POLITECNICO DI TORINO

Master of Science in Biomedical Engineering

Master Thesis

Synthesis and characterization of innovative silica-based bioactive glass doped with tellurium

Supervisors

Prof. Enrica Vernè

Prof. Marta Miola

Candidate

Edoardo Renzi

March 2019

Contents

Abstract

In the last decades the research on innovative materials and technologies for applications in medicine improved considerably the quality of life and reduced the social costs of several diseases. Among materials for biomedical applications, bioactive glasses have been widely studied, since the 1970s, as third generation bone substitutes and biomaterials for tissue regeneration. The term “bioactive” is related to the ability of these glasses to stimulate bone regeneration trough a peculiar reactivity that induces the formation of a hydroxyapatite layer on their surface. A further peculiar property of bioactive glasses is the possibility of being doped with ions of therapeutic interest. Among them, tellurium is still under investigation and very few works report its introduction into bioactive glasses. The purpose of this work is to investigate the effect of the introduction of tellurium oxide in the composition of a silica-based bioactive glass in two different ratios. The tellurium-doped glasses have been synthesized by traditional melt and quenching route. The obtained glasses have been subsequently characterized in terms of their characteristic temperatures by Differential Thermal analysis (DSC), phase analysis by X-ray diffraction (XRD) and structural analysis by means of spectroscopic techniques (Raman and Fourier-transform infrared spectroscopy - FTIR). In addition, the obtained bioactive glasses were immersed in solutions similar to biological body fluid in order to investigate their bioactivity, evaluating pH evolution over time in solution, ion release and hydroxyapatite formation. In addition, cell viability assay and reactive oxygen species evaluation tests are in progress in order to investigate the role of tellurium as a biologically relevant ion. The findings suggested that the addition of tellurium oxide into a bioactive glass does not affect negatively the bioactivity and potentially may play a helpful role in the realization of a new class of bioactive materials with antimicrobial and antioxidant activities.

Negli ultimi anni, la ricerca nel campo delle tecnologie e dei materiali biomedici ha apportato miglioramenti considerevoli nella qualità della vita di ognuno e nei costi sociali associati a molte malattie. I vetri bioattivi sono, tra i materiali impiegati nel settore biomedico, quelli più ampiamente studiati fin dal 1970 in quanto appartengono alla terza generazione di materiali bioattivi. Il termine bioattivo è associato proprio alla capacità di questi vetri di formare un legame diretto con l'osso e stimolare, sulla sua superficie, la formazione di idrossiapatite. Un ulteriore vantaggio offerto da questo materiale consiste nel fatto che può essere drogato con ioni dagli effetti terapeutici. Il tellurio è fra questi, anche se i dati disponibili in letteratura non sono sufficienti per trarre conclusioni riguardo alla sua efficacia e le applicazioni in medicina sono del tutto assenti. L'obbiettivo di questo lavoro è quindi quello di andare a investigare l'effetto che può avere drogare un vetro bioattivo a base di silice con il tellurio in due percentuali in peso differenti. Questo materiale è stato realizzato con la tecnica classica di fusione e tempra. Dopo di che, sono stati individuati i suoi punti caratteristici di temperature tramite Analisi Termica Differenziale, determinate le fasi cristalline e amorfe tramite Diffrattometria a raggi X e la struttura atomica tramite la spettroscopia (Raman e Infrarossa). Inoltre, il materiale è stato immerso per tempi differenti in una soluzione simile al plasma sanguigno al fine di valutare la bioattività, il pH, il rilascio di ioni e la formazione di idrossiapatite. Test di citocompatibilità e valutazione dei ROS sono attualmente in corso per dare un quadro più chiaro del ruolo del tellurio impiegabile come ione terapeutico. I risultati ottenuti fino ad ora hanno mostrato che il tellurio non sembra influenzare negativamente la bioattività della composizione e pertanto potrebbe in future essere impiegato nei vetri bioattivi in come agente antibatterico e antiossidanti.

Aims and objectives

This work is expected to contribute to new knowledge development regarding the bioactive glasses. The main objective of the research is to synthesize and characterize new bioactive silica-based glasses doped with tellurium. On the basis of my knowledge, this is an innovative research topic since bioactive glasses doped with tellurium have not been previously documented in literature. Then, the aim of this work is to investigate the possible tellurium influence on the bioactive glass synthesis, its characteristic temperatures and its reactivity (i.e. bioactivity), the cytocompatibility and biological effect (e.g. antibacterial effect and ROS production) by means of several investigation tests. Finally, the last step will be to estimate if any improvements are required to facilitate material synthesis or application.
This thesis is basically dived into five sections:

1. Introduction: a literature review that provides a clear in-depth overview of the topics concerning this research: from the concept of glass to the state of art and global market.

2. Materials and Methods: a chapter specifically dedicated to describe compositions of interest, all experimental procedures, all experimental conditions and methods of determining quantitative measurements.

3. Results: data sets and plots emerged from this work.

4. Discussion: a debate on the performed analysis and obtained results.

5. Conclusions: a brief summary with generalized statements in answer to research questions and a list of suggestions to overcome in future works the current obstacles encountered.

1. Introduction

1.1 Background

Technological and scientific progress are strongly affected by the available materials. Generally speaking, it can be said that the choice of the appropriate material for a specific application is central to find solutions to a technological problem. To satisfy all different requirements, research has also focused on the development of new materials and the improvement of those materials already known. A very interesting class of materials is represented by glasses. They have distinct characteristics, and this fact makes them suitable for optical products, applications to sensors and biomaterials. The interest in the latter family has been growing on a surprising scale because of their well-established compatibility with living tissues. For centuries mankind has been trying to identify innovative materials aimed at producing safer and healthier prosthesis in order to replace or improve body tissue functions. Human body, however, is corrosive and aggressive towards implants, and therefore materials must be chosen to make sure the properties are fit for that purpose. This is where material science intervenes. Its role is to search for materials mimicking those already present in the body. There is also a number of materials that causes no reaction from the body and is stable enough not to get chemically broken down. This compatibility can be increased by making their shape such that the body can grow into the material rather than just encapsulate it in scar tissue. However, the next step in biomedical technology will be utilizing biomaterials to emulate entirely synthetic organs programmed specifically to our genomes in order to cure our illnesses, disorders, and diseases. By utilizing biomaterials, there is the hope that one day the man will be able to replace damaged nervous tissues, to regulate the chain of electrical signals and provide the ability to walk again to many confined to the wheelchair. Humans can replace organs like lungs and someday hearts in order to save those seriously injured in every day tragedies like severe automotive accidents. By creating artificial bone structures with our genetic and anti-genetic markers, humans can bypass the rejection therapy often accompanying transplants. A million different worlds of possibilities exist in this emerging field of science and the consequence will inevitably be that people will live longer, more fulfilling lives. From the loved ones that would have

survived had been a cure available at the time, to those who desperately need medical care at the start of life, biomaterials will completely change the procedures of health care as humans know them today.

1.2 Glass

Glasses are amorphous materials obtained by the gradual hardening of a liquid that has not crystallized during cooling [1]. In inorganic oxide-based glasses the framework typically consists of corner sharing MO_4 tetrahedra or MO_3 trigonal planes as indicated in this report [2]. The material produced is characterized by an absence of long range order within the atomic structure likewise the liquid from which takes origin (**figure 1.1**).

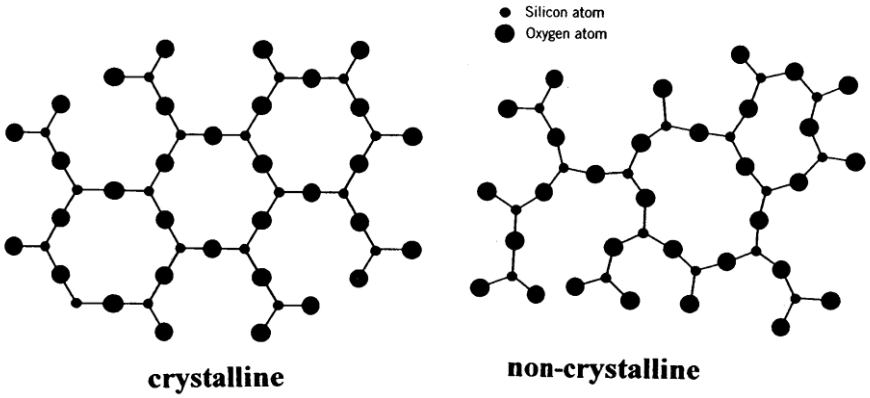

Figure 1.1: Crystalline and amorphous silica based-glass structure [3].

However, molecules of a regular solid don't move unless there is a change in the environment. This suggests that glass molecules can flow, like some sort of an extremely viscous liquid, hence glass is referred to as a super-cooled liquid when it is below its melting point but still hot and malleable. The freezing process starts forming small bits of crystals in a process called nucleation. The problem is that this nucleation requires an input of energy, called the activation energy. Since the activation energy can be high, freezing can take a very long time to set in. To achieve phase transformation at the equilibrium temperature requires a nucleation center or centers. As liquid is cooled from a high temperature, it may either crystallize or become super-cooled [4].

As shown in **figure 1.2**, the transition from the solid to the liquid state is sharp. The diagram shows a plot of specific volume versus temperature for a fully crystalline solid.

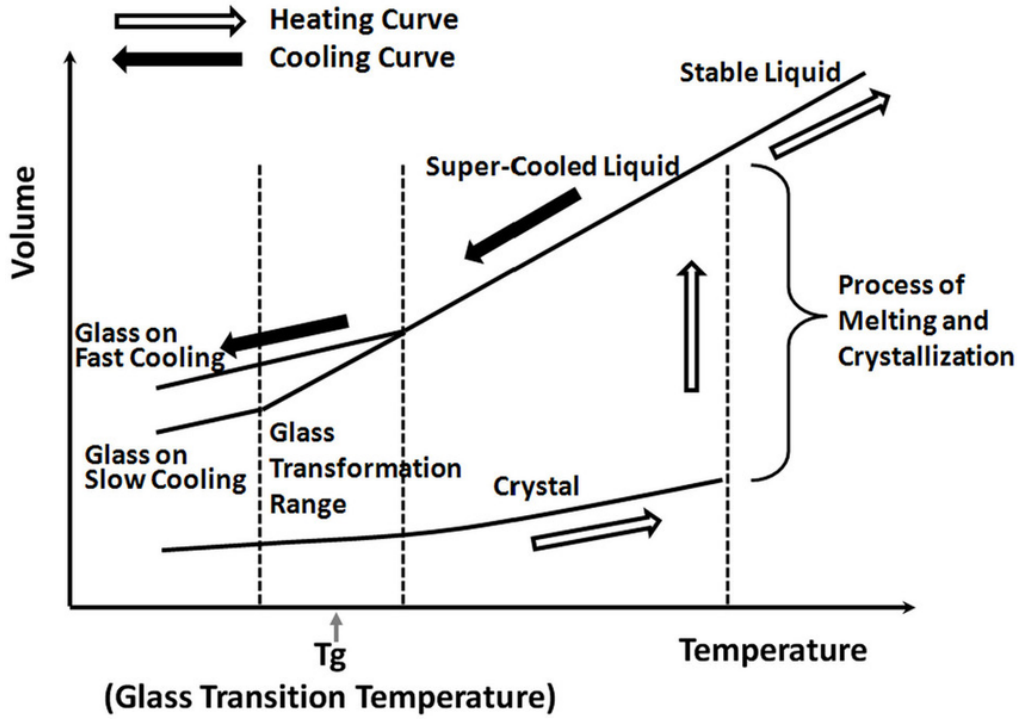

Figure 1.2: Plot of specific volume versus temperature for glasses [5].

T_m is the melting point, while T_g is the glass transition point. At the glass transition temperature, it can be observed a sudden increase in viscosity due to the change from liquid to a solid state. Besides, at the melting point, it is possible to notice a considerable drop in specific volume followed by a distinct decrease in the rate of decline of specific volume with decline in temperature. On the contrary, the region over which glass transition point occurs, shows only a change in the rate of decline of specific volume with decline in temperature. Above the glass transition, the material has a lot of mobility. When materials reach a precise temperature, a mass transfer of a solute from the liquid solution to a pure solid crystalline phase occurs [6]. In this process, the atoms or molecules are highly organized in a structure known as crystal and this defines the crystallization temperature T_c. If material is heated past its T_c, eventually it reaches another thermal transition, one called melting. Those crystals begin to fall apart. The chains come out of their ordered arrangements and begin to move around freely [7]. When glass is worked between T_g and T_m, one can achieve virtually any shape and the glass is considered a super-cooled liquid [7]. It is well known that the values of T_g depend both on heating rates and rates of cooling of samples [8]. The optimum results are obtained in the cases when an initial cooling rate is equal to a heating rate. If the material is not cooled slowly, it determines the formation of region with different specific volume and consequently the establishment of residual stress. This stress can weaken the glass and degrade its properties, so it is necessary to remove these internal stresses by reheating glass to an adequate temperature in glass transition region. This temperature is called annealing temperature. At this point, the glass is too tight to distort and remains soft enough for any built up stresses to relax. The time required for this process can vary depending on the mass and type of glass. The glass temperature shall remain

constant for a definite time period before cooling slowly to room temperature. The quicker the glass is cooled down, the more the amount of stress that can be built up in the glass [9]. This temperature to anneal any glass is a range, so it is not important to reach an exact temperature, in this way, the volume of glass will shrink until the target value is reached on the diagram of metastable equilibrium. As a liquid is cooled its viscosity normally increase, but viscosity also has a tendency to prevent crystallization, so if the viscosity rises enough as it is cooled further, it may never crystallize, in such way the molecules have a sufficient cohesion to maintain rigidity [10]. The higher the viscosity at the melting point, the more easily the glassy state of material is reachable. (Vogel-Tamman-Fulcher-bassler viscosity glass). In general, the requirements for the formation of glasses are the following:

1. Rapidly cooling;

2. A high viscosity at Tm;

3. No heterogeneous nucleation sites [11];

4. A large liquid-crystal interfacial energy [11];

1.2.1 Mechanical Properties

Glass is a brittle material. The typical Stress Strain diagram for glass looks like this figure (**figure 1.3**).

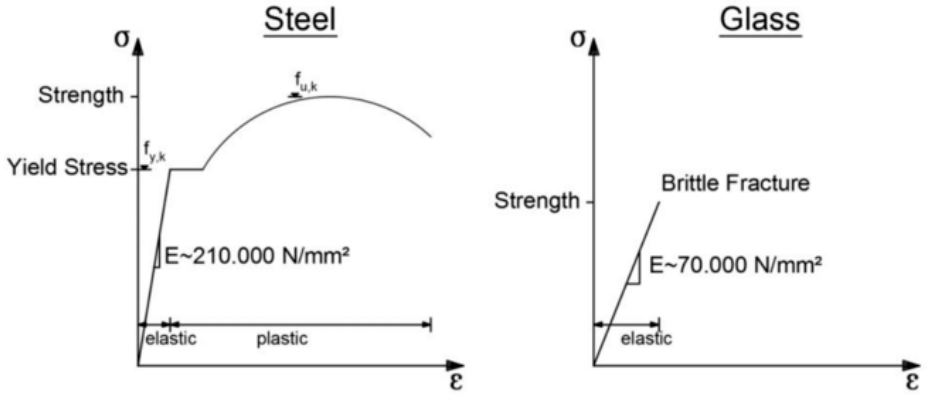

Figure 1.3: Comparision between stress-strain curves of steel and glass for an uniaxial tensile loading test [12].

The linear relationship till sudden failure and fracture can be observed. Glass fails quite easily under low/moderate cyclic loading, or sudden impulse loading, its fatigue strength isn't that high if compared to metals. Glass material behavior is similar to that of a ceramic. Conventional glass fractures and breaks quite easily, and never shows plastic deformation. Compared with a ductile material, the difference in energy absorbing capabilities can be also observed in **figure 1.4**.

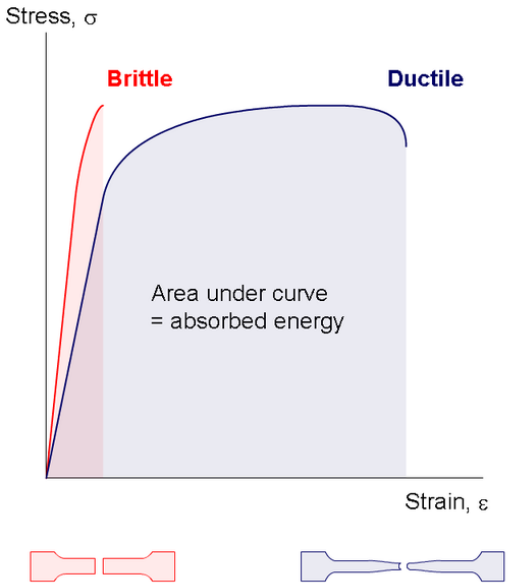

Figure 1.4: Brittle against ductile stress-strain behaviour [13].

So, materials like glass, which are brittle, can only absorb a bit of energy before failing. The compressive strength of a glass can reach up to 10 GPa, but in tension, when stress level exceeds 100 MPa, glass fails easily [14]. Even the slightest crack in the surface of glass can act as a "seed" for brittle fracture. Round such a crack, if it is stretched by tension or bending, there is a concentration of stress. The interatomic bonds are easily broken by the high stress values that build up near cracks [15]. On the other hand, when glass is compressed, the crack propagation is more difficult as it tends to close up the cracks. For the most of commercial glasses, Young's modulus of elasticity E ranges from 55-90 GPa and the Poisson's ratio γ ranges from 0.16-0.28 as recalled in this article [15]. For glass specimens with pre-existing surface flaws (with length a), the fracture is controlled by crack propagation. When the applied stress σ_a reaches the critical stress level σ^{fr}_a with proper orientation the flaw opens into a larger crack [16]. Griffith' criterion is expressed with $\sigma_a \geq \sigma^{fr}_a$ formula, indicating catastrophic failure. Griffith explained that the discrepancy is due to the inherent defects in brittle materials leading to stress concentration and lowers the fracture strength of the materials [17]. Crack propagation occurs when the released elastic strain energy is at least equal to the energy required to generate new crack surface. However, if $\sigma_a < \sigma^{fr}_a$, there will be no failure. Unless the glass part exhibits static fatigue, or delayed failure (which consists of slow crack growth), brittle fracture occurs when the most severe crack reaches the length 2a [17].

$$\sigma = \left(\frac{2E\gamma}{\pi a}\right)^{\frac{1}{2}}$$

Equation. 1.1: Griffith's equation for strength of materials [18].

$$P_f = 1 - e^{\left[-\left(\frac{\sigma}{\sigma_0}\right)^m\right]}$$

Equation. 1.2: Weibull distribution [19].

The Griffith equation (**equation 1.1**) is strongly dependent on the crack size and satisfies only ideally brittle materials like glass [20]. Other experimental results of fracture strength can often be described by the Weibull distribution (**equation 1.2**). The Weibull distribution is a cumulative probability distribution. It predicts the fraction of samples which survive or fall at stresses up to the stress in question, but it does not give the probability of failure at that stress. P_f is a probability of surviving. σ is stress assumed. σ_0 is a normalizing stress, which depends on the material and also on the size of component and stress distribution in the component. m is a shape factor, usually referred to as the Weibull modulus, which reflects the degree of variability in strength. The higher the m is, the less variable is the strength [20].

1.2.2 Rheological properties

Viscosity is a motion of atoms or molecules relative to their neighbors. Viscous flow in amorphous materials is a thermally activated process: where Q is activation energy, T is temperature, R is the molar gas constant and A is approximately a constant. The viscous flow in an amorphous material is characterize by a deviation form from Arrhenius-type behavior [21]: Q changes from a high value Q_H at low temperatures (in the glassy state) to a low value Q_L at high temperatures (in the liquid state). Depending on this change, amorphous materials are classified as either: strong when, $Q_H - Q_L < Q_L$ or fragile when, $Q_H - Q_L \geq Q_L$ [21].

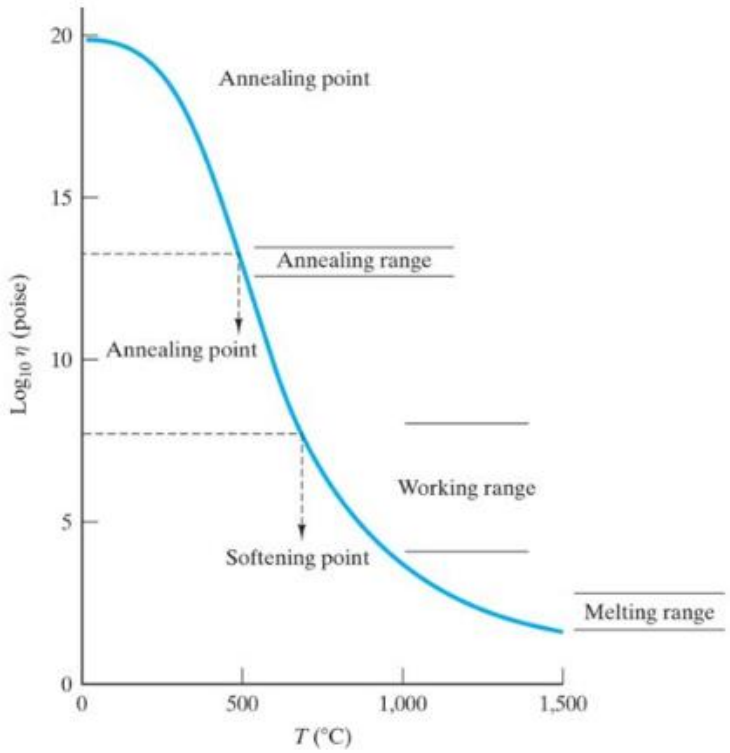

Figure 1.5: Viscosity of a silica-based glass [22].

All along the cooling process, the viscosity of glasses increases (**figure 1.5**), from a low-viscosity melt, to a rigid material with a higher viscosity. For a good annealing of the constraints, the viscosity of the glass should be not too high and not too low. At annealing point, the internal thermal stresses present in the glass are relieved by viscous relaxation within 15 minutes [23]. Below the strain point, relieving the internal stresses is practically impossible. Characteristic temperatures vs viscosity diagram gives a clearer overview.

1.2.3 Thermal properties

Since glasses are amorphous solids, which exhibit a high structural disorder, the mean free path of phonon is short and that's the reason why glasses are poor heat conductors. The coefficient of thermal conductivity shows how efficiently heat can be transferred in the considered material and, in the case of soda-lime glasses, it is low (around 1 W/mK in practice) [15]. An additional parameter that describes thermal behaviour is thermal transmittance. It is the loss of heat through one square meter in constant conditions of a material, divided by the difference in temperature across that material. The lower the thermal transmittance, the lower the heat loss. The risk of thermal breakage is influenced by condition of the glass edge, so when the central area of glass becomes hotter than the edge. The center of glass expands but is restricted from natural expansion by the cool edges, therefore this results in stress within the glass [15]. For applications where thermal breakage is a concern, heat treated glass should be specified.

1.2.4 Optical properties

The optical properties of a glass determine how it will interact with light. For this purpose, optical properties can in principle be divided into categories: refractive index, optical dispersion, refraction and reflection. The index of refraction refers to the ratio of the speed of light in a vacuum to the speed of light through a given material at a given wavelength, thus it is defined as follows: where c is the speed of light in a vacuum and v is speed of light through a given material. Typical values for glasses are n ~ 1.5-2 [24]. Refractive index depends on wavelength and this dependence is called dispersion, so refractive index should be quoted at a specific wavelength. Refractive index represents the interaction of light with electrons of the constituent atoms in a glass, therefore "n" increases with electron density or polarizability. The structure of the glass therefore plays a secondary role, but if a change in structure results in a change in electron density, then "n" should also change. Further specific feature of glasses is the dispersion which is a description of the variation of the refractive index with wavelength. It is specified using the Abbe number defined as where n_f, n_d and n_c are the refractive indices blue (F), yellow (D) and red (C) of Fraunhofer lines [25]. The Abbe number of a glass quantifies the amount of dispersion for a specific spectral range. A high Abbe number generally gives less color dispersion and reduces color aberration. Lastly, glasses offer high transmission throughout the entire visible spectrum and beyond in the near ultraviolet and near infrared ranges [26].

1.2.5 Electrical properties

At room temperature, glass performs as good an insulator. The electrons of the last layer are travelling between the owner atoms which is negatively charged and the beggar atoms which is missing one electron. The stable chemical bond that give physical strength to glass is the reason electric current is not allowed. Additionally, glass becomes more conductive (less electrical resistance) the hotter it becomes, when heated above 800°C [27]. Unlike most other materials which become less conductive (more electrical resistance) when heated. The exact conductivity will depend on the ions present in the silica, but a typical value is 10^7 Ω·cm, so immobile ions are able to drift further between collisions under the influence of an applied electric field [15]. In physics terminology, free electrons in a material are electrons having energy levels in what's known as the material's conduction band. In room temperature glass the conduction band energy levels are too high for any of the electrons to reach.

1.2.6 Chemical properties

Glasses are made for special purposes because of its outstanding durability and excellent resistance to chemical or water attack. The corrosion attack on glasses can vary greatly depending on the pH and strength of the attacking, but the chemical stability of SiO_2 is the reason for glass chemical stability [28]. The Si - O bond has a very high enthalpy of formation, which is a measure of how much effort is required to break apart the chemical bond. In fact, a good example is silicon-based compounds being used as a protecting group in organic chemistry, in order to prevent normally easily reacted portions of a molecule from reacting under harsh reaction conditions. The strong acids, as HCl, H_2SO_4, don't attack glass because SiO_2 is a covalent compound with strong bonds and because the resultant Si^{4+} ion

of the hypothetical reaction is a too strong Lewis acid to form in presence of water, so it would immediately react with the water formed, re-generating the initial acid and the silicon dioxide [29]. Although not all chemical should be stored in glass, as strong as SiO_2 bond is. SiO_2 will still dissolve slightly by basic solutions with high pH and by certain acids. Furthermore, a very small amount of silicon ions will still diffuse out of the glass based on the quality of the glass. It can pretty much only be removed with fluorine containing reagents because almost nothing else will react with it. Fluorine and silicon have a high affinity for each other. HF etches SiO_2 and this reaction happened (**equation 1.3**):

$$SiO_2 + 6\,HF \rightarrow H_2SiF_6 + 2\,H_2O$$

Equation 1.3: Chemical interaction between silica and phosphoric acid [30].

The degree of attack is determined by the amount of alkali released from the glass under the influence of the attacking, even water can be very aggressive especially when it reaches the critical pH of 9 by dissolution of alkalis from the glass surface [31]. This quantity of alkali is extremely small in case of the more resistant glass. It is clear that removal rate of ions alkaline is highly dependent on chemical composition of glass. Silicon oxide is relatively water insoluble compared to the other minerals. The release of silicon to solution is proportional to the square root of time, consistent with a surface diffusion process [32]. There is an alkaline ion exchange of glass through hydrogen ions of water. This chemical reaction generates siloxan groups and hydroxide ions, which increases pH in solution. Then, a second reaction can be formulated (**equation 1.4**):

$$\equiv Si - O - Si \equiv + OH^- \leftrightarrow \equiv Si - OH + \equiv SiO^-$$

Equation 1.4: Chemical interaction between silica and hydroxil [33].

An increase in the pH level leads to the break of siloxan groups and generates silanol groups on the surface. This mechanism will be studied in detail hereafter. The stability of the Si-O bond is the key to the stability of glass. The only element that silicon likes bonding to more than oxygen is fluorine which is why HF does attack glass. Furthermore, if a break glass exposes fresh surface, it gets exposed silicon atoms and exposed oxygen atoms. Oxygen from the air quickly bonds to the exposed silicon atoms. So, in a while, oxygen atoms of surface bond to silicons that are bonded back into the bulk of the glass. These exposed oxygen atoms have unpaired electrons and may bond to hydrogen, carbon, nitrogen and more complex ions. But these interactions between surface oxygens and the atmosphere do not weaken or break the Si-O bonds that reach back into the glass. Moreover, glass is different, perfectly clean glass will allow water to adhere to the surface. Actually, glass is right on the border and can sometimes be hydrophobic, especially if it is not perfectly clean. The slightest amount of soap or detergent will ensure full wet-ability of a glass surface. It is controlled by the angle that water makes with the surface, less than 90 degrees will result in a wet surface, more than 90 degrees will cause water to roll off the surface like water of a duck's back. Silicon dioxide, which is the main component of glass, is slightly polar, which means it can attract water molecules [34]. Therefore, glass is wettable. Further, other components added to glass, such as calcium carbonate, would also make the surface wettable.

1.3 Glass transition

Unlike crystalline solid, glasses do not have a specific melting temperature, but as temperature increases, the material softens over a wide temperature range and gradually changes its phase from solid to liquid leading to a decrease in viscosity. The glass transition is the reversible transition in amorphous materials from a hard and relatively brittle state into a molten or rubber-like state [7]. Glass transition from the solid state to the liquid state is basically a kinetic phenomenon therefore, it depends upon the kinetics of the process (**figure 1.6**). Starting from the melt, if the cooling rate is much larger, structural rearrangements is unable to volumetrically relax. Temperature plot related to glass changes from a flexible rubbery material to a brittle and rigid material can be defined as glass transition temperature (T_g). Above T_g, glass molecules have greater mobility and are able to achieve their equilibrium conformations which corresponds to an increase in free volume as mentioned in the article [35]. Below T_g, glass mobility is greatly decreased corresponding to a reduction in glass free volume. At temperatures T_g, viscosity is roughly equal to 10^{12} Pa, then the liquid transforms into a glass stopping achieved configuration [36].

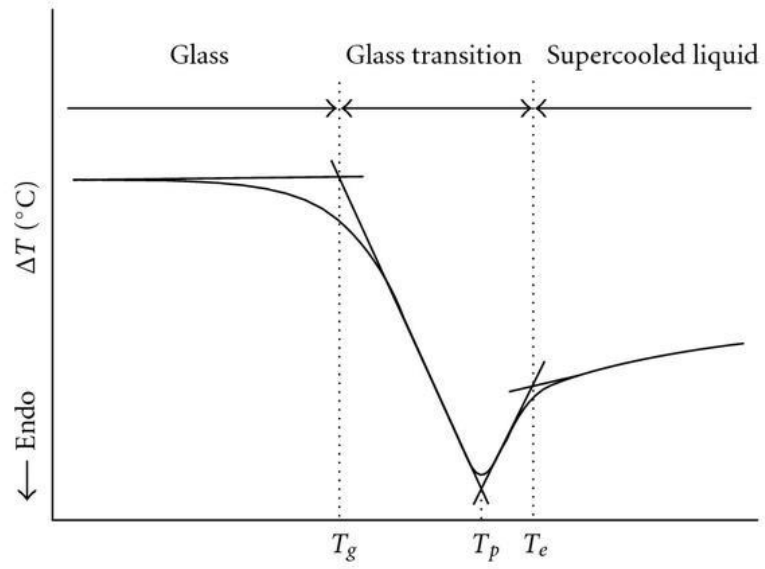

Figure 1.6: Determination of glass transition temperature based on differential temperature analysis (DTA), below the T_g the material is glassy whereas above the T_e the material is liquid [37].

Since T_g is determined by cooling down processes, it can present different values according to the cooling rate. The faster the heating rate, the higher the observed T_g will be, due to the thermal lag of the material. Conversely, the higher the cooling rate, the lower the T_g will appear to be if observing on a cooling cycle. Glass transition does not always occur. The liquid changes properties and structures only if it is given sufficient time to change. It can therefore be affirmed that glass transition occurs when cooling rate of the substance concerned is lower than melting point and greater than crystallization rate. It is generally known that glass transition temperature can be roughly estimated as 2/3 of the liquidus temperature for a given composition in the phase diagram of the system considered [36].

This definition shall be supplemented by a more accurate description. When a liquid is cooled rapidly enough, it led to the formation of a glass and the considered glass transition temperature will be a function of the quenching rate (q). Over a limited temperature range, the relationship (**equation 1.5**) becomes:

$$q = q_0 \cdot e^{\left[\frac{E_a}{RT_g}\right]}$$

Equation 1.5: Quenching rate equation [4].

where q_0 is a constant, E_a is an activation energy with a value related to viscous flow activation energy, while R is Boltzmann costant. T_g decreases exponentially with increasing q [4]. A number of theories have been put forward to try to further explain the nature of glass transition. The most reliable theories are free volume theory and the Gibbs theory. The first theory was elaborated by Beuche, Turnball and Cohen. The free volume is associated with the space between molecules in a glass, therefore liquid diffusion is due to molecules jump into vacancies. The probability of the motion of molecules per unit time is associated with an activation energy which depends on the amount of free volume in a sample. More free volume is related to a lower activation barrier [38]. As regards the second theory, the statistical calculation of the entropy can also be used to determine the basis of the glass transition. According to Gibbs, diffusion and viscosity are due to cooperative rearrangement in the melt. Glass transition shall be achieved when the configurational entropy has reached a minimum.

1.4 Glass formers, intermediates and modifiers

Glass formers are oxides of elements which are surrounded by four oxygen atoms in the tetrahedral chain forming glass (**figure 1.7**). Glass forming-oxides are essential in the formation of glass because they form the basis of the random three dimensional network of glass [39]. Some examples of oxides can be found here: SiO_2, GeO_2, B_2O_3, P_2O_5 etc. which form glasses when quenched from high temperatures.

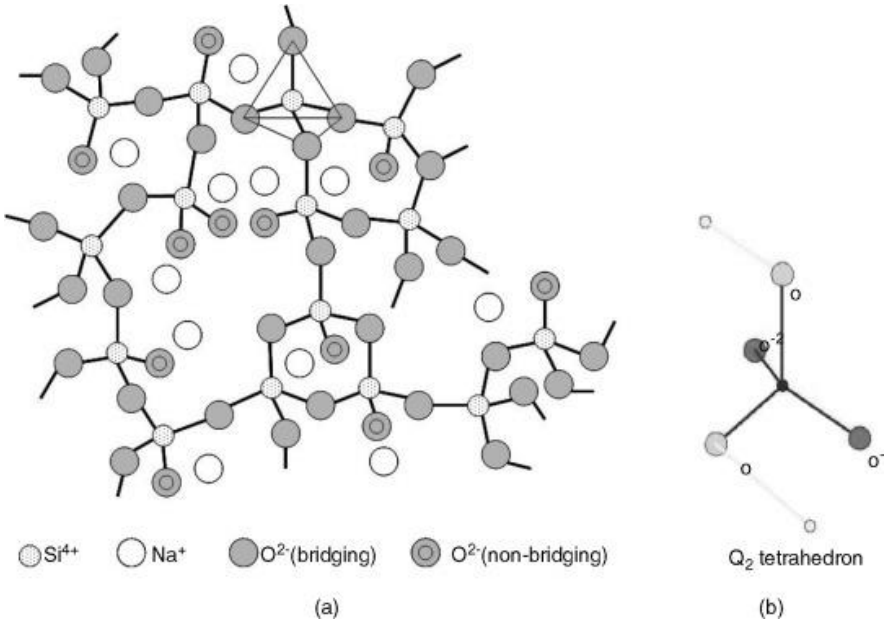

Figure 1.7: (a) Structure of silicate glasses; (b) a Q_n structural unit: Q_2 comprises two bridging oxygen atoms and two non-brdging oxygens (NBO) [40].

The work of some researchers has greatly contributed to the evolution of chemistry and structural characteristics of glasses. Indeed, there are different structural theories of glass formation. Goldschmidt's radius ratio theory was one of the first model proposed. Glass formation is only possible when the cation/anion ratio r_a/r_c (where c denotes cation and a anion) falls between 0,2 to 0,4. This ratio determines how many anions can be packed around a given cation [41]. Most crystals with radius ratio of 0,2 to 0,4 have a coordination number of 4 with anions at the corners of tetrahedron. Tetrahedral arrangement of oxygen ions around a cation necessary for glass formation [41]. A Norwegian physicist of name William Holder Zachariasen elaborated its theoretical model known as Zachariasen's Random Network Theory (1932) [41]. Glasses lack the periodic long range order, characteristic of crystals, and have the same average packing and properties in all directions [41]. Zachariasen's rules for glass formation based on an empirical observation on oxides:

- No anions (oxygen) may be linked to more than two cations (metals) [41]
- The former cation coordination number is less than four [41]
- Unit cells share corners, not edges or faces
- Unit polyhedra cells are bonded in a 3D network (at least three corners must be shared) [41]

All four rules should be satisfied for glass formation to occur. This structural approach to glass formation is based on coordination number and can apply only to oxide glasses. Stanworth, in the early 1950s, proposed another model based on bond type. Stanworth has introduced the concept of ion percentage related to the difference of electronegativity

between cation and oxygen. The electronegativity of the cations, of which the oxides are glass-forming, falls within a certain range between 1.90 and 2.20, so the tendency to form a glass increases as the cation size decreases [42]. Instead, the Sun's bond strength model is based on bond strength. It establishes a relation between glass forming tendency and the bond energies of elements with the anion atom in the glass (**table 1.1**).

Table 1.1 Elettronegativites of glass forming oxide and network modifiers [1].

Element	Pauling electronegativity
Glass network formers	
Te	2.1
B	2.0
Si	1.8
P	2.1
Ge	1.7
As	2.0
Sb	1.8
Glass network modifiers	
Li	1.0
Na	0.9
K	0.8

This theory asserts that, when a melt is quenched to form a glass, the stronger the M-O bonds, the more difficult are the structural rearrangements necessary for crystallization and, hence, the easier is glass formation as said in the paper [43] This model has a limitation: the exclusion of the chalcogenide glasses. Intermediate glasses oxides are oxides that do not form glasses on their own, but when mixed with glass formers may either act as network formers or network modifiers (Al_2O_3, SnO_2, TiO_2 etc.) [43]. These oxides are added in high proportion for linking up with the basic glass network to retain structural continuity. For example, aluminum oxides can replace many of the SiO4 groups in the silica network with AlO_4 tetrahedra [43]. Dietzel's field strength model has been introduced to highlight difference between glass former and intermediate. More factors are important than just bond strength:

- Small cations with high charge => network formers
- Large cations with small charge => network modifiers [44]
- Medium size cations with medium charge => intermediates [44]

Dietzel classified elements according to their field strength F. This considers the forces (attraction/repulsion) between cations and anions in the glass:

$F = Z/(r_c + r_a)^2$ where Z is valence of the cation, r is ionic radius of the cation or anion (**table 1.2**).

Table 1.2 Ions classification according to Dietzel's model [45].

Element	Valence Z	Ionic radius	Coordination number	Ionic distance	Field strength Z/a^2	Function in glass structure
K	1	0.133	8	0.277	0.13	Network-modifiers $Z/a^2 \approx 0.1–0.4$
Na	1	0.098	6	0.230	0.19	
Li	1	0.078	6	0.210	0.23	
Ba	2	0.143	8	0.286	0.24	
Pb	2	0.132	8	0.274	0.27	
Sr	2	0.127	8	0.269	0.28	
Ca	2	0.106	8	0.248	0.33	
Mn	2	0.091	6	0.223	0.40	
Fe	2	0.083	6	0.215	0.43	
Mn	2	0.083	4	0.203	0.49	
Mg	2	0.078	6	0.210	0.45	Intermediates $Z/a^2 \approx 0.5–1.0$
			4	0.196	0.53	
Zr	4	0.087	8	0.228	0.77	
Be	2	0.034	4	0.153	0.86	
Fe	3	0.067	6	0.199	0.76	
			4	0.188	0.85	
Al	3	0.057	6	0.189	0.84	
			4	0.177	0.96	
Ti	4	0.064	6	0.196	1.04	
B	3	0.020	4	0.150	1.34	Network-formers $Z/a^2 \approx 1.3–2.0$
Ge	4	0.044	4	0.166	1.45	
Si	4	0.039	4	0.160	1.57	
P	5	0.034	4	0.155	2.1	
B	3	0.020	3		1.63	

Glass modifiers are oxides that can be mixed with network formers to yield glasses and to modify the properties of glass. Modifiers include Li_2O, BaO, CaO, SrO, Na_2O and K_2O. The oxygen atoms from these oxides enter the silica network (for example) at points joining the tetrahedra and break up the network, producing oxygen atoms with an unmatched electron [46]. Modifiers remain as metal ions ionically bonded in the interstices of the network [46]. Rawnson has proposed to use, as a means to discriminate formers from modifiers, ratio of the bond strength to the energy available at the freezing point. The higher the value, the lower the probability for bonds to break at T_m, and hence the higher the tendency for glass formation. This criterion shows its efficacy, above all if applied to binary systems. Glass formation occurs usually in a composition range close to eutectic one, with a liquidus temperature with the lowest possible melting temperature [46].

1.5 Glasses crystallization

Crystallization in glasses is generally a phenomenon that happens when ordinary window glass is held for long enough just bel [47]ow its liquidus temperature, crystals will begin to form in the undercooled material [47]. Crystallization from a glass is known as

devitrification and usually forms tiny crystallites with dendritic morphologies and textures indicating heterogeneous nucleation, therefore the crystals formed have highly regular internal structure. Crystallization is the result of two processes: nucleation and growth of crystals, under the influence of a temperature gradient normal to the boundary (**figure 1.8**). Nucleation usually takes place when molecules meet and form clusters than can grow further to form crystals [48]. Nucleation is a competition between surface energies that resist the creation of new interfaces and a driving force to grow a more stable phase, therefore this is a stochastic process, and as such, nucleation can be somewhat unpredictable. Nucleation involves the lining up of atoms from their disordered liquid state to an ordered crystal state. The driving force for this is the free energy change on moving from liquid to crystal [48]. However, nucleation creates an interface between the two phases, which has an energy penalty. There is therefore a critical size of nucleus that must be reached, below this size, the nucleus is unstable and can dissolve back into solution; above this size, the nucleus is stable and can grow into a larger crystal.

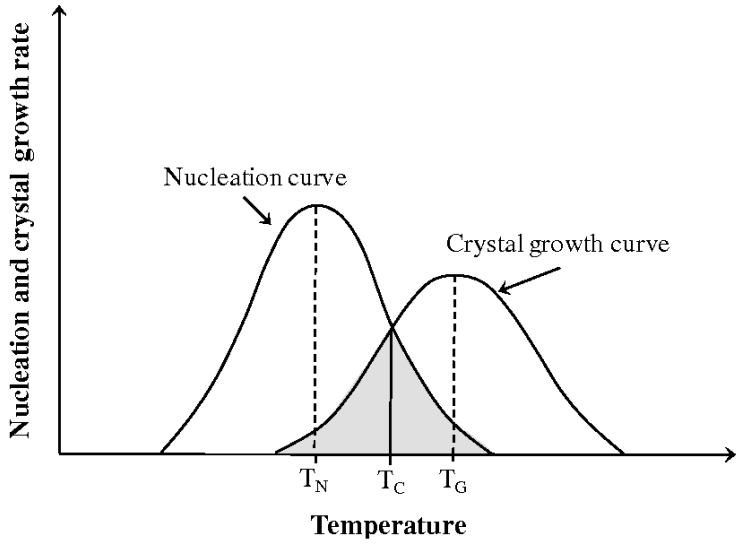

Figure 1.8: Relative position of the nucleation and crystal growth curves with temperature [49].

The formation of stable nuclei only happens if the increase in interfacial energy resulting from the formation of a solid liquid interface is offset by a decrease in energy released by the formation of a solid [50]. The second stage is the growth of the nucleated crystals. This is a thermally activated process, which means that its rate is dependent on the temperature. For growth to proceed, constituents must diffuse through the melt and reaches the crystal surface, so rapid growth and slow nucleation produce fewer coarse-grained crystals. If the cooling rate is very slow, equilibrium is maintained or closely approximated [50]. Crystallization is favored by high enthalpy of fusion and a low viscosity. The critical Gibbs free energy for the nucleation of a crystal is related to the enthalpy of fusion. Large enthalpy of fusion implies a lower critical Gibbs free energy, which further implies ease of crystallization. An embryo becomes a nucleus by jump of atom across the interface from liquid to crystal. This requires an activation enthalpy. The activation enthalpy is related to the log of viscosity. This implies that a lower viscosity allows for easier atomic jumps, which in turn favors crystallization [50].

1.6 Phase separation

Several glass-forming systems exhibit, for certain compositions and preparation conditions, the phenomenon of phase separation or immiscibility. All happens when a glass mixture under certain cases tends to separate into more than one phase. Both phases have their own internal or free energy, which is derived from the second law of thermodynamics that, with some simple assumptions, can be re-expressed as a change in entropy and a change in enthalpy [51].

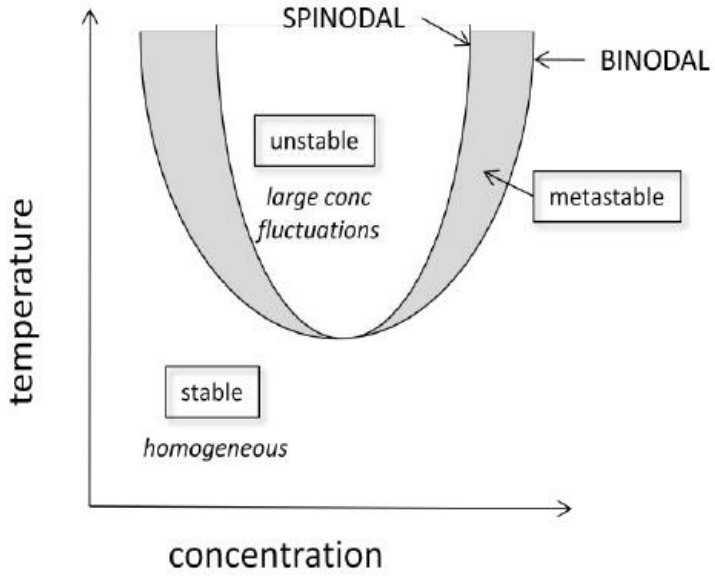

Figure 1.9: Schematic phase diagram showing different phase separation mechanisms [52].

The variation entropy is strongly associated with entropy of single components contained in the mixture which varies linearly with the same component concentration (**figure 1.9**). On the other hand, a change of enthalpy depends on connection between components in the mixture. As in any chemical process, the favorability of mixing is determined by a combination of entropy and enthalpy, so while entropy and enthalpy of a system change, the free energy changes lead to total or partially miscibility [51]. Therefore, whether two components will mix or not is usually determined by whether it is enthalpically favorable for them to do so. In brief terms, because mixing entails no covalent bond breaking, enthalpy considerations for mixing boil down basically to the sum total strength of electrostatic interactions in the pure substances versus those in the mixture [53]. Generally, on a glass phase diagram the phase separation will happen within the binodal region while spinodal decomposition happens within the spinode. On the binodal, the chemical potentials of the two phases are equal. The unstable state of the system is reached on spinodal. A substance, being in a labile state, rapidly loses its spatial homogeneity, and during relaxation its structure becomes more granular-cellular, without the phase boundaries. The binodal structure will have spherical particles in it while the spinodal structure looks loop like [53]. Since the structures are metastable, with time the loops break up into spherical particles as

well. The kinetics of the processes are quite complex. Phase separation is a nucleation and growth event while spinodal decomposition is diffusion controlled.

1.7 Preparation techniques

Many methods are adopted for preparation of glass. Some of these are discussed below.

1.7.1 Melt-quenching technique

This is historically the oldest established method of producing a glass and it still widely used. The technique consists of weighting out suitable proportions for the required composition and mixing the high purity materials followed by melting in sealed evacuated ampoules. Once the mixed substances are melted, it is either poured into molds and subsequently, the melt will vitrify when cooled by quenching in water. Common glass can be liquified at very high temperatures like 1500 °C [54]. An important factor is to keep the melt at a high temperature, so that solubility of gasses is low and the viscosity is low enough for the bubbles to escape. After this, it is necessary to decrease the temperature to re-dissolve the remaining gas bubbles. Usually, adding some suitable chemical fining agent to melt composition helps to remove bubbles from molten glass [55]. If the surface cooling is fast enough the glass at the surface structurally freezes remaining at lower density values, the density observed in glass depends on the cooling rate since it is a metastable structure, while the center cools down slower increasing its density and pulling the surface into compression. The atoms are fixed in position, but in their disordered, liquid positions, not an ordered crystal. This sort of frozen-in-place liquid. When a glass is heated to its glass transition temperature, the atoms gain enough thermal energy to move [55]. Unlike in crystalline melting, there is no breaking of bonds. Instead, bonds become free to rotate.

1.7.2 Sol-Gel Technique

The sol-gel method was developed in the 1960s, when glass where made without high temperature melting processes [56]. The sol-gel method typically refers to the production of a ceramic oxide material by creating a sol, a solution of precursor molecules in a blend of water and alcohol, turning it into a gel, an amorphous material that results after the precursor is hydrolyzed and starts to form metal-oxide bonds. Then, optionally, firing the gel to convert it into a ceramic. In some of these processes, the gel is the final state, like metal oxide particles suspended in solvent and turned into a gel somehow [56]. The metal/semi-metal atoms are still atomically dispersed in the sol-gel process, which has some advantages. Whereas in the case of nanoparticles, there is a bunch of tiny objects, each with their own pre-existing atomic structure. The mixtures of precursors are treated by stirring with magnetic stir bar and ageing for 24 hours at room temperature [57]. Sol-gel is often used as a synthesis method for solid-state chemists when uniformity, shape control, and atomic-level homogeneous mixing are important. Therefore, various parameters are involved to convert solution into gel in the mentioned sol-gel synthesis process: these are

temperature of synthesis, molarity of the precursors or concentration of chemicals, solvent amount and time of synthesis [57].

1.8 Bioactive Materials

Biomaterials are materials that are applied in medical devices or in contact with biological systems. Since the time of its birth, approximately half century ago, the field of biomaterials has seen a steady growth as a result of ideas from materials science, chemistry, biology, medicine and engineering [58]. Since the Bronze Age, it saw that materials could be used to heal, but effects on human health were not known (**figure 1.10**). The Egyptians were the first ones to do primitive prosthesis; in fact, a female mummy have been found in Egypt with a wooden toe. Treatment for broken bones was often performed through use of bronze and copper objects with good results.

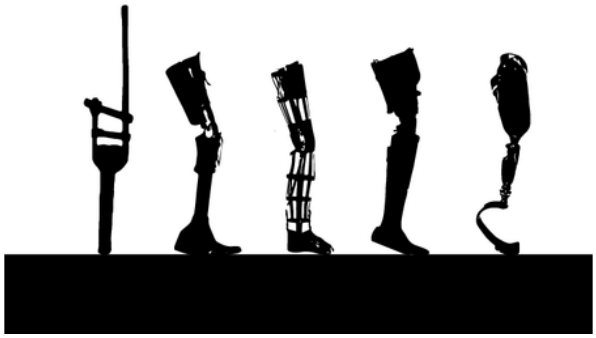

Figure 1.10: Evolution of the Prosthetic [59].

In this case, implant failure was resulted from copper toxic effect. Another area which offered plausible solutions with regard to both function and esthetics is dentistry. The Etruscans were particularly skilled in the product of metals, enabling them to build first pontics using golden bands. The Middle Ages was characterized by an alarming decline in ideas and the notions of medicine were in some cases not detailed enough. The concept of compatibility began to emerge only toward the end of 1800 due to the Industrial Revolution. Indeed, an urgent action was needed to address work accidents and their consequences. During this period, ivory was being use as a bone graft material for the repair or augmentation of bone defects [1]. Biocompatibility is not quite as pedestrian as that, in fact, it took more than thirty years with a view to arriving at an acceptable definition. Furthermore, biocompatibility has evolved, allowing it to be adapted both to developments in medical and material science. Today, biomaterial is defined as a substance which is surgically implanted or come into contact with the body for a limited or an unlimited period and forms a stable interface with living host tissue. However, the definition of biomaterial has undergone a continuous evolution during the period 1940 – 2000. A first generation of biomaterials has been designed to ensure the slightest response with its surrounding tissue. Then, it was time for second generation of biomaterials which, once brought into contact with the body, change their characteristics over the passage

of time releasing beneficial substances for the body. Finally, third-generation biomaterials exploit a full range of characteristics, which enable not only repair process, but also stimulates them specifically [60]. Since there are different types of materials, the biological response is going to be different from each other, when it is implanted in the body; therefore, materials can be divided into two different broad classes: biocompatible (bioinert, bioactive, biomimetic and bioresorbable) and toxic (tissue becomes necrotic). Biocompatibility of materials also depends on the bulk composition and the surface properties, the latter is affected by several parameters: contaminations, crystalline degree, surface topography, composition, roughness and hydrophobicity. Despite all these considerations, a biomaterial can be subject to substantial deviations: reduction/oxidation, diffusion of the ions, leaching of metal ions or free radicals, hydrolysis, material degradation and rearrangement of surface chemical groups [60]. Many reactions occur at different scales: for example, a material may degrade over time realizing ions at nanometer scale, while it interacts with cells at the macro scale. It is therefore important how the body is going to respond to surface of a foreign material. When material that comes into contact with living tissue because of injuries, it activates a series of protective reactions to repair the damage causing inflammatory processes. These processes may be described, in brief, as follows.

1. Implant
2. Proteins adsorption
3. Cell attachment (lymphocytes and macrophages)
4. Release of cytokines by macrophages
5. Fibroblast recruitment in situ
6. Fibrotic capsule formation (**figure 1.11**)

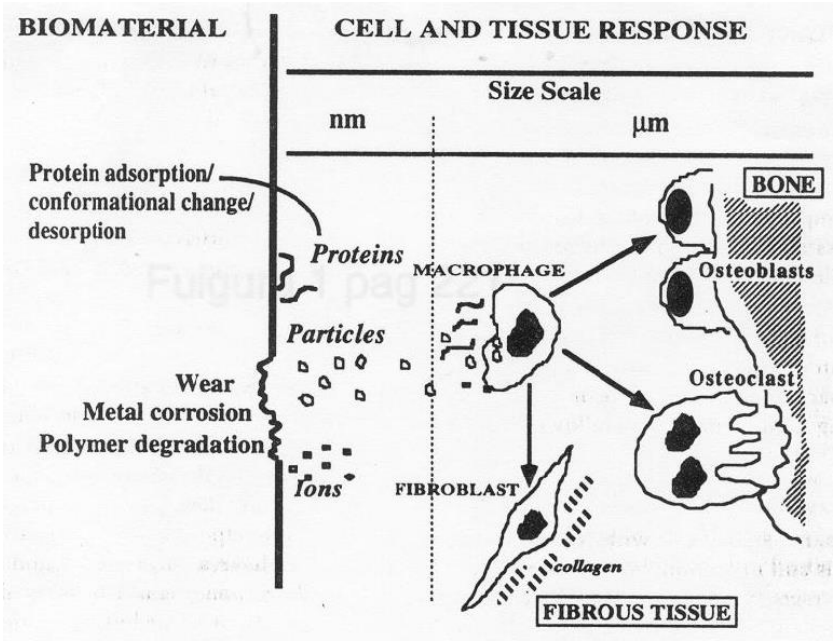

Figure 1.11: Schematic example of an interaction between biomaterial and living tissue [1].

The purpose is to avoid as far as possible this natural fibrous encapsulation to ensure successful implant integration. Consequently, a material has optimal biocompatibility, when new-tissue formation on exposed surface area is guaranteed. In addition, the interface between implant material and host tissue must be capable of withstanding the stress applied locally. A material that create chemical and mechanical bonds with tissues should therefore be carried out. More specifically, this category is populated by calcium phosphate-based ceramics, bioactive glasses, bioactive glass-ceramics, bioactive composite materials. The strength of a chemical bond can differ depending on the chemical nature of materials and the interactions that take place between biomaterial and tissue [1]. Bioactivity concept describes the behavior of tissue approaching the material surface of interest in more detail than biocompatibilty and it is a direct extension of that. On the tissue level, the biomaterial has to allow for regeneration, wound healing, and tissue remodeling. This means that the cells have to be able to break the biomaterial down, and replace it with natural biomaterials or the biomaterial can be integrated by cells in the human body. If the biomaterial cannot be broken down, then blood vessel networks to supply oxygen will have trouble forming. If the there is an injury or damage to the biomaterial, it may not repair properly. The systemic properties could be summarized twofold: immune response and material degradation. If the biomaterial ellicits an immune response, then the host will either actively destroy the tissue, or create a fibrotic barrier between the foreign biomaterial and the host. This fibrotic barrier will prevent cells, oxygen, and nutrients from entering the biomaterial, rendering it effectively inert [60]. This is bad, as the biomaterial must interact with the host, and foster the regeneration of the tissue. Lastly, material degradation is important. Some materials are designed to degrade, and others are not. If the material does degrade, metabolites, degradation and reaction products will be floating in the blood stream. This is foreign material that the body needs to handle properly, lest it build up and clog arteries. Typically, these materials are sent to one of two places: the kidneys or the liver. If the kidneys pick it up, they will dump it into urine, and the degradation and reaction products will through in urine. If the degradation and reaction products are too large, or there are too much, the kidneys could be overloaded and cause irreversible kidney damage. If these degradation and reaction products go to the liver, they are either reprocessed into another material, or they are stored permanently. Again, overloading the

liver causes liver damage. A benchmark, called bioactivity index, has been determined in order to quantify body-material interactions involved [1]. It shall be calculated by dividing by one hundred the number of days to take for more than half of the interface to bond. The reaction speed is different for each class of material and the times get longer as material gets far from bioactivity. Moreover, in vitro or vivo tests are carried out to evaluate biocompatibility and toxicity of the used materials. In vitro tests are performed with biological fluids, although often simulated physiological solutions (artificial saliva, Ringer solution, Hanks solution etc.) are used to check changes in both materials and fluids. These are salt solutions, markedly concentrated, speeds up surface material degradation processes, enabling to understand what would happen if material were to lie directly on living environment.

1.9 Testing Biomaterials

Biomaterial should have a suitable composition or desired function like in terms of biological properties, mechanical properties, and that should match with the specific tissues or specific organs, where this biomaterial will be implanted. Therefore, biocompatibility evaluation essentially will address or will focus some of the important properties: cytotoxicity and genotoxicity. Consequently, testing of the biomaterials will try to address how to characterize the material that will be processed into a medical device or implant. Biomaterials can be evaluated to determine whether they function appropriately in the in vivo or in vitro environment (**table 1.3**). In vitro experiment are laboratories scale simulated experiments, where essentially trying to simulate as close as environment possible, which is prevailing in the human patient or human body. In vivo models have a demanding protocols like animal welfare act.

Table 1.3 Advantage and disadvantage of in vivo and in vitro test [61].

In vitro tests	**In vivo tests**
Advantage	Advantage
Experimentally controllable	Simulate real body condition
Repeatable	Clinically relevant
Fast	
Inexpensive	
Simple	
Small amount of test material is required.	
Decreasing the use of animal	
Have a quality control	
Range of applications is vast	
Disadvantage	Disadvantage
Chronic effects cannot be tested	Expensive
	Time consuming
	Ethical and regulatory issues

1.9.1 In vitro tests

- Direct Contact: it consists in cell culture on the surface of materials and the cells considered should be the same that will interact with the material *in vivo*. The choice of which type of cells depends on the application of material: osteoblast cells in case of bone applications, endothelial cells in case of vascular applications, cardiomyocytes in case of

cardiac applications. In direct contact test, different aspects can be evaluated: the cell attachment on the material surface after different time points using scan electron microscope, the cell proliferation or the phenotype by immunofluorescence staining [62].

- Indirect contact: materials will be immersed in media at a final concentration expressed by the ratio between material and the media that it is going to use according to the cell type for 12-72 hours to check whether material can leash or release some toxic elements into media or not [63]. This is called preconditioned medium. Prior to being immersed in the preconditioned medium with the material, the cells are [63]cultivated in a normal medium. When the cells are transferred in the preconditioned medium, they need approximately 12-24 hours to attach to the material [64]. The response of cells to that preconditioned medium can be checked using MTT assay or any cell viability assay. Afterwards, results can be compared with negative control groups, cells cultured in normal medium, and positive control groups, cells cultured in presence of toxic material [64].

1.9.2 In vivo tests

The main advantage of in vivo experimentation is that it allows to gather knowledge about some biological processes with a lesser ethical and practical burden than equivalent human experimentation. There are various in vivo tests:

• Sensitization: sensibilisation as having antibodies for a specific substances or potential allergens

• Systemic toxicity: each compound has a different toxicity profile and produces different symptoms. Very small particles of implanted material become much more reactive and are more likely to form compounds that are absorbed into the body.

• Genotoxicity: if chemistry or composition of the material results indicate potential genetic mutation

• Implantation test: it is difficult to predict who will have reactions, even in those with established pre-implant metal allergy

• Eye irritation test: estimation of ocular irritation potential to chemicals

• Skin irritation test: like the previous

• Pyrogen testing: potential febrile reaction of extractable substances derived from material leaching

• Carcinogenicity: determine the tumorigenic potential of medical devices

• Hemocompatibility: device contact with circulating blood

1.9.3 Simulated Body Fluid

A simulated body fluid (SBF) is an aqueous based-solution,in which the nature of ions (**table 1.5**) and their concentration are close to that of human blood plasma (**table 1.4**). Temperature and pH are carefully monitored with regard to physiological safety. Kokubo introduced the first protocol to prepare SBF for the purpose of evaluate in vitro the changes on a surface of a bioactive glass ceramic after implant [65].

Table 1.4 Ion concentration of SBF in comparison with human blood plasma [66].

Ion species	Ion concentration (mM)	
	SBF solution	Human blood plasma
Na^+	142.0	142.0
K^+	5.0	5.0
Mg^{2+}	1.5	1.5
Ca^{2+}	2.5	2.5
Cl^-	148.8	103.0
HCO_3^-	4.2	27.0
HPO_4^{2-}	1.0	1.0
SO_4^{2-}	0.5	0.5

Table 1.5 Chemical composition of simulated body fluid (SBF) solution [67].

S. no.	Reagents	Amount in 1000 ml
1	NaCl	8.035 g
2	$NaHCO_3$	0.355 g
3	KCl	0.225 g
4	$K_2HPO_4 \cdot 3H_2O$	0.231 g
5	$MgCl_2 \cdot 6H_2O$	0.311 g
6	1.0 M HCl	39.0 ml
7	$CaCl_2$	0.292 g
8	Na_2SO_4	0.072 g
9	$((HOCH_2)_3CNH_2)$	6.118 g
10	1.0 M HCl	Appropriate amount for adjusting the pH $\sim$ 7.4

1.9.4 Tris(hydroxymethyl)aminomethane

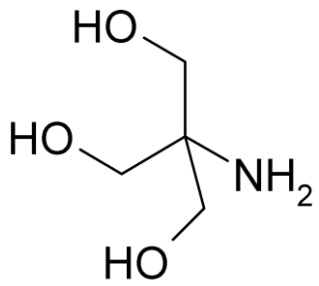

Figure 1.12: Tris(hydroxymethyl)aminomethane [TRIS] Formula [68].

A widely used buffer for studying biological system is tris(hydroxymethyl)aminomethane $(HOCH_2)_3CNH_2$ called "TRIS" for short (**figure 1.12**). It is a biologically inert amino alcohol that buffers carbon dioxide and acids in vitro and in vivo. The pKa = 8.072 for the conjugate acid of TRIS [65].

1.9.5 Cytocompatibility

Cytocompatibility is a term referred to the evaluation of the cytotoxicity via the measurement of cell survival on material surface. Cytotoxicity is the destruction of cells caused by certain external and internal factors. Internal cytotoxic factors include cytokines, interlukins, tumor necrosis factors secreted by cytotoxic T lymphocytes. External factors include certain allergens or drugs. As far as mechanism is concerned, cytotoxic elements exert damage to cell membranes or destabilize them increasing their permeability ultimately leading to the cell lysis [69]. On the cellular level, cells have to be able to grow on/in the biomaterial and to behave the way they normally would. For example, a hard, rigid, porous biomaterial could support cellular growth for a large number of cells, but would be most likely ideal for bone cells, and not ideal for liver cells. Moreover, the immune system recognizes all foreign chemical substances. Native surfaces have heparin protein chains coming off the surface. Heparin prevents the adhesion of C3 proteins to surfaces. Lack of heparin leads to C3 sticking to the surface and cleaving into C3a and C3b [70]. C3b stays on the surface and starts a chain reaction that will lead to the death of the cellit is stuck upon.C3a floats off to act as chemoattractant to neutrophils and other immune response agents to come attack the foreign body [70]. In the case of an implanted device macrophages will eventually get involved and form a giant body of cells that grows until they form a fibrous capsule, isolating the foreign material from the body. Fibrous capsule formation often inhibits device functioning and the timeline of its formation often determines the maximum usable duration. Therefore, treating cells with a cytotoxic compound can result in a variety of consequences. The cells may undergo necrosis, in which they lose membrane integrity and die rapidly as a result of cell lysis [71]. The cells can stop actively growing and or the cells can activate a genetic program of controlled cell death []. Cytocompatibility

tests can be divided into two categories: indirect and direct contact tests, whose description can be found in chapter 1.8.1.

1.9.6 Reactive Oxygen Species (ROS) production

Cells work through a very delicate system of biochemical reactions. Some of these are oxidation or reduction reactions where electrons are shuttled around. ROSs are certain types of molecules containing oxygen, and oxygen has a strong ability to steal electrons from other molecules. Thus it impacts on their abilities to perform their normal biological functions. Sometimes these oxidants are important for inter-cells communication, because they are used as messengers to active different processes inside the cell. Free radical reactive oxygen species such as peroxides or hydroxls, are highly reactive molecules that are a normal part of metabolism, but cause cellular damage, and bodies are built to detoxify and repair this damage. The dangerousness of oxygen is given by the fact that it can trigger a chain of reactions destructive for all cells, either human or bacterial [73].

$$OH - RH \rightarrow H_2O + R\cdot$$

Equation 1.6: ROS chemical mechanism [72].

Analysing in details the chemical reaction (**equation 1.6**), the oxidant takes a proton and an electron from a reactant R, leaving it with a high energy unpaired electron, thus creating a ROS. When oxidants reach high concentrations in a body, they can react with important biomolecules like DNA, leading to mutations and other side effects. In this way, a chain of radical reactions is started leading to a series of damages, like mutations, dimers and possibly strand breaks. Another big targets of damage are the components of cell membranes, like phospholipids, because they feed the chain reaction producing more free radicals [73]. This is why ROS are usually dangerous because one molecule can react with certain parts of cells to create more ROS.

The main types of ROS are called superoxide and hydroxyl radicals. Oxidative stress basically occurs when there are more free radicals than the amount that can be handled by the body itself. However, antioxidants can be used to prevent ROS damage by reacting with it in a way to stop the chain reaction effect. Antioxidants attach to peroxides and turn them into chemicals that the body can dispose through the liver and lymphatic system [73]. Not all antioxidants are ingested from food, many are made by the body. Certain vitamins and minerals like Vitamin C, Calcium and Vitamin E are used in large quantities by the body to make these antioxidants. Some of these vitamins, such as Vitamin E, can even be absorbed through the skin and will promote the skin to repair itself from sun damage more quickly [73].

1.9.7 Antimicrobial activity

In the 1900s, 1 in 3 children were expected to die of an infectious disease before the age of five, but the introduction of modern drugs (antibiotics) in the 1930's was a medical revolution [74]. Each antibiotic has a spectrum of bacterial species it can target, depending on the mechanism of the drug. Antibiotics may, for instance, inhibit bacterial cell wall

synthesis or bind ribosomal subunits to prevent protein synthesis [75]. There are generally two large categories of antibiotics: those that target the cell wall building mechanism and those that target bacterial ribosomes. By disrupting building cell walls the bacteria are unable to multiply, which makes them weaker towards the immune system (the primary weapon that all pathogens have against the immune system is replication) [76]. By disrupting the activity of bacterial ribosomes the cells are unable to translate messenger RNA into proteins, so the cells stop functioning and die [75].

A *bacterium* is a microscopic single celled living organism that reproduces itself by binary fission. Thanks to their relative simplicity, they can adapt quickly to the extreme conditions in which they can thrive and their survival depends in part on their ability to detect changes in their surroundings. Some bacteria are characterized by different sensors that are used to build up a complete picture of the its environment. They have an outer layer that consists of two things: rigid cell wall and an underlying cytoplasmic membrane or plasma membrane that it includes granules, ribosomes, mesosomes and circular DNA [75].

Bacteria can be classified according to morphological characteristics like their cell shape, size and structure and their specific arrangement like motility and flagellar arrangement. They can be divided into two main categories according to their cell wall: Gram positive or Gram negative. There are many other differences but the membrane/peptidoglycan layer (cell wall) is the major difference used to classify bacteria. Both Gram positive and negative bacteria have an internal cytoplasmic membrane surrounded by a peptidoglycan layer [77]. The peptidoglycan layer is much thicker in Gram positive bacteria, and Gram negative bacteria also have an outer membrane surrounding the peptidoglycan layer that is not present on Gram positive bacteria [75]. Lipopolysaccharide is a major component of the outer membrane and during an infection, this component is sometimes able to over activate the immune system causing septic shock [75].

There are two main ways through which substances (mostly water, gasses, biomolecules and ions) move between cells through cell walls. Some substances can move through the cell wall freely. Sometimes, the cell walls have waxy materials that block this pathway. There are two different kind of processes that cells use: direct transport and endocytosis. Direct transport usually involves secreting enzymes out of the cell onto the substances to break them down into simpler forms. After this the substances are absorbed through the plasma membrane by diffusion or facilitated diffusion by transmembrane proteins or ions channel or active transport by pumps. Furthermore, many channels open or close in response to a small signaling molecule called ligands [76]. They are able to bind substance and pass into the membrane channel. The others method is known as endocytosis, where the cell literally swallows the substances by surrounding it and pinching off its membrane to form a capsule.

$$(M^{n+}) + H_2O_2 \rightarrow (M^{n+1}) + OH^- + OH^\bullet$$

Figure 1.13: Fenton's reaction (M^{n+} is a cation of a metal) [79].

When it involves solids it is known as phagocytosis, for liquids it is pinocytosis. With these types of mechanism, it can be understood how bacteria are affected by toxic metal activity. Metals have been used as antimicrobial agents prior to the discovery of antibiotics. A Recent

research has demonstrated that some metals can affect resistant bacteria and can disrupt biofilms [77]. In the majority of cells, metals work as a cofactor in enzymes, but they also promote free radicalsaccording to Fenton reaction. The Fenton reaction (**figure 1.13**) is also known as hydroxyl hydrogenation and has the ability to oxidize a wide variety of organic contaminants into non-regulated compounds, in fact, in this reaction OH^* free radical is formed. The kinetics reaction is fast and may damage biomolecules [78]. Several researches have shown that ROS created by Fenton reaction can damage DNA in E. coli and lead to the cell death [78].

Drugs and disinfectants aren't the only ways mankind can use against the spread of disease. Many heavy metal cations have antimicrobial activities and can be very toxic to living organism [80]. This toxicity, called oligodynamic effect, is related to ion concentration but it also depends on the size of the cell in contact. These metals (**figure 1.14**) interfere with the functioning of the bacteria, fungus etc. resulting in the death of the microorganism [80]. In particular, it is supposed that the metal interferes with the correct functioning of proteins needed for the survival of these microorganisms. The phenomenon at the root of this are the following: donor atom selectivity, reduction potential and speciation [74].

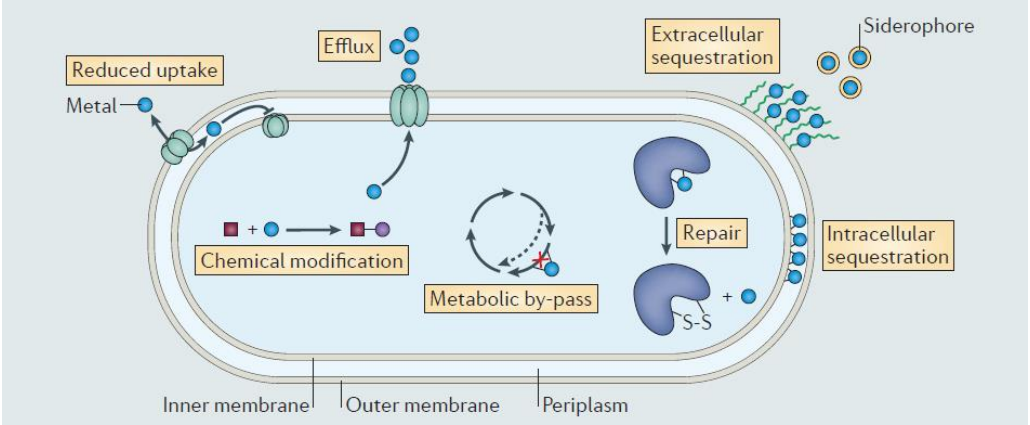

Figure 1.14: How bacteria deal with deadly metals [74].

• Donor atom selectivity is based on ligand field theory, which considers the effect of different ligand environments on the energies of the d-orbitals, which determines the magnetic and electron spectral properties of transition metal complexes [74]. The effect depends on the coordination geometry of the ligands. This fact promotes the formation and deconstruction of transition-metal containing proteins. In terms of formation, if the metal is more easily released by its previous ligands (either water or some compound that delivers the metal to the site of enzyme construction), it can form the necessary enzyme more quickly [74]. However, even if a metal-containing enzyme plays a useful role, it should not be too stable, because it is necessary to adjust the level of enzyme concentration for optimum activity, or remove enzyme if it becomes damaged. Thus, it is important that the metal ion can be removed easily [77].

• Reduction potential: reduction-oxidation reactions involve the transfer of electrons between proteins and metals. Certain metals in solution will produce hydroxyl radicals,

which are very reactive and can damage just about any cellular component through oxidation. Some evidence suggests that some metals can cause lipid peroxidation of the bacteria membrane by interacting with highly electronegative chemical groups which stand as sites of adsorption for metal ions [74].

- Speciation: metals can exist in different physic-chemical states in biological environments depending on oxidation states. Different species of the same metal can vary widely in toxicity. Thus, the chemical form of a metal determines its reactivity and solubility [81]. It has to be noted that there are distinct binding protein sites for metals. They lead to formation of carbonyl groups which disable function of enzymes [81]. Metal species have a similar structure to the cofactors of enzymes using ionic or molecular mimic and are able to replace cofactors in binding sites. Also, with regard to nutrient assimilation, metal ions can competitively inhibit the uptake of essential ions for bacteria survival [81].

1.10 Bioactive Glasses

Bioactive glasses belong to a particular class of biomaterials, which are able to induce the precipitation of a layer of hydroxyapatite/hydroxicarbonate apatite, main constituent of the bone tissue, when put in contact with body fluid, leading to the formation of a chemical bond with living tissue. The bioactivity of these materials is expressed through a change over time in material surface when they are put in contact with the physiological environment or biological fluids. The result is a series of chemical processes occurring at their surface, leading to the formation of a strong and stable bonding interface connecting the glass to the living tissues [82]. A bioactive glass is different from other biomaterials because chemical composition affects the development of interface between material and living tissue.

1.10.1 Hydroxyapatite

Hydroxyapatite (HA) is an inorganic substance, which can exist in nature in different forms, such as rock and in living organisms [83]. Hydroxyapatite (Hap) with multiple substitutions at all sites and containing 4% to 6% carbonate is the primary component of bones (70% wt) and teeth (96%) [84]. Chemically speaking (**figure 1.15**), it is a double salt of calcium orthophosphate in tetrahedral units, which has in its structure hydroxyl groups and its stoichiometry is expressed by the formula:

$$Ca_{10}(PO_4)_6(OH)_2$$

Figure 1.15: Hydroxyapatite formula [85].

In fact, unit cell of the HA is composed of 10 calcium ions, 6 phosphate ions and 2 hydroxyl groups [83]. It crystallizes in the hexagonal crystal system as shown in **figure 1.16**: calcium and hydroxyl groups are packed into columns while oxygen is part of both hydroxyl and phosphate groups.

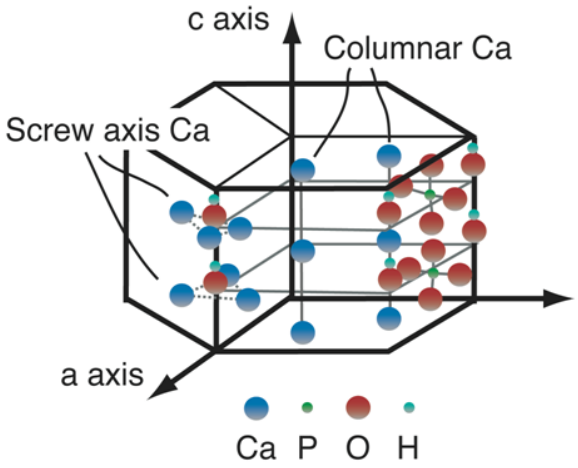

Figure 1.16: Hydroxyapatite crystal [85].

This column structure gives it piezoelectric properties causing formation of dipoles and limiting the size of HA, since oxygen is more electronegative than hydrogen. Thus, all the apatites are double salts, but from a medical standpoint, only those with calcium phosphates are interesting, while those apatites in which calcium is replaced by another equivalent cations or phosphorus and hydroxyl are replaced by halogens are not of interest. However, this great possibility of cations/anions substitution constitutes an advantage for the apatites, for istance, the replacement of OH^- with F^- gives a less soluble apatite (fluoroapatite) [83].

1.10.2 Bioactive glasses: State of the Art

The first and most famous bioactive glass was developed at the University of Florida by Larry Hench in 1967 and its name is Bioglass® (45S5) [58]. The idea stems from a fortuitous encounter with Colonel Klinker, returning from Vietnam. Colonel Klinker asked Larry Hench to design a material capable of protecting human body from energy radiation [58]. Bioglass was the first man-made material to bond to living tissue and that led to the foundation for the second generation of biomaterials. Nowadays, it is used worldwide for repair bones and teeth and it is even an active ingredient in some toothpastes [86].

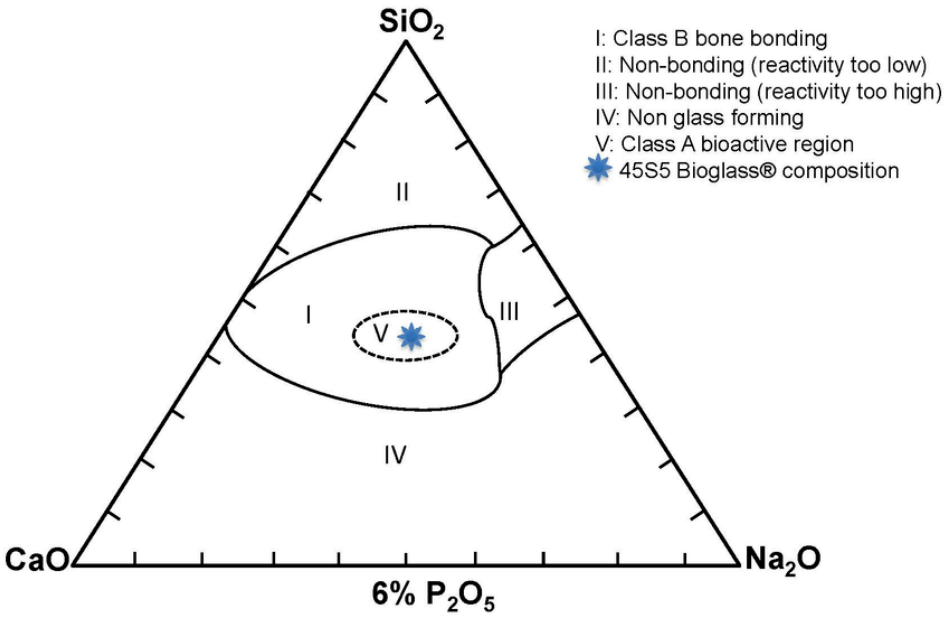

Figure 1.17: Compositional dependence of bone and soft tissue bonding to bioactive glasses [1].

Bioglass is a multicomponent oxide glass with the following composition (in wt%):

$$45\%\, SiO_2 -\ 24.5\%\, Na_2O -\ 24.5\%\, CaO -\ 6\%\, P_2O_5$$

Figure 1.18: Chemical composition (wt%) of 45S5 Bioglass® [1]

These compositional (**figure 1.17**) features make the surface of the 45S5 Bioglass® highly reactive when exposed to an aqueous medium [86]. Hench also showed that these glasses activate healing responses not only in bones, but also in connective soft tissues. Bioactive glasses have different families and each of these families have different compositions of oxides for everyday applications. A comprehensive ternary phase diagram (**figure 1.17**) shows probable internal structures in different regions [87]. When the composition is low on CaO, the glass is dissolved more rapidly. A low concentration of Na_2O in the glass composition leads to the formation of hydration layer in contact with physiological solution. The SiO_2 region has the possibility to bond to soft tissue with the formation of carbonated hydroxyapatite, while the region between CaO and Na_2O contains non-glass forming. Glasses with the highest bioactivity level belong to the central region (**figure 1.17**). This composition is very closed to eutectic ternary system and it is for this reason that it can be easily cast. Bioglass, as well as bioactive glass, has very poor mechanical properties, low tensile strength and a high modulus of elasticity, thus cannot be used for load bearing applications (**table 1.6**). On the contrary, 45S5 Bioglass® is ideal as bone cement filler and coating due to its biological activity [87].

Table 1.6 Selected properties of melt-derived 45S5 Bioglass® [87].

Property	Value
Density	2.7 g cm^{-3}
Network connectivity	2.12
Glass transition temperature	538 °C
Onset of crystallization	677 °C
Thermal expansion coefficient	15.1 × 10^{-6} $°C^{-1}$
Young's modulus (stiffness)	35 MPa

As argued above, composition makes the surface highly reactive when it is exposed to an aqueous environment and start stages of reaction to form an interface with living tissue. This mechanism was explained by Larry Hench following specific steps (**figure 1.19**). All of this applies to the basis of the bone bonding property of bioactive glasses.

• The first step is a rapid reaction, which consists in ion exchange between hydrogen in the body fluid and sodium or calcium ions from the surface of the glass. This generates an alkaline surface layer with a net negative surface charge. The loss of Na and Ca causes a breakdown of the silica network (Si-O-Si) leading to the formation of $SiOH_4$ [89].

• Release of $SiOH_4$ in soluble form resulting from breakdown of silica network following action by ions in water with the consequent formation of silanol groups.

• Dissolution and polycondensation of silanol groups to form hydrated silica gel.

• Precipitation of Ca^{+2} and $[PO_4]^{3-}$ from body fluid to form an amorphous film rich of calcium phosphate.

• Crystallization of amorphous $CaO\text{-}P_2O_5$ film by incorporation of OH- and CO_3 to form the hydroxycarbonateapatite (HCA) layer [89].

• Adsorption of biological molecules (growth factor, proteins) on HCA layer. The thickness of this HCA layer forms a mechanically compliant interface that is essential for maintaining the bioactive bonding of implant to the natural tissue [89].

• Action of macrophages to remove debris from site allowing cells to occupy the space [89].

• Attachment of stem cells on bioactive surface [89].

• Differentation of stem cells to form osteoblast [89].

• Crystallization of inorganic calcium phosphate.

• Proliferation and growth of bone.

Steps 1-5 are chemical reactions of the glass that can occur also in vitro, while steps 6-11 are biological reactions between bioglass and bone, which occurs only in vivo.

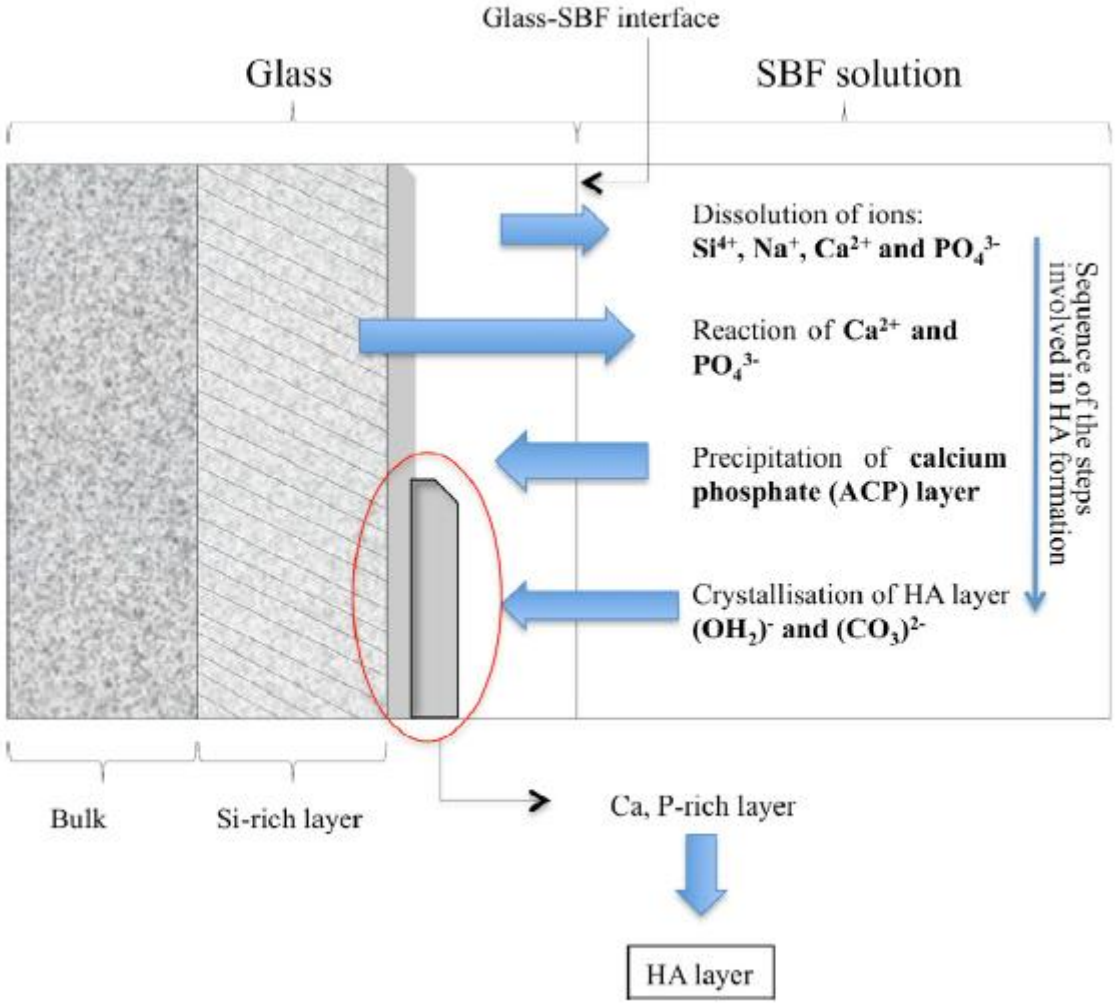

Figure 1.19: Sequence of stages taking place on the bioactive glass surface when it is put in contact with physiological fluids [78].

Turning to another bioactive glass class, professor Tadashi Kokubo developed the most widely used bioactive glass for bone replacement. It is called Cerabone® (**figure 1.20**) and it is based on a ceramic belonging to A/W glass, where A/W means apatite/wollastonite (crystalline phase). In this case, modifiers are not monovalent but only bivalent.

$$33\%\, SiO_2 - \ 44.7\%\, CaO - 4.6\%\, MgO - \ 16.2\%\, P_2O_2 - \ 0.5\%\, CaF_2$$

Figure 1.20: Chemical composition (wt%) of Cerabone® [1].

Proportions have been chosen in order to to achieve crystallization of the fluoroapatite and wollastonite, in this way the result is an amorphous phase reinforced by needle-like

wollastonite crystals [90]. The properties of A/W include good mechanical strength and fracture toughness (**table 1.7**), but the surface nucleation and rapid growth of large wollastonite crystals caused internal cracks [91]. Here again, the bioactivity of this glass is attributed to apatite formation on its surface in the body, but since wollastonite is stable in amorphous phase, the release of ions from glass suface is slow, this is also due to the presence of bivalent ions who are deeply tied to silica network [91]. The bioactivity is explained in the next steps:

• Due to the different composition, polycondensation happens less frequently in Cerabone®, nonetheless hydrogen ions exchange with oxygen ions creating a silanol layer negatively charged ensuring the growth of hydroxycarbonato apatite.

• Partially charged state due to silanol attracts ions from solution. The pH value increases because of dissolution of Ca ions leading to apatite precipitation.

• Ca ions begin to attach by electrostatic attraction to the negatively charged surface, but in this case gel of silica is not formed [92].

• A layer of bone-like apatite is formed on the surface [92].

Table 1.7 Cerabone® properties [93].

CERABONE®
Empirical formula $[Ca_{10}(PO_4)_6(OH)_2]$
Pentacalcium-hydroxide-[tris]-phosphate
Bovine origin
pH: 8.2
CaO content: 0.005 (w/w)%
Calcium/Phosphate ratio: 1.67
Average pore diameter: 800 μm

George H. Beall began to develop a new more complex type of glass-ceramic biomaterial in Germany (**figure 1.21**).

$$SiO_2 - Al_2O_3 - CaO - MgO - Na_2O - K_2O - P_2O_5 - F$$

Figure 1.21: Chemical composition of George H. Beall system [1].

This system is based on tetrasilic mica and trisilic mica phases (**figure 1.22**).

$$(Na, K)Mg_3((AlSi_3O_{10})F_2$$

Figure: 1.22: Chemical composition of trisilic mica phase [1].

The purpose of a mica phase is to include machinability to the apatite-mica [94]. This material typically has a low hardness, which generally is correlated with machinability and it is able to redirect the propagating crack preventing catastrophic fracture. Glasses belonging to this system are called Bioverit® and they differ significantly in oxide proportions. Bioverit I is composed of small apatite crystals and large mica crystals (**figure 1.23**) [94]. The mica crystals are $Mg_3(AlSi_3O_{10}F_2)K/Na$ or tetrasilic mica $Mg_3(Si_4O_{10}F_2)K/Na$ [94]. Instead, Bioverit® II is constituted by apatite crystals and curved fluorphlogopite mica crystals [95]. Bioverit® I and II have the advantage to be shaped by the surgeon prior to implantation thanks to their machinability (**table 1.8**) [95].

$$30.5\%\ SiO_2 - 15.9\%\ Al_2O_3 - 14.8\%\ MgO - 14.4\%\ CaO - 11.4\%\ P_2O_5 - 2.3\%\ Na_2O - 5.8\%\ K_2O - 4.9\%\ F$$

Figure 1.23: Chemical composition (wt%) of Bioverit® I [94].

Bioverit® III consists of a silica-free network with mono- and diphosphate units [1]. This glass-ceramic is called invert-glass because phosphate replaces the silica. Bioverit® III contains apatite, $AlPO_4$ crystals of the berlinite and other phosphates. Its mechanical properties are low, but the release of calcium ions act as osteoconductive.

Table 1.8 Mechanical properties of Bioverit® I and II [95].

Properties	Bioverit® I	Bioverit® II
Density (g/cm^3)	2.8	2.5
Bending strength (MPa)	140–180	90–140
Compressive strength (MPa)	500	450
Young's modulus (GPa)	70–88	70
Hardness Vickers (GPa)	5	~8
Fracture toughness (MPa·m$^{1/2}$)	1.2–2.1	1.2–1.8

The first bioactive glass for clinical application was developed by H. Bromer. These other types of glass are called Ceravital®.

$$42.2\%\ SiO_2 - 27.5\%\ CaO - 2.9\%\ MgO - 4.8\%\ Na_2O - 0.4\%\ K_2O - 18.2\%\ P_2O_5$$

Figure 1.24: Chemical composition (wt%) of Ceravital® [1].

The composition of Ceravital® (**figure 1.24**) is similar to bioglass in SiO_2 content but differ in CaO, MgO and Na_2O; in fact, reaction kinetics is not fast as Bioglass, but it is stable with a very low thermal coefficient of expansion [96]. In addition, Ceravital has controlled gain size and improved resistance to surface damage and this means more tensile strength [96].

In 1993, FDA released the PerioGlas® (**figure 1.25**), a bioactive glass composed by minerals andoral/periodontal bone grafting material that body needs to grow new healthy bones, and it will dissolve as new bone growth occurs [97].

$$46.1\%\ SiO_2 - 24.4\%\ Na_2O - 26.9\%\ CaO - 2.6\%\ P_2O_5$$

Figure 1.25: Chemical composition (wt%) of PerioGlass® [97].

It is used in the form of irregular particles measuring 90 to 170 micrometers [97]. The surface of the materials is covered with hydroxy-carbonate apatite when it comes in contact with biological fluids. This layer incorporates organic ground proteins such as chondroitin sulfate and glycosaminoglycans and attracts osteoblast that rapidly form bone [98].

In 1999, NovaBone® was developed and it consisted of a calcium phospho-silicated composition equal to 45S5 Bioglass® in the form of particulate (with different sizes). It is used in orthopedic applications in non-loading-bearing sites [99]. The synthetic binder is a blend of polyethylene glycols (PEGs) and glycerol that acts as a temporary binding agent for the bioactive glass [98]. Novabone® is highly malleable, easy to mold and pack into any defect, moreover stays at the surgical site and does not migrate during irrigation, as mentioned in this paper [99].

As regards bioactivity mechanism, NovaBone® starts a series of chemical reaction on its surface immediately upon introduction to the body. This biomaterial releases ions and stimulate osteoblasts activity modifying the surface of material, which attracts and binds all the necessary components for bone regeneration [98]. The ion release continues to go forward over time and this release is particularly critical in the initial weeks of healing. As the ion release progresses, the NovaBone® material is transformed into an increasingly porous scaffold with a resulting increase of surface area [99].

A new bioactive glass was introduced in the year 1990s knows as BonAlive® and has started to be marketed from 2006 in the form of powders [100]. This bioactive glass was developed in Finland by ensuring a high rate of bioactivity and a completely matched with human body bones.

$$53\%\ SiO_2 - 23\%\ Na_2O - 20\%\ CaO - 4\%\ P_2O_5$$

Figure 1.26: Chemical composition (wt%) of BonAlive® [100].

When BonAlive® comes in contact with body fluids, it releases out ions leading to the development of a silica gel layer on the surface of the glass [100]. A reaction between the silica gel layer and biological fluids occurs through exchange of the Ca and P that has been released from the granules [100]. As a result of precipitation, some crystals grow on the surface with a similar mineral component of bone. This new layer will promote bone bonding and osteointegration.

Based on what has been said, silica-based glasses can be divided into several classes according to their bioactivity mechanism [1]. When silica-based glass is placed in wet environment, it is necessary to control their solubility because glasses show a huge range of solubility form inert to soluble [1].

Type 1: Inert glasses are, de facto, rich in silica, therefore, they don't make ion exchanges possible.

Type 2: glasses having a silica content less than 60% by weight. Reactive layers formed on the surface can create a silica gel, but this protect surface from further attachments making glass less biocompatible.

Type 3: there are two options: the first one consists in silica glasses containing multivalent cations. Multiple layers of ion from the salts have been built on the surface and they do not satisfy the necessary requirements of apatite formation. In the second one, silica gel on the surface is rich in Ca^{++} and PO^{3-}_4 and apatite can precipitate;

Type 4: Fast ion exchange with H^+ from solution forms a thick layer, which is easily detachable.

Type 5: If the pH is over 9, breaking Si-O-Si bond and $Si(OH)_4$ to solution can be observed.

Table 1.9 Different type of bioactive glass [101].

Sl. No.	Name of the bioactive glass	Composition (%)												
		SiO_2	P_2O_5	CaO	$Ca(PO_3)_2$	CaF_2	MgO	MgF_2	Na_2O	K_2O	Al_2O_3	B_2O_3	Ta_2O_5/TiO_2	ZnO
1.	45S5 Bioglass®	45	6	24.5	–	–	–	–	24.5	–	–	–	–	–
2.	45S5.4F Bioglass®	45	6	14.7	–	9.8	–	–	24.5	–	–	–	–	–
3.	45B15S5 Bioglass®	30	6	24.5	–	–	–	–	24.5	–	–	15	–	–
4.	52S4.6 Bioglass®	52	6	21	–	–	–	–	21	–	–	–	–	–
5.	55S4.3 Bioglass®	55	6	19.5	–	–	–	–	19.5	–	–	–	–	–
6.	KGC Ceravital®	46.2	–	20.2	25.5	–	2.9	–	4.8	0.4	–	–	–	–
7.	KGS Ceravital®	46	–	33	16	–	–	–	5	–	–	–	–	–
8.	KGy213 Ceravital®	38	–	31	13.5	–	–	–	4	–	7	–	6.5	–
9.	A/W glass-ceramics	34.2	16.3	44.9	–	0.5	4.6	–	–	–	–	–	–	–
10.	MB glass-ceramics	19-52	4-24	9-3	–	–	5-15	–	3-5	3-5	12-33	–	–	–
11.	S45P7	45	7	22	–	–	–	–	24	–	–	2	–	–
12.	S53P4	53	4	20	–	–	–	–	23	–	–	–	–	–
13.	13-93	53	4	20	–	–	5	–	6	12	–	–	–	–
14.	4-Mar	50.5	1	22.5	–	–	6	–	5	15	–	–	–	–
15.	18-04	54.5	4	20	–	–	4.5	–	15	–	–	2	–	–
16.	23-04	56.25	1	20	–	–	4.5	–	5	11.25	–	2	–	–
17.	H2-02	53	2	22	–	–	4.5	–	6	11	0.5	1	–	–
18.	CEL-2	45	3	26	–	–	7	–	15	4	–	–	–	–
19.	55S	55	4	41	–	–	–	–	–	–	–	–	–	–
20.	H	46.2	2.6	26.9	–	–	–	–	24.3	–	–	–	–	–
21.	HZ5	44.4	2.5	25.9	–	–	–	–	23.4	–	–	–	–	3.8
22.	HZ10	42.5	2.4	4.8	–	–	–	–	22.5	–	–	–	–	7.8
23.	HZ20	38.8	2.2	22.6	–	–	–	–	20.5	–	–	–	–	15.9

Today a great variety of bioactive glasses is known (**table 1.9**); they differ in composition and molecular structure providing a wide range of properties, consequently bioactive glasses have a wide range of applications. Nowadays, bioactive glasses are used for coating of metal prostheses, in reconstruction of dental defects, for filling space vacated by bone screws, donor bone, diseased bone loss, for correcting periodontal defects and in replacing subperiosteal teeth, etc. [102] Results and perspectives of bioactive glasses look scientifically and clinically rosy and very attractive in these uncertain times. Many of bioactive glasses based on composite and synthetic materials, composite resins, amalgam, for istance, are already at an advanced stage of completion, Inaddition, bioactive glasses can be successfully used as delivery systems for proteins, grow factors or other biomolecules affecting bone growth. Actually, the global market of bioactive glasses continues to be dominated by calcium phosphate glasses probably due to the fact that they satisfy requirements in hard and soft-tissue application and owing to the increasing demand for healing replacement.

1.10.3 Global Bioactive Glass Market

As explained above, bioactive glasses have a wide number of applications in medicine, especially in tissue and bone replacement. For example, bioactive glass powders might be

used as coatings for various ceramic and polymer substrates, with the aim of preventing ionic accumulation or corrosion of the surface. A combination of bioactive glass and bone harvested outside the patient's body has proved as durable as the patient's own bone [96]. Furthermore, bioactive glasses have also been using in the manufacture of non-biological applications such as medical instruments for surgery and endoscopy. The intake of antibacterial agents orally or intravenously causes a poor vascular perfusion, resulting in orthopedic infection.

For these reasons, the global bioactive glass market was valued at 284.55 $ million in 2014 and is expected to grow at a CAGR (Compound Annual Growth Rate) of roughly 7.6% over the next five years and to increase from 130 million US$ in 2017 to 200 million US$ in 2023, [103] [104]. The analysis shows some market drivers that are contributing to the growth of the global bioactive glass market:

- New clinical application: bioactive glass is actually used in bone graft substitute in various clinical applications, therefore an increasing number of researches are developing many different systems of bioactive glass in order to guarantee a better composition, bone forming properties, antibacterial properties, and degradability [104].

- Increasing number of aging population: elderly people require more and more implant treatments because of their physiological health problems related to the ageing process (many people start losing their teeth as they get older). Improving surgeries, where bioactive glass is used, will likely enable them to lead more comfortable lives [104].

- Increasing demand from emerging countries: nowadays, lots of new jobs in manufacturing and industrialized industries are emerging in some countries. In these countries, people are moving from rural to urban areas for education, employment, higher salaries, better life styles and healthcare system [105].

The bioactive glass market is dominated by companies like Biomet 3i, Stryker, Bonalive Biomaterials, Novabone, Schott, Mo-Sci Corporation, Synergy Biomedical, Dingsheng Biology and others [103]. In terms of regions, North America is the largest global market of bioactive glass, followed by Europe. Pacific Asia is estimated to grow at the highest rate, due to the improvement of the medical level and the enhancement of medical consciousness in the area [103]. Bioactive glass market may be categorized according to synthesis process (melt-quenching, sol-gel, etc), to product (powders, scaffold, etc) or to applications (orthopedic, dentistry, etc.) [105].

1.10.4 Ion Doping

Doping refers to the addition of specific and controlled amounts of impurity into materials. The practical use of impurity doping mainly changes the properties of the materials. For years, research has been conducted to investigate the effect of metal ions on material biocompatibility. Their study has focused on the role of metal ions involved in biological systems as well as the role of externally introduced metal ions. In the body, where metallic elements are required in very small quantities, they are usually present in monoatomic form and thus do not show any properties. As single-atom elements, they perform duties much

like any other element the human body needs. Because of their specific properties and interactions with other elements, the human body uses them in the construction of proteins with specific forms and functions depending on the nature of the metal ions and the type of enzyme activity [108]. An iron atom, for example, gives the ability to proteins to bind or unbind oxygen atoms. In addition, some metal ions could aid in increasing the enzyme activity acting as an allosteric effector. In other case, they could also affect the conformational shape of the enzyme and thus reduce the rate of enzyme activity. Metal ions are required for many critical functions in the human body which are involved in the transfer of genetic information from DNA, leading to the synthesis of specific proteins [108]. Lastly, lack of some metal ions can lead to diseases or growth retardation. Bioactive glasses can also embed metallic ions in different ways. Depending on the element, ion doping a bioactive glass can result in the enhancement of bioactivity or antibacterial effect (**figure 1.27**) or in the promotion of angiogenesis and osteogenesis. In particular, they have highly selective toxicity to the pathogenic microorganism in host body with less or no toxicity to the host as reported in this article [74]. Some metallic ions are antimicrobial because they interfere with proteins of the outer membrane of microbial cells, thus destroying the cells or inhibiting their growth.

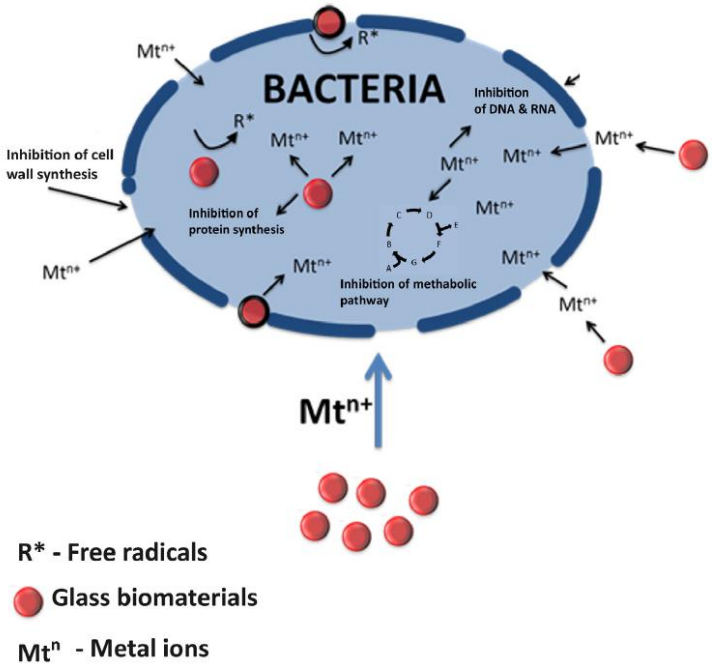

Figure 1.27: Mechanism associated with the antibacterial activity of metal ions [78].

- Calcium

A healthy human adult has about 1,05 kg Ca of which 99% exists as phosphates as inorganic part of the endoskeletons [109]. The small remainder is in cellular fluids, existing in partly ionized or protein bound form with functions such as signaling, muscle contraction and enzyme regulation. Ca^{+2} acts as a messenger by activating, regulating secretion of hormones and reinforcing signals necessary for transmission of nerve impulse. It can take over the role of a co-factor in hydrolases and exert structure function in proteins [110]. Calcium ions

could be used as therapeutic ions to regulate cell proliferation, migration and death. Bioactive glasses contained calcium and phosphate, that form calcium phosphate precipitates (HA), as previously described.

- Magnesium

Magnesium is vital to both plant and animal life. Half of it is present in the skeleton, about a 40% is in muscles and soft tissues and the remaining in enzymes. All enzymatic reactions in living systems such as oxidative phosphorylation, DNA transcription, RNA function, protein synthesis and critical cell membrane functions are dependent upon optimal Mg concentration as these are catalyzed by ATP, which require Mg as a cofactor [111]. Deficiency leads to muscle cramps. Magnesium alloys can match the needs of specific implants in a range of applications. Besides, when magnesium implant degrades and is reabsorbed, it enables the growth of new bone. The bioresorbability prevents the need for secondary surgical procedures. Magnesium has both the strength and mechanical benefits, so it can be used in high-load-bearing areas [111]. Magnesium is also widely accepted as a therapeutic agent to treat constipation, dyspepsia, eclampsia, headache, preeclampsia and rapid atrial fibrillation [111]. However, a higher dosage could be used only for these specific medical problems. Magnesium is often included in the composition of bioactive glass to produce different effect and to make different products. Among these effects, magnesium helps with the production of new bone tissue or with attachment of osteoblasts. Therefore, this ion can be included into bioactive glass in various mass fraction using sol-gel method [110].

- Iron

Iron is the most abundant transition metal in biology and it is used by plants, animals and bacteria as well. The average human adults have about 4-5 g of Fe. About 60-70% Of this amount is present in hemoglobin in red blood cells, the rest is in muscle myoglobin, Fe storage cellular protein, ferritin; 0,2% occurs as a component of critical respiratory enzymes and bound to the serum transport protein transferrin [112]. Iron deficiency causes anemia because red cells of blood containing less hemoglobin than in normal condition. Iron poisoning leads to vomiting, pallor, shock and circulatory collapse. Many diseases such as cancer, kidney or hearth problems can cause anemia, therefore, taking iron along with other medications can prevent or treat anemia in people with kidney or hearth problems or being treated for cancer with chemotherapy [112]. Besides, the incorporation of iron into bioactive glass allows treatment with magnetic fields with the functions of local hyperthermia [113]. From the purely physical point of view, the heating ability of the particles, due to its superparamagnetic property, can be quickly increased using an electromagnet by alternating the. Anyway, big magnetic particles are usually not colloidal stable and are not able to cross biological barriers. But for a given material, the smaller the particle, the lower the heating ability. The aim is to find a compromise between the optimal physical and biological properties of the particles [113]. A typical application is on the cancerous cells which are destroyed while the normal cells can survive at specific temperature points. This happens because tumors don't tend to have blood supplies as good as normal tissue, so heating the area can cause cell death because the blood cannot cool the tumor fast enough [113]. Heat in normal tissue can more easily dissipate. Hyperthermia will target the tumor to minimize heating of any normal tissue.

- Copper

Cu has vital role in metalloenzymes involving several critical biochemical pathways, such as superoxide dismutase, which metabolize the potentially damaging superoxide anion. Dopamine β-hydroxylase, amine oxidase and tyrosinase are all Cu containing enzymes that interconvert the major neurotransmitters dopamine, noradrenaline and adrenaline in brain [114]. CytochromecC oxidase is the key and terminal enzyme of the respiratory chain, accounting for more than 90% of the energy of muscular contraction. Cu often participate together with Fe in proteins or has equivalent redox roles in same biological reactions like reversible binding, O_2 activation or dismutation, electron transfer [114]. Copper has been used by humans for thousands of years as a treatment of chest wounds and the purifying of drinking water []. Nowadays, it has been proven that copper helps prevent inflammation in arthritis and similar diseases [114]. Research is also going on into anti-ulcer and anti-inflammatory drugs containing copper, and its use in radiology for treating convulsions and epilepsy as this article says [115]. Copper can be incorporated into bioactive glass acting for the prevention of infectious diseases or helping treatment of bone defects. Copper has an affinity to bind to intracellular thiols such as glutathione, creating sulfides which can be harmful to internal bacteria processes. One of the most likely mechanisms is the inactivation of enzymes inside bacteria due to affinity for amino-, carboxyl-, phosphate-, and imidazole-groups [116]. That is obviously not good for the bacteria and can quickly kill it. Copper also generates free radicals of reactive oxygen, like H_2O_2 which induces vascular endothelial growth factor (vegf) expression in human keratinocytes [116]. Vegf is is a homodimeric glycoprotein which induces migration and proliferation of endothelial cells and enhances vascular permeability. Therefore, copper can be involved as an angiogensis factor. Copper nanoparticles can be included inside a composition of a bioactive glass or in scaffolds [110].

- Zinc

Zinc is the second most abundant mineral in the body, being present in all tissues [117]. Inside the body, zinc possesses three main roles: catalytic, structural and regulatory. All of these roles involve cellular activity, from working as a cofactor, to an antioxidant with other vitamins, reducing inflammation, and boosting the immune system. The Zinc ions are transcription factors necessary for the protein to adopt the proper shape which allows it to interact with DNA as this report suggests [118]. It is not known if zinc ions play more than a structural role in these proteins or whether the Zn^{+2} concentrations are also used to regulate gene expression [117]. On the other hand, zinc can interfere with other vitamins and nutrients, it must be carefully used. For example, too much zinc causes calcium excretion and vice versa, and the same phenomenon has been exhibited with supplemental iron. Zinc plays also a role in diarrhea, male fertility because it has a big impact on hormonal balance and Alzheimer disease [119]. In addition, Zinc acts like an antioxidant within the body, fighting free-radical damage and slow the aging process [119]. Bioactive glasses incorporating Zn have a drastic reduction in the leaching activity of glass reducing solubility and bioactivity but accelerates bones growth and protects bones health [110]. Zinc can be added to an organoapatite coating of titanium fibres, on bioactive glass scaffold or in order to realize disk made by sol-gel [110].

- Cobalt

Cobalt has a vital role in a number of biochemical metal-enzyme reactions [120]. Cobalt is a hard ferromagnetic, silver-white, brittle element. Cobalt is readily available in our diets already, and an essential element to our survival in fact. It is an essential mineral for red

blood cells and other body cells functioning even if our body only needs a small amount. However, cobalt plays a role in the creation of vitamin B12 [120]. Vitamin B12, also called cobalamin, is a water-soluble vitamin that contains the biochemically rare element cobalt positioned in the center of the molecule [120]. Cobalt is involved in various enzymatic reaction of iron metabolism and it is very important for the growth and development of body weight. Some activities of endocrine glands are stimulated by cobalt as well as production of red bloods cells, speeding-up the growth and survival processes [121]. Due to its low absorption rate and high excretion rate, cobalt toxicity is not common, but excess can lead to enlargement of the thyroid gland. Cobalt is important in treatments of radiotherapy in the form of the isotope Co^{60} which is a gamma and beta ray emitter [122]. Finally, it is also used in the prosthetic alloys sector, being utilized in hip, knee and dental replacements. Bioactive glass compositions can be modified introducing cobalt as therapeutic ions for cartilage repair applications and increase considerably densities and mechanical properties of the scaffold structure. Furthermore, cobalt releasing materials function as angiogenic agent [110].

- Silver

Silver has no known function in the body and it is not an essential mineral supplement. The use of silver in the past was relegated to sterilize water for domestic use [123]. The modern use of silver is almost exclusively as an antiseptic and anti-infective element [123]. High concentration or frequent dosing can cause the silver to become stuck in the skin, turning it grey-blue. Ag^{+} is a bioactive species because catalyzes the reaction of oxygen with thiols, -SH groups that frequently terminate organic molecules, into disulfides, -C-S-S-C-, releasing water [123]. The interaction of silver ions with thiol groups in enzymes and proteins plays an essential role in silver antimicrobial action. Many enzymes, which are specialized proteins that run most of the chemical reactions in living organism, have a sulfur molecule in them, called thiol group. The binding of silver to this sulfur blocks the action of some enzymes, which prevents normal chemical reaction from occurring and causing the microbial cells to die [123]. Silver ions also directly induce chromosomal instability and DNA strand breaks, which if extensive or very rapidly evolved may be catastrophic for bacteria [123]. In conclusion, silver is a very potent antibiotic/antimicrobial agent and it is widely used also in medical sector. Bioactive glasses containing silver and silver nanoparticles have been widely studied as bone substituted, scaffold, coatings and filler [110]. Silver ions can be introduced into bioactive glass through an ion-exchange process or incorporated on surface of scaffolds as a coating [110].

- Gallium

Gallium does not exist in any compounds in nature and it also has no appearance in any natural form. Gallium is used for treating high calcium levels in the blood caused by cancer in patients who do not respond to proper fluid intake or fluid injected into the vein [124]. In fact, gallium is a calcium resorption inhibitor [124]. It works by inhibiting the usual release of calcium form the bone into the blood. Gallium salts are used in medical imaging as gallium scan, which is a diagnostic test that looks for infection, inflammation and tumors [125]. The addition of Ga^{+3} in bioactive glasses would induce hemostatic and antibacterial effects. A typical application consists of making a bioactive glass gallium-doped with gallium using a conventional melt quenching technique [110].

- Manganese

Manganese is a part of many enzyme systems, including the enzymes involved in blood sugar control, energy metabolism, and thyroid hormone function [126]. Manganese is an essential enzyme cofactor for certain superoxide dismutases. The disproportionation of superoxide requires redox active cofactors such as Cu, Mn, Fe, or Ni, depending on the class [127]. It is useful for changing the oxidation state because it itself is easily reduced and oxidized [127]. A manganese deficiency inhibits the production of collagen in wound healing, joint pain, arthritis, skin rash that is why manganese is used for inflammation. Moreover, further studies suggest that it helps prevent or treat diabetes and its associated complication [128]. Bioactive glasses containing manganese can favor osteogenic differentiation and these glasses can be produced by the wet chemical method coupled with ion-exchange mechanism [110].

- Strontium

Strontium (Sr) is a member of the alkaline earth metals. Most strontium compounds are regarded as harmless to plants and animals, and have relatively few commercial uses [129]. Strontium may play a role in bone formation and also may inhibits bone breakdown. Strontium acts on receptors and regulatory proteins that calcium usually does to downregulate bone resorption by osteoclasts and increase bone deposition by osteoblasts. However, it has no biological function in humans, but it is easily absorbed and can replace calcium in bone [130]. It is harmless in small quantities. The average adult human has around 0.05% to 0.1% strontium substitution in their bones [130]. Furthermore, research shows that using strontium in toothpaste relieve pain in sensitive teeth. The incorporation of strontium in bioactive glasses has the capacity to increase regenerative properties of bone cells. Calcium phosphate bone implants doped with strontium show superior bone regrowth, for instance [110]. Bioactive glasses Sr-doped can be produced by sol-gel technique above all [110].

- Vanadium

The biological role that vanadium plays is still being investigated. Very little is known about its biological function. It is most commonly found in the +4 and +5 oxidation state acting as oxidizing agents [131]. In tissues, vanadium is bound with proteins and 10% is present in the ionic form. There is some evidence that vanadium may offer certain health benefits. It may improve the boby's metabolism of blood sugar [131]. So far, very few clinical trials have tested use of vanadium in the treatment of diabetes. But on the other hand, vanadium seems promising for cancer treatment, in fact it may promote apoptosis of cancer cells and suppress the growth of cancerous tumors [132]. Vanadium compounds may help promote osteogenisis for treatment or prevention of bone disorders. Bioactive glasses containing vanadium are promising candidates for bone tissue repairmen [110].

- Boron

Boron is a miner found in the environment and in certain foods and it has a wide range of uses form toys to medicine [133]. Humans are exposed to boron on a daily basis via water, air, fruit and vegetables. Boron seems to be essential for the growth and maintenance of bone because boron affects calcium metabolism and this is linked with osteoarthitis. Boron supplement may improve symptoms and replenish stores. It also seems to increase estrogen levels in order women and healthy man giving beneficially impacts on the body's use of estrogen, testosterone, and vitamin D [133]. Besides, boron is important to aid in the

adsorption of magnesium and calcium since it reduces urinary loss of them [133]. The addition of boron to composition of bioactive glasses helps for the treatment and regeneration of bone defects because of their osteostimulation potential [133]. But it also has demonstrated preventive and therapeutic effects in a number of cancers, such as prostate, cervical, and lung cancers [134]. In addition, boron raises levels of antioxidant enzymes, such as superoxide dismutase (SOD), catalase, and glutathione peroxidase protecting against pesticide-induced oxidative stress and heavy-metal toxicity [135].

- Silicon

After oxygen, silicon is the most abundant element present in the earth's crust. It is present in clay and sand and also exists as a major part of rocks like quartz and granite. Earlier in human history, silicon was not regarded as a physiologically important element due to its substantial presence in the animal and plant tissues [136]. The exact biological roles of silicon in bone health have been clearly demonstrated, although a number of possible mechanisms have been suggested, including the synthesis of collagen and its stabilization, and matrix mineralization [136]. In addition, silicon is useful for skin health, and in the health of blood vessels. In the end, it helps in brightening the eyes as well [137]. Silicon increases bone strength when obtained from foods, which could reduce the risk of osteoporosis. That's why bioactive glass is characterized by the presence of silica, it has very strong network of bonds.

- Tellurium

Tellurium is the 52th element on the periodic table. It is found in the form of elemental crystals. Its electronic configuration is [Kr] $4d^{10}5s^{2}5p^{2}$ [138]. The element is a poor conductor of heat and only a fair conductor of electricity. Tellurium is unaffected by water or hydrochloric acid, but dissolves in nitric acid [139]. It has an atomic mass of 127.6 g/mol^{-1} and a density of 6.24 $g\text{-}cm^{-3}$ [138]. Its boiling point is at 450°C and its melting point is at 1390 °C. The element crystallizes in the rhombohedral form [140]. It is silvery white and isomorphous, while the structure and dimensions of the crystals are very similar to selenium. It is brittle but not very hard. The tellurium atoms form spiral chains in the crystal with Te–Te distances of 3.74 Å [140]. As already mentioned in chapter 1.3, tellurium, in the form of oxides, is generally regarded as excellent glass formers because since tellurium has an electronegativity value of 2.1 [1]. Te was discovered by Franz Joseph Moller von Reichenstein in the 18th in a gold mine in Romania [138].

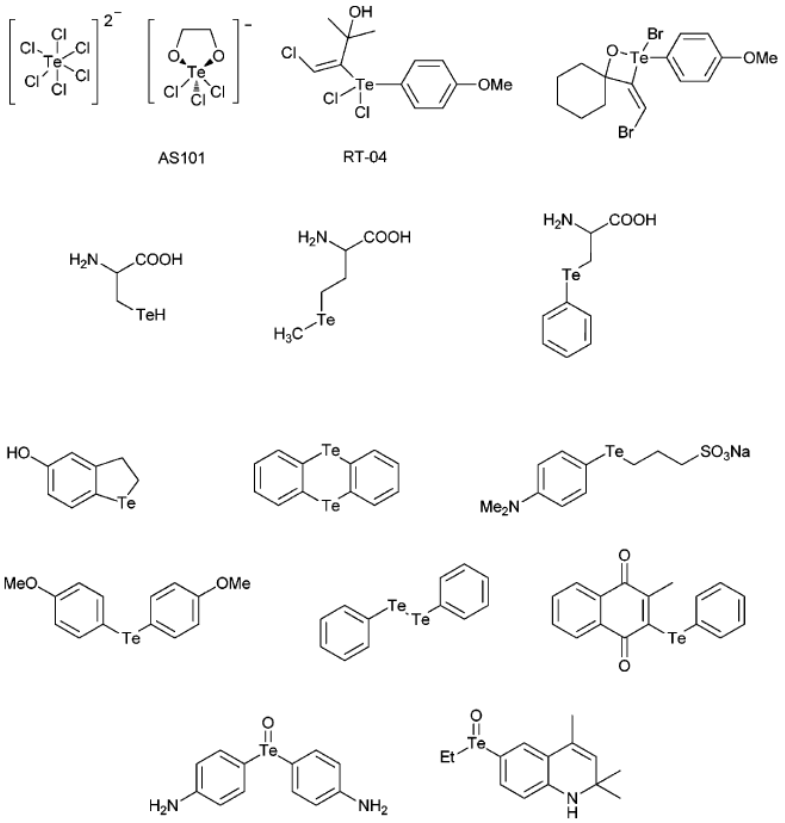

Figure 1.28: A selection of tellurium compounds which illustrates the chemical diversity of these agents [138].

Tellurium belongs to metalloids, a group of elements on the periodic table that have chemical characteristics partially from metallic elements and partially from non-metallic elements. Practically, they are known to be semi-conductors of energy in from of heat and electricity. Tellurium is additive for semiconductor part, black melting, alloy, glass, rubber [141]. Except those uses, it could be used as polishing in electroplating solution, heavy oil cracking catalyst, pigment for ceramic and glass. When added in iron, it strength ductility. When added in lead, it could strength hardness and corrosion stability [142]. It is also used as a coloring agent in ceramics. Tellurium is an important component of infrared detectors used by the military in a variety of fields including medicine, science, and security. CdTe films are one of the highest efficiency photovoltaics, metals that convert sunlight directly into electrical power, therefore, widely used in solar panels [143]. As mentioned before, tellurium can be used also in medicine, even if it is yet poorly investigated. Since tellurium is closely allied with selenium in chemical and physical properties, tellurium organo-compounds (**figure 1.28**) should behave similarly to selenium organo-compounds, which are widely studied in the literature [138]. Selenium is essential for humans in form of selenocysteine, which forms the catalytic center in a number of enzymes. Some of those are thought to have anti-cancerous properties [138].

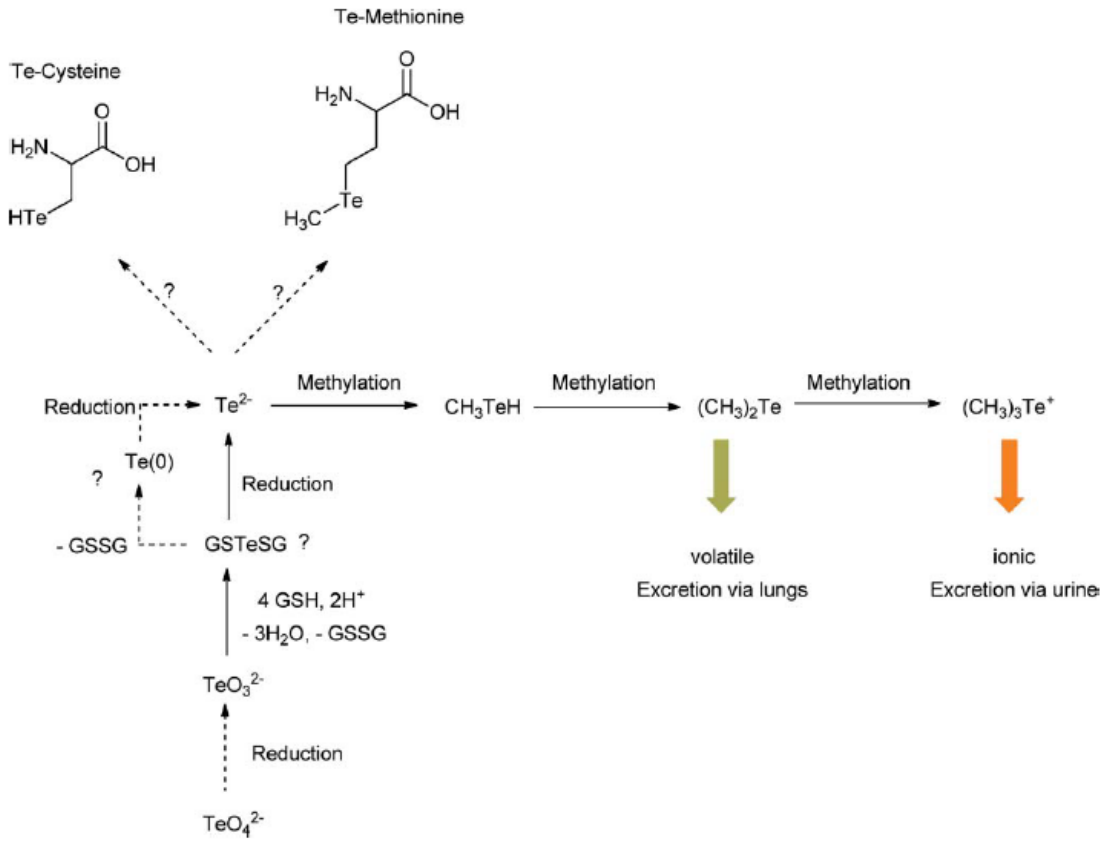

Figure 1.29: Aspects of human tellurium metabolism. The scheme is still speculative at this time. [138].

In contrast to oxygen, sulfur, and selenium, tellurium has no essential physiological role in cell biology. However, due to its chemical versatility, Te has been extensively used in chemistry. Research conducted during the last decade has indicated that certain organoselenium and organotellurium compounds (**figure 1.29**) exert a rather diverse biological activity based on redox modulation of pre-existing intracellular redox states [138]. Such compounds may act as pro or antioxidants or both, depending on their precise redox properties and the cellular environment they are placed in. Certain selenium and tellurium compounds are potent redox modulators and hence to interfere with various cellular signalling events [138]. As these interferences may result in cell cycle arrest and the induction of apoptosis in cells particularly rich in ROS (**figure 1.30**). These seem promise as effective and selective cytotoxic agents against a range of important therapeutic targets, including cancer cells under oxidative stress and bacteria [144] [141]. The antibacterial effect of the organo-tellurium compounds enables to inhibit biofilm formation and to penetrate the bacterial cell, causing damage and ultrastructural changes [145]. All tellurium compounds can be highly toxic as they cause, at high concentration, a morphologically observable demyelination of Schwann cell. Tellurium compounds are teratogenic since ingestion in even small amounts causes charmingly potent garlic breath and appalling body odor [138]. In humans and other animals, tellurium has no known biological role, but the body can metabolize it to create a volatile gaseous compound,

dimethyl telluride, which may produce a garlic breath. However, tellurium dioxide or tellurium ion exhibit inhibitory systems against many bacteria growth, gram positive and gram negative [141]. But tellurium is not limited only to its antibacterial effect, it has demonstrated relevant antioxidant activity. Before proceeding, it is necessary to introduce thiols. An important role is played by intracellular thiols since they are related to kinetics transport of metals into the cell. If thiols are depleted, bacteria are more vulnerable to ROS. Depletion of thiols has been noted that Tellurium affected E. coli for once exposure has occurred [145]. An example of this would be tellurium inhibition of E. coli because metalloid oxyanion Te causes indirect oxidation of Fe-S clusters, a family of bacteria enzymes [146]. As regards bioactive glass, application in literature are limited, almost entirely absent. Among them, tellurite glass melt-derived were used in order to study tellurium bioactivity and tellurium as a network former [147]. In this overview, tellurium was exploited for its antimicrobial and antioxidant properties creating calcite silicate nanocomposites with tellurium nanorods and tellurium dioxide nanoparticles [148] [149].

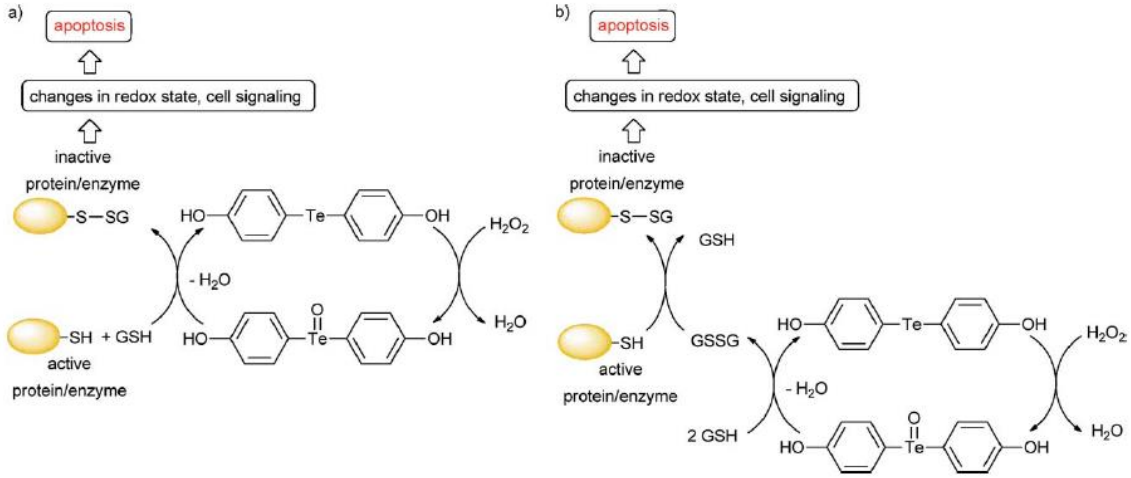

Figure 1.30: Tellurium-based agents are able to sense the presence of ROS and subsequntly oxidize key cysteine-containing proteins and enzymes [138].

2. Material and methods

In this thesis, a tellurium-containing bioactive glass has been prepared from a starting composition without tellurium (Te), by replacing silica with a different molar fraction of Te. This chapter contains information on the preparation of samples and on methodologies used for their characterization. In addition, every performed technique will be described in detail. The composition without tellurium has been called STe0, while compositions containing Te up to 1 mol% and 5 mol% have been named STe1 and STe5 respectively.

2.1 Preparation of Bioactive Glass systems STe0, STe1 and STe5

The produced bioactive glasses belong to the specific bioactive system called 45S5 Bioglass® (**table 2.1**), already seen in chapter 1, which contains oxides in specific mass fraction proportions shown in the **table 2.3.**

Table 2.1 45S5 Bioglass® oxides mass fraction proportions.

Oxide	**wt%**
SiO_2	45.0
CaO	24.5
Na_2O	24.5
P_2O_5	6.0

It possible to noticed that the STe compositions slightly vary from the 45S5 Bioglass®

Table 2.2 Molar fraction of STe0, STe1 and STe5.

	%mol		
	STe0	**STe1**	**STe5**
SiO_2	48,6	47,6	43,6
Na_2O	16,7	16,7	16,7
CaO	34,2	34,2	34,2
P_2O_5	0,5	0,5	0,5
TeO_2	0,0	1,0	5,0
sum	100,00	100,00	100,00

Table 2.3: Mass fraction of STe0, STe1 and STe5.

	wt%		
	STe0	**STe1**	**STe5**
SiO_2	49,08	47,28	40,63
Na_2O	17,45	17,16	16,10
CaO	32,20	31,67	29,71
P_2O_5	1,27	1,25	1,17
TeO_2	0,00	2,64	12,39
sum	100,00	100,00	100,00

The exact amount of required reactants in order to get 100 grams of glass was determined using the following procedure starting from amount of needed oxides:

$$Na_2CaO_3 \rightarrow Na_2O + CaO_2$$

$$CaCO_3 \rightarrow CaO + CO_2$$

$$Ca_3(PO_4)_2 \rightarrow 3CaO + P_2O_5$$

$$m_{Na_2O} = n_{Na_2O} M_{Na_2O}$$

$$m_{CaO} = n_{CaO} M_{CaO}$$

$$m_{P_2O_5} = n_{P_2O_5} M_{P_2O_5}$$

$$m_{Na_2O} = n_{Na_2CaO_3} M_{Na_2O}$$

$$m_{CaO} = n_{CaCO_3} M_{CaO} + 3 \cdot n_{Ca_2(PO_4)_2} M_{CaO}$$

$$m_{P_2O_5} = n_{Ca_2(PO_4)_2} M_{P_2O_5}$$

$$n_{Ca_2(PO_4)_2} = \frac{m_{Ca_2(PO_4)_2}}{M_{Ca_2(PO_4)_2}}$$

$$n_{CaCO_3} = \frac{m_{CaCO_3}}{M_{CaCO_3}}$$

$$n_{Na_2CaO_3} = \frac{m_{Na_2CaO_3}}{M_{Na_2CaO_3}}$$

$$n_{SiO_2} = \frac{m_{SiO_2}}{M_{SiO_2}}$$

$$n_{TeO_2} = \frac{m_{TeO_2}}{M_{TeO_2}}$$

Formulas of for silica and tellurium oxide were not included as they are already inserted as reactants.

$$mol\%_{SiO_2} = \frac{n_{SiO_2}}{n_{tot}}$$

$$wt\%_{tot} = \frac{m_{SiO_2}}{m_{tot}}$$

The same procedure was applied for the purpose of calculating molar (**table 2.2**) and mass fraction (**table 2.3**) of oxides.

m: mass of oxide

mol%: mole percentage

wt%: mass percentage

M: molar mass

n: number of moles

The following table (**table 2.4**) gives masses of reactants to be weighted to obtain 100 grams of glass. they were calculated according to the equation above.

Table 2.4: Mass of each compounds in ST0, STe1 and STe5.

Amount of oxides present (grams) in each composition			
	STe0	**STe1**	**STe5**
SiO_2	49,08	47,28	40,63
Na_2CO_3	29,83	29,34	27,52
$CaCO_3$	54,82	53,91	50,57
$Ca_3(PO_4)_2$	2,77	2,73	2,56
TeO_2	0,00	2,64	12,39

All the reactants were weighted using an analytical balance (ORMA BCA120S) with a weighing capacity of 12 0g and a readability of 0,1 mg. The reactants powders were carefully weighted prior to mixing step; then the powders mixtures were placed in a platinum crucible, as it is an inert material (that does not react with the powders and offers high temperature strength). The powder mixtures were melted inside platinum crucible for 1 hour at 1500 °C with heating rate at 12 °C per minute inside an electric chamber furnace. The bioactive glass was obtained in two different forms depending on its intended use: bulk and powders. In order to obtain the powders, the molten glass was immediately quenched into distilled water to obtain glass frit. Then, the frit was dried before proceeding with milling. The bioactive glass powders were prepared by milling the glass frit for 15 minutes in a zirconia grinding jar with 10 mm zirconia balls. Subsequently, the glass was sieved through stainless steel sieves to obtain powders with particle size finer than 25µm. As regard bulk, the melt was poured on a brass mold and placed in a prepared annealing furnace for 13 h at 550°C and then cooled down to room temperature. Annealing treatment was necessary to relieve stresses and allows the surface and interior to cool uniformly. The bulk samples were cut into thick (about 2 mm) slices using Brillant 220 ATA. Then each slice was polished to remove the roughness using Struers Loboforce-1 and uniform the surface for further test. The described procedure was followed for each composition.

2.2 Characterization of bioactive glass systems STe0, STe1 and STe5

Some tests were performed on the powders to evaluate the morphological, thermal and compositional properties of the glasses and their bioactivity. Other tests, in particular test to evaluate the biological effect of the glasses, were performed on the slices. The techniques used to these purposes are set out below: Differential Thermal Analysis (DTA), Field-Emission Scanning Electron Microscope and Electron Dispersive Spectroscopy (FESEM-EDS), X-Ray Diffraction (XRD), pH Evolution, In Vitro Bioactivity Test, Fourier Transform Infrared Spectroscope (FTIR), Inductively Coupled Plasma - Optical Emission Spectroscopy (ICP-OES), Raman Spectroscopy and Cell Culture Tests (Cytocompatibility Evaluation and Antimicrobial Activity).

2.2.1 Field-emission Scanning Electron Microscope and Electron Dispersive Spectroscopy

FESEM-EDS analyses were performed to investigate morphological and compositional properties before and after immersion if samples in SBF solution, especially they were employed to identify the nucleation and growth of hydroxyapatite.

FESEM is based on SEM principles but compared with conventional scanning electron microscopy (SEM), field emission SEM (FESEM) offers clearer images with a less distortion and a spatial resolution greatly improved. SEM is based on a beam of electrons generated by a suitable source, typically a tungsten filament. High temperature is generated by applying current to the tungsten filament and, as a result, electrons gain a sufficient energy to overcome potential barrier which anchoring them on material surface (**figure 2.1**) [150]. The electron beam is accelerated through a high voltage and goes through an electromagnetic lens system to obtain a thin beam of electrons. After that, the beam scans the surface of the sample. Objective lens (**figure 2.1**) provides the formation of either image or diffraction pattern of the sample. Electrons emitted from the sample by the action of the scanning beam are captured by suitable positioned detectors [151]. The energy of incident electrons ranges between 100 eV and 20 eV, hence it is possible use different detectors depending on the intensity of the incident electrons. Electrons interact with the atoms of samples and, as a result, signals containing properties about the surface sample is produced. When speaking of backscattered electrons (**figure 2.1**), electrons are ejected by an elastic collision of an incident electron with high-energy. These electrons conserve their energy at incidence but their direction of propagation has been modified upon interaction [152]. Backscattering electrons enable to obtain information not only on the morphology but also on the chemical composition of the sample. On the contrary, secondary electron are generated from an inelastic collision in which the transferred energy of the primary beam is transferred to an electron that is then emitted from the atom of sample. Secondary electrons (**figure 2.1**) typically have low-energy [152]. The bombarding electrons can penetrate in the electrons shells of the atoms composing the surface of the sample. The energy of these incident electrons can be converted to eject local electrons [152]. The main difference between the SEM and the FESEM is emitter type, which is thermionic emitter and field emitter respectively [152]. Basically, what happens in thermionic emission is that the tungsten filament is heated. When a metal is heated sufficiently, its free electrons gain enough kinetic energy to leave the metal. Thermionic sources have higher efficiency and high power density, but a thermal breaking is possible during operation and there is a possibility of vaporization of emitter surface [152]. Field Emission is also a way of bypassing this problem using electrons [152]. A Field Emission Gun does not require heating the filament. In this case, the increase of the beam density increases significantly the brightness of the images.

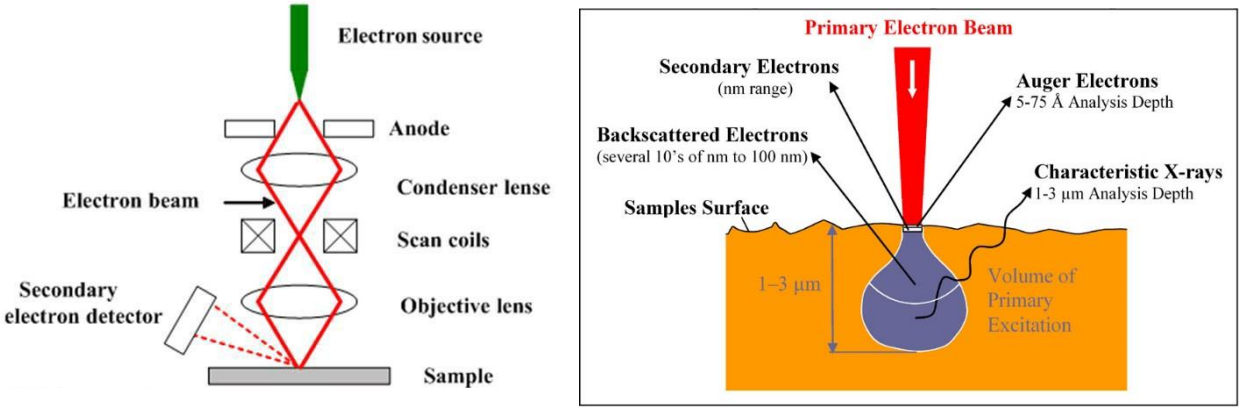

Figure 2.1: On the right, a schematic representation of the basic SEM components; on the left, the beam samples interaction [153] [154].

The filament usually is made of a single crystal tungsten sharpened to a tip of radius and placed in a huge electrical potential gradient between filament and nearby anode. Because of the electrical field, electrons can jump the energy barrier to the nearby anode. Electrons generated from Field Emission Gun comes into contact with surface of a sample generating secondary electrons with low energy [155]. Each image pixel corresponds to a point on the specimen surface, which is obtained as a function of the signal intensity of secondary electrons captured by the detector at each specific point [155].

Advantages of FESEM include:

- Smaller final electron spot giving high resolution

- Spot diameter also less compared to thermionic emission [155]

- The brightness will be very high compared to others thermionic source [155]

- Need for placing conducting coating on insulating materials is virtually eliminated [155]

One of the most common ways to determine the composition of a material is Electron Dispersive Spectroscopy (EDS). It is able to fit an EDS detector to an electron microscope and analyze what sample is looking at. EDS uses the photons generated by electrons hitting the surface to figure out what is in the sample [155]. When high energy electrons hit the sample, the electrons in the sample are excited and, as a result, they emit x-rays (**figure 2.1**) when relaxing. The energies of these x-rays depend on which elements are present, therefore results show what elements are there, the relative % and even map where elements are on the sample [155].The detector displays the signal as a spectrum of intensity as a function X-ray energy. Standard SEM procedures for non-conductive samples involve coating with a metal (chromium, gold, platinum, etc.) to avoid charging effects but this makes the process destructive [152].

FESEM micrographs were obtained using the secondary electrons detector in an SUPTRA^{TM} 40 Zeiss. Before observation samples were coated with a thin Cr film to guarantee the conduction.

2.2.2 In Vitro Bioactivity Test

Bioactivity is one of the most important properties of a bioactive glass. It should chemically react to form a strong bond with bones or soft tissues through the formation of a stable calcium phosphate layer on its surface. Bioactivity was investigated using in vitro assays using both SBF and TRIS. SBF were prepared according to the protocol of Kokubo [156]. Therefore, the powders were soaked in simulated body fluid and the protocol for preparing SBF is described below:

- Pour 700 ml of deionized water into a cleaned beaker

- Heat the water to 36,5±1,5°C.

- Added one at a time the reactants until 8 in water respecting the order. Mixing with a magnetic stir.

- if the solution has a volume less than 900 ml, add water to reach 900 ml.

- Calibrate the pH meter with fresh standard buffer solution and place the electrode of pH meter in the solution.

• Dissolve gradually the TRIS, checking the temperature of the solution in the beaker and measuring its pH while the temperature is at 36.5±1,5°C. pH should not increase above 7,45±0,01. Reached that point, do not add more TRIS.

• Titrate 1M-HCl solution with pipette to adjust the pH at 7,42±0,01. pH must not fall below 7,40±0,01.

• When the pH-value is 7,42±0,01, re-dissolve gradually the remaining TRIS, until a pH of 7,45±0,01.

• Repeat steps 6-7-8, until TRIS is exhausted.

• Add 1M-HCl solution with pipette to adjust the pH at 7,40±0,01.

• Transfer the solution from the beaker to a glass volumetric flask of 1000 mL.

• Keep the flask at room temperature until its temperature should be approximately 20 ºC.

• After cooling, add ultra-pure water again, the solution to the total volume of the solution to 1000 mL.

Moreover, the same experiment was carried out immersing the powders in a TRIS solution. Bioactive glass powders (150 mg in 100 ml of SBF or TRIS) were immersed in a container containing the soaking fluid, SBF or TRIS, which was continuously stirred at 100 rpm and thermostated at 37°C using an Orbital Shaker IKA KS4000i control. At the beginning of the test, the pH of SBF was 7.4. The pH was measured after 1 day and every 48 hours for 3, 7 and 14 days. At the schedule time, the glass powders were washed in bi-distillated water, filtered using filter paper and dried inside a dessicator. 2 ml of the solution were removed with a syringe from each container for leaching analysis and all the samples were placed in dessicator.

2.2.3 Differential Thermal Analysis

Differential Thermal Analysis is a technique used to measure the difference in temperature between a substance under investigation and an inert reference, the temperature as a function of time [157]. Both materials are monitored in during heating or cooling at controlled rate. Differential thermal analysis (DTA) is suited for the determination of characteristic temperatures of a material in every atmosphere of interest. Modern instrumentation (**figure 2.2**) used for thermal analysis usually consists of the following parts:

- a sample holder: alumina block, which contains sample and reference material [158]
- sensors: two low impedance differential thermocouples [158].
- furnace: sample and the reference should be heated or cooled in identical manner [158].
- temperature controller: monitoring furnace atmosphere and heating rate [158].

- recording system: derivative weight loss versus temperature recorded [158].

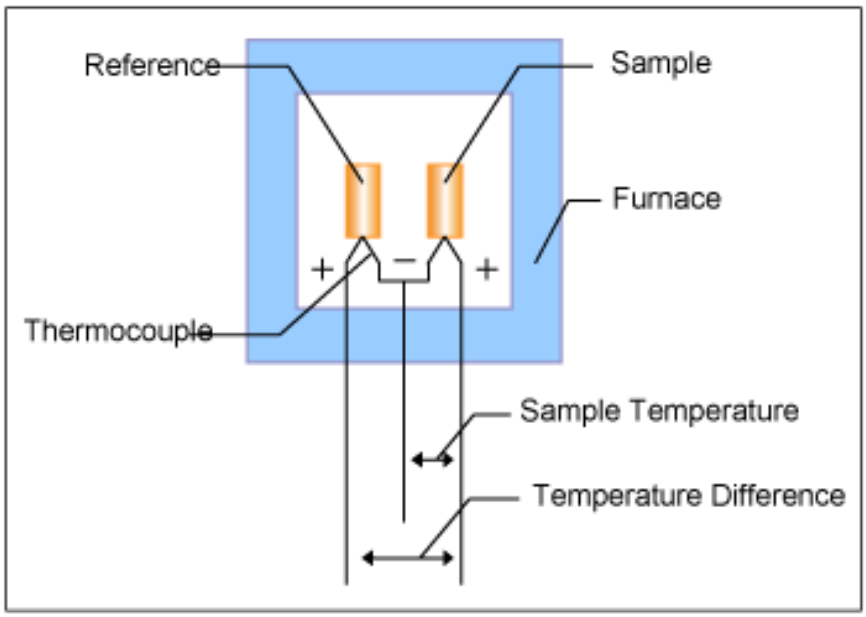

Figure 2.2: Block diagram of DTA [159].

Operating temperatures of DTA instruments are generally room temperature to about 1600°C, even though one manufacture makes a DTA capable of operating from 150°C to 2400°C [160]. To reach the very low sub-ambient temperature, a liquid nitrogen cooling accessory is required, even if some low temperature may be reached with electrical cooling device [158]. When the program begins, the reference and the sample begin heating with a slight delay depending on their respective thermal conductivity [158]. ΔT changes until a state of equilibrium is reached. The signal at the state of equilibrium is known as the baseline. When the temperature rises and melting occurs in the sample, the temperature rise stops, and the ΔT increases. When the melting ends, the temperature curve rapidly reverts to the baseline [161]. At this point, the ΔT signal reaches the peak. When the reaction has completed, the ΔT position, before the curve returns to the baseline, will depend on the type of the reaction. This is true for reactions other than melting [161]. From this, it is possible to detect the sample transition temperature and the reaction temperature from the ΔT signal. In an endothermic (**figure 2.3**) change (melting, vaporization, sublimation, etc), the temperature of the sample is slower than that of the reference material. In an exothermic (**figure 2.3**) change (crystallization, etc), the sample temperature is higher than that of the reference material [158]. There are also physical changes that are not simple; for example, phase changes still cause changes on the sample temperature. Another example of such physical changes includes glass transition.

DTA curve (**figure 2.3**) is a plot of the temperature difference $\Delta T=T_s-T_r$ versus the temperature. DTA curves help in the identification of transformation that have occurred and, in addition, their peak areas provide quantitative information regarding mass of samples and heat of reactions [162]. The peaks of a DTA curve correspond to the temperature at which max degradation occurs.

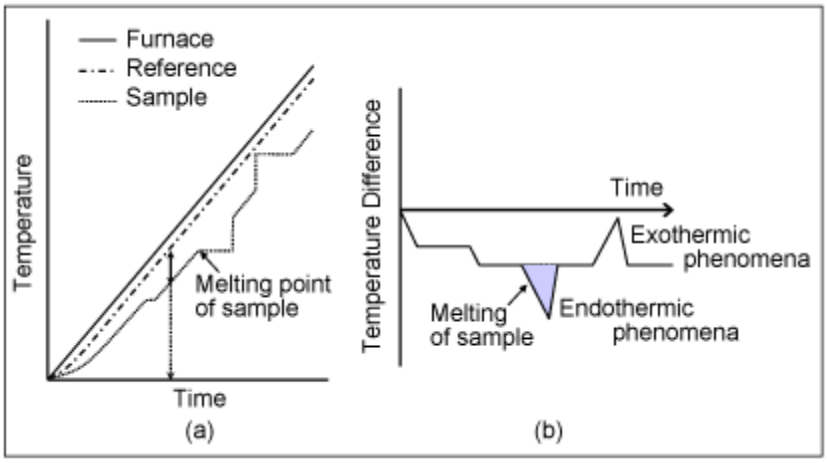

Figure 2.3: Graph (a) shows the temperature change of the furnace, the reference and the sample against time. Graph (b) shows the change in temperature difference (ΔT) against time detected with the differential thermocouple [163].

The peak area is defined as the area between peak and interpolated line. The following relation (**equation 2.1**) is based on a purely theoretical analysis:

$$A = \frac{m\Delta H}{g\lambda}$$

Equation 2.1: Peak area equation [164].

m: mass of the processed sample

ΔH: the enthalpy change associated with a phase change

λ: thermal conductivity of the sample

g: geometric factor

Total heat is proportional to peak area regardless of the physical properties of the sample, thus the area can be used in quantitative analysis [164]. The main aim of such analysis is to describe the shape of the DTA peak in terms of the heat transfer from the source to the sample. Proportionality of formula (**equation 2.1**) assumes that thermal conductivity of sample doesn't change during the processing. This requirement is hardly applicable, as the process is made more complicated by machine geometry and used technique [164]. The advantages offered are numerous, for example:

- Instruments are capable of withstanding the high temperatures

- Highly sensitive

- Identification of characteristic temperatures is very accurate

- Flexibility in crucible volume/form

On the contrary, the main disadvantages of DTA is the signal too low. Moreover, when samples with big mass are used due to the temperature difference between the center and surface of the sample, the relationship between mass of sample and peak area is not linear any more [164].

DTA was used to determine the glass transition, the crystallization and the melting temperature of STe0, STe1 and STe5, and to verify any influence of Te introduction. The analysis was carried out on both unsieved and sieved powders. DTA analysis were carried out using STA449

F1 Jupiter and heating 40 mg for each glass samples in a Pt-crucible under heating rate of 1300 °C/min.

2.2.4 X-ray diffraction

The diffraction of X-rays gives deep information about the atomic structure of matter and, therefore, is a very useful tool for a wide range of investigations. A beam of X-rays hits the electrons in the atoms of the crystal and thus, x-ray wavelengths are about the same size as the typical distance between atoms in a crystal [165]. This means that the x-rays are small enough to get a little bit into the crystal by sliding between the holes within atoms. As light waves pass through the different gaps in an object, the waves recombine on the other side in patterns that are very much dependent on where the holes are, how are spaced, and how big are [165]. The direction that approaches the crystal surface is subjected to changes and how long the difference in distance is for bouncing off the first layer versus bouncing off a different layer. This depends on the angle and the distance between the two layers. The concept of diffraction was first proposed by William Lawrence Bragg and William Henry Bragg in 1913 [166]. More specifically, Bragg's Law relates the spacing of a specific set of atomic planes to the wavelength of x-rays and the angle the waves are bouncing off interested crystal [166]. By mixing that with some math relating to constructive and destructive interference, it is possible to predict the XRD pattern for any crystal structure, real or theoretical. W. L. Bragg basically explains that when particles scatter off of different scattering centers, the geometry of the scattering centers will determine what angles will yield constructive and destructive interference [166]. The angles that make for constructive interference will have to line up with the planes, because otherwise there will be considerable destructive interference [166]. That gives Bragg condition. At each atom, a small part of the incident beam gets absorbed and another smaller part gets scattered, more or less equally in all directions. Hence, the beams retain their phase and can interfere.

Bragg's law [imagine] says that constructive interference happens when a certain relation between the wavelength, lattice spacing and angle of incidence is satisfied [165]. When, the path length difference, between rays scattered by successive planes of the lattice is equal to an integral number of wavelength of the incident x-rays, the rays interfere constructively to produce peaks of intensity.

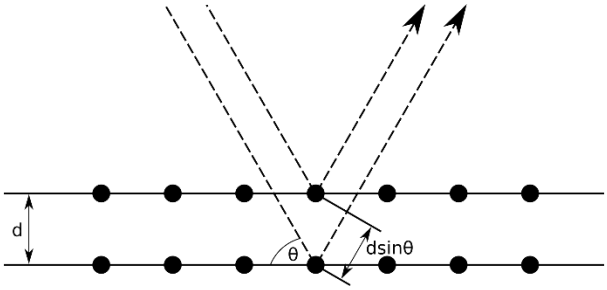

Figure 2.4: Schematic illustration of Bragg condition [167].

$$2dsin\theta = n\lambda$$

Equation 2.2: Bragg's Law equation [167].

The equation explains this phenomenon (**equation 2.2**) where, d is the spacing of the planes and n is the order of diffraction. Bragg reflection can only occur for wavelength $n\lambda<2d$. No diffraction occurs when the above condition is not satisfied [168].

In contrast to the Bragg diffraction, in Fraunhofer diffraction every points at the opening/aperture are regarded as secondary sources of waves. If one extends the idea to a crystal lattice where there are periodic structural positions acting as scatterers, then waves diffracted from each position of the particles (atoms, ions, molecules etc.) can be regarded as point sources [168]. More precisely, the particles scatter the incoming waves with regular phase differences (related by their Miller indices) giving their specific positions [168].

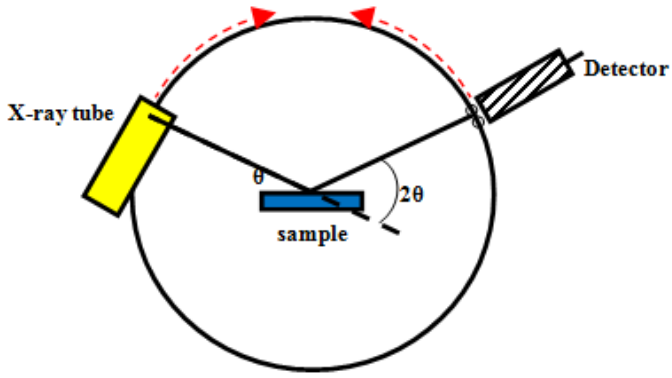

Figure 2.5: X-Ray tube working principle [169].

Source of X-rays shoots highly collimated energy beams against a target, then it changes the angle of incidence (around the Bragg condition) towards a detector to observe the effect of interference by counting incoming particles [170]. The detector position is recorded as the angle 2ϑ. The spectrometer picks up the photons and analyzes the distribution. Depending on which frequencies are detected, it can determine what kind of atoms emit those frequencies and thus what kind of atoms make up the material [170]. The detector records the number of X-ray observed at each angle 2ϑ. Each phase produces a unique diffraction pattern when hit by X-ray. Each diffraction line is based on of a set of small spots, each form a separate unit cell parameters. Each spot is so small as to give the appearance of a continuous line. On the contrary, XRD pattern of an amorphous compound consists of one or more broad diffuse halos. The diffraction pattern of a mixture is a simple sum of diffraction patterns of each individual phase. From the XRD pattern, it is possible determine:

- crystalline phase
- ordered-disordered molecular arrangement

- amount of each phase

X-ray diffraction analysis were performed on STe0, STe1 and STe5 sieved powders before and after in SBF to verify their amorphous nature and to estimate the precipitation of hydroxyapatite after in vitro test in SBF. X-ray curves was plotted and then analyzed using X'Pert High Score software.

2.2.5 Fourier Transform Infrared Spectroscope

FT-IR is a method of infrared spectroscopy. The basic principle behind molecular spectroscopy is that every chemical bond absorbs light at different frequency. When a sample is irradiated with infrared radiation, a part of the radiation is absorbed by the sample, while the remainder goes through the sample [171]. The spectrum obtained represents the absorption of infrared radiation by the sample material versus wavelength. Since each compound has a unique combination functional groups or part of molecules, every molecule has a unique infrared spectrum, but the IR spectra of any two molecules cannot be same [171]. Therefore, infrared spectroscopy can identify every different kind of material.

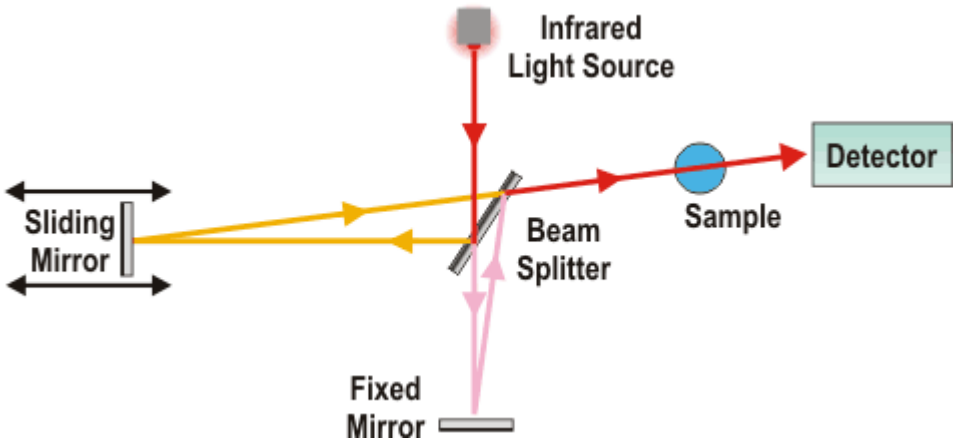

Figure 2.6: FTIR measuring principle [172].

The FTIR instrumentation is composed by the following parts:

1. The Source (**figure 2.7**): the infrared beam is emitted (**figure 2.6**) from a solid material, which is heated to a high temperature (rare earth oxides or silicon carbide). Then the beam passes through a hole, which monitors the amount of energy sent to the sample [171].
2. The Interferometer (**figure 2.7**): the radiation enters and splits into two beams by beam splitter (**figure 2.6**). One beam is transmitted to a fixed mirror [171]. The other is transmitted to a moving mirror that can move a very short distance away from the beam-splitter. The two beams reflect off of their respective mirrors and are recombined when they meet back at the beam-splitter. The path that one beam travels is a fixed length and the other is constantly changing as its mirror moves, thus the signal which exits

from the interferometer is the result of these two beams interfering which each other [171].

3. The Sample: the beam strikes the sample (**figure 2.6**) and it is transmitted through or reflected off of the surface of the sample, depending on the type of analysis being accomplished [171].
4. The Detector (**figure 2.7**): the transmitted beam finally reaches the detector (**figure 2.6**) for final measurement. The detector reads information about every wavelength in the infrared range [171].
5. The Computer (**figure 2.7**): the measured signal is sent to the computer where Fourier transformation algorithm takes place to convert it into a single beam spectrum [171].

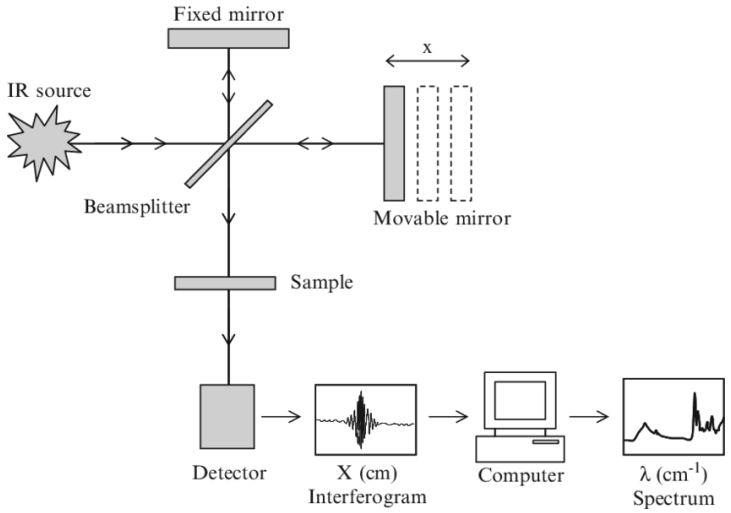

Figure 2.7: FTIR instrumentation [173].

By looking at the signal on the detector as a function of position, it would be possible to see a sine wave traced out. The frequency of that sine wave is the frequency of the light, and the amplitude is the transmission through the sample, just like in normal absorption spectroscopy [174]. Therefore, if broadband is used as source of light, the same thing will be observed, except with a lot of waves of different frequencies superimposed in an interferogram. All of the information corresponding to the amplitudes and frequencies are there, just combined into a single waveform [174]. Fourier transform returns those amplitudes and frequencies, which gives the spectra.

It should be clear that all matter contains molecules and these molecules have bonds. The bonds between the atoms vibrate and possess a vibrational motion called stretching and bending (v) [175]. Linear molecules have 3*N*-5 (where N is the number of atoms) modes of vibration (for instance CO_2) because 3 of all the modes vibrate along the axis of symmetry and 2 vibrate out of the axis of symmetry, while bent molecules have 3*N*-6 modes of vibration (for instance H_2O) because 3 of all the modes vibrate along the axis of symmetry and 3 vibrate out of the axis of symmetry [175]. The term Q_{ab}^{n} represents the tetrahedral unit, where *n* is the number of bridging oxygens for each tetrahedron and *ab* the molecule of interest. In the stretching, the bond length is increased or decreased at regular intervals. Stretching can either be symmetric, if bond length increases or decreases, or asymmetric, if length of one bond increases and the other one decreases [175]. In the bending, the vibrations change the bond angle between bonds with a common atom or a group of atoms moves respect to the other molecules. In other words, a

photon of light that has a frequency in the range will be absorbed if the bonds between atoms in the target material allow these atoms to vibrate in this frequency [175]. These frequencies are related generally to the part of the electromagnetic spectrum which lies between the visible and microwave regions. For a vibration to be visible by infra-red spectroscopy, it needs to result in a change in the dipole moment of the molecule. Some atoms are more electronegative than others, resulting in a dipole across a molecule [175]. When some atoms move in a vibration, a change in the magnitude or direction of the dipole moment is possible. In such cases the vibration is visible by IR. Unfortunately it follows that symmetrical diatomics (like H_2, N_2, O_2) cannot undergo a dipole moment change from any possible vibration, so those bonds are not visible by IR [175]. It shoud be noted that an IR spectrum usually extends from radiation around 4000 cm^{-1} to 600 cm^{-1}.

The molecular structure of STe0, STe1 and STe5 after and before immersion in TRIS or SBF and the formation of hydroxyapatite were investigated by FT-IR. FT-IR spectra were recorded from 4000 cm^{-1} to 400 cm^{-1}. FTIR spectra were plotted and then analyzed using Origin8.

2.2.6 Inductively Coupled Plasma – Optical Emission Spectroscopy

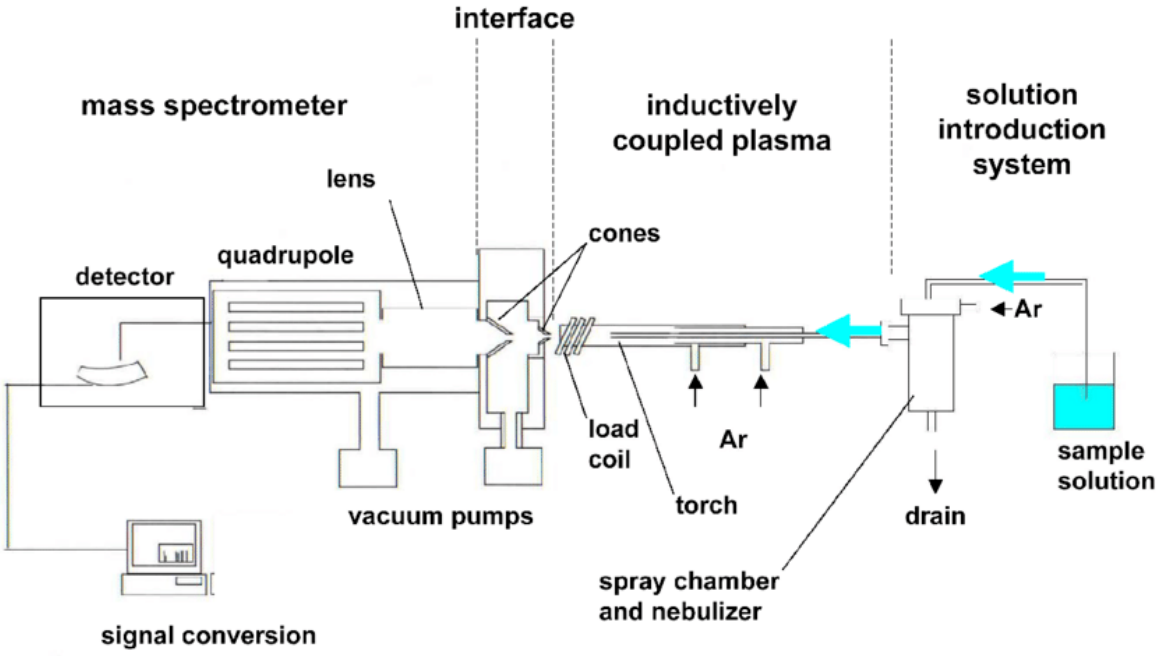

Figure 2.8: The principle and major components of a typical ICP-OES instrument [176].

ICP is an analytical technique, which uses plasma to ionize the sample. Then, the ionized sample (**figure 2.8**) emits light at wavelengths characteristic of the elements present in the sample [177]. The intensity of the light at the specific wavelengths also gives information about the amount of that element, therefore, it is possible to work out concentrations and relative amounts. Most common ICP uses argon (**figure 2.8**) gas system to generate plasma [177]. It is important that the plasma gas is pure since contaminants in the gas might quench the torch [177]. The instrument has ICP torch where the argon gas flows. The ICP torch (**figure 2.8**) is surrounded by radio-frequency load coil, whom are connected to the radio-frequency generator

[177]. As the power is generated from the generator, there is a generation of oscillating electric and magnetic field at the end of the torch. It is followed by generation of a spark (**figure 2.8**) which ionize the argon gas flowing through the torch to argon ions [177]. These ions will get caught in the oscillating field and collide with the other argon ions which would generate the plasma or discharge [177]. The used sample in ICP is in aerosol form. This form can be achieved by aspirating the liquid sample or dissolved sample into the nebulizer. This aero-sol is transferred towards the plasma torch and then, the solid sample are converted to a gaseous state which is ionized at the end of the torch. The plasma or the argon discharge has a temperature of around 6000-10000 K [177] [178]. The electrons of the atoms of elements contained in the sample undergo a transition to excited state by absorbing thermal energy from the plasma source that are then re-emitted at a characteristic frequency as they return to lower energy state [179]. Thus, the elements present may be determined by resolving individual spectral lines of the element of interest, choosing and measuring the intensity of one or more of the carefully selected lines for each element [180]. However, most of the ions generated by the plasma are positively charged and thus, negatively charged ions such as Cl, F, Br, I etc. cannot be ionized. But these elements can be analyzed easily with the help of ICP-MS. It is an elemental analysis tool which works by vaporizing the sample and then ionizing the sample through the use of the plasma, which is tuned to between 4500-5800 Kelvin [181]. Once the elements in the sample are converted into ions, pass through into the mass spectrometer via the interface cones. The purpose of these cones is set up to sample the central portion of the ion beam coming from the ICP torch. A shadow stop will block the extra photons coming from the ICP torch [177]. Despite the ICP-MS is very accurate and beneficial for analyzing compounds, the small opening of the sampler cone and skimmer cone limits the amount of the solid sample dissolved and analyzed. If the total dissolved solids in the sample are high, then the opening of the cone will be blocked [179]. Now, the ions are focused towards the entrance of mass spectrometer. This is facilitated by the electrostatic lens which is positively charged [179]. As the ions ejected from the ICP are positively charged, they would get repelled by the parallel positively charged electrostatic plated and focused on entrance aperture or slit of the mass spectrometer [179].

The concentrations of Ca, Na, P, Si and Te ions from STe0, STe1 and STe5 after 1, 3, 7 and 14 days of SBF/TRIS immersion were determined by ICP-OES using Agilent Technologies 5110 ICP-OES. 1 ml of every samples was diluted in 9 ml of 1M HNO_3 before performing ICP-OES test. The samples stand in acid for at least 24 hours before analysis to ensure that each analyte is completely dissolved.

In order to show the results derived from ICP test, the following calculations were carried out before the plotting.

1. The molar mass percentage of ions ($\%_{molar\ mass}$) in compound was achieved starting for the molar mass of compounds ($M_{compound}$) and ions (M_{ion}):

$$\%_{molar\ mass} = \frac{M_{ion}}{M_{compound}} \cdot 100$$

2. Then, the weight of the ion ($m_{ion,100}$) in compound considering 100 grams of sample was calculated as follows:

$$m_{ion,100} = \frac{\%_{molar\ mass}}{100} \cdot m_{compound,100}$$

Where $m_{compound,100}$ is the mass of the compound in 100 grams of sample.

3. The total theoretical amount of ion was determined on the basis of this relation:

$$m_{ion,100}: 100 = m_{ion,150}: 150$$

Where $m_{ion,150}$ is the total theoretical amount of the ion in 150 milligrams of sample.

4. After obtaining the solution concentrations for the sample from ICP-OES test, the dilution factor (DF) was calculated since it is necessary for analysis:

$$DF = \frac{V_f}{V_i}$$

Where V_f is the final volume (after digested in nitric acid) V_i is the solute volume (volume used for analysis). Therefore, once obtained (DF), it was multiplied by the ICP-OES measured concentration value (C).

5. The measured concentration value was multiplied by the assayed volume (V) to give the total real amount of ion in the sample. Then, the value obtained was divided by the sample mass (m) to get the mass of analyte per mass unit of sample (Q):

$$Q = C \cdot \frac{V}{m}$$

6. To obtain the percentage of ion dissolved, the total amount of analyte in the sample was divided by the theoretic amount of analyte in the sample:

$$\%_{dissolved} = \frac{C \cdot V}{m_{ion,150}}$$

2.2.7 Raman Spectroscopy

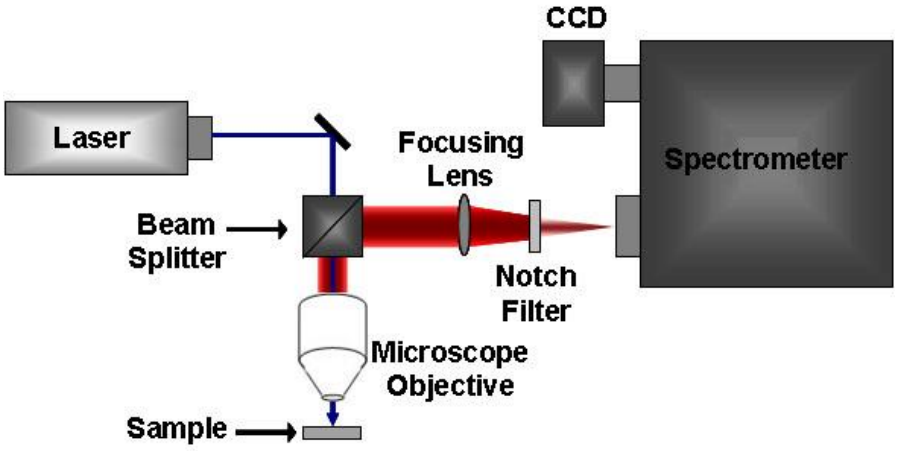

Figure 2.9: Raman spectroscopy setup [182].

Raman spectroscopy is a spectroscopic technique, which gives data about molecular vibrations and rotations that can be utilized for test distinguishing proof and quantization. Raman spectroscopy provides an invaluable analytical tool for molecular finger printing as well as monitoring changes in molecular bond structure [183]. When a photon hits molecules in the right way, it gives a kick to the bond, hence the molecule starts bouncing about. It could bounce to and fro, twist left and right or bounce in all kinds of complex ways depending on the structure of the molecule [183]. Not just any photon can kick a molecule's bonds into bouncing like this. The photon has to have just the right amount of energy thus it will pass right through. A photon with lots of energy has a high frequency, and less energy has a lower frequency [184]. What happens is basically inelastic scattering of photons. Unfortunately, only about 1 in 10 million photons gets Raman scattered. Detectors (**figure 2.9**) around the analyzed substance detect any photons that bounced off the molecule in different directions, and measure their frequencies even though all the incoming light was at one frequency [184]. This effect, changes in the wavelength of light that occurs when a light beam is deflected by molecules. When a beam of light traverses a transparent sample of a chemical compound, a small fraction of the light emerges in directions other than that of the incident beam [184]. A small part, however, has wavelengths different from that of the incident light; its presence is a result of the Raman effect. A Raman spectrum then shows the frequencies of reflected light that comes from shining light at one frequency on the substance [185]. The electron in the atoms and molecules might get to a new energy level by absorbing photon, and when it comes back, it might emit the photon with same wavelength. Therefore, the same electron excited to higher energy level may jump in one of its vibrational excited state emitting a photon but with wavelength larger than incident photon [183]. So, when the laser light interacts with molecular vibrations in the system, photons being shifted up or down. The shift in energy gives information about the vibrational modes in the system. In general, the ionic bonds have vibration frequencies that will appear in the Raman spectrum, and the covalent bonds will appear in the IR spectrum [185]. This means that Raman and IR spectroscopy together judge the types of bonds in an unknown substance, but they provide complementary information. Some molecules having dipole moment, such as symmetric vibrations, do not vibrate but rotate, leading to interaction with microwave spectra. Molecules not having dipole moment but have polarization can be studied using Raman spectrometry [185]. If the molecule is symmetric it is unlikely for a single vibrational mode to cause the molecule's dipole moment and polarizability to change much. In an asymmetric molecule, they can both change but a strong change in dipole moment corresponds to a weak change in polarizability and vice versa [185].

Raman analyses were performed on STe0, STe1 and STe5 powders immersed for 1 and 14 days in TRIS and SBF. Raman spectra were plotted and then analyzed using Origin8. Raman spectra were recorded from 2000 cm^{-1} to 100 cm^{-1}.

2.2.8 Cell Culture Tests

Square specimens (1cm side size) were stored at room temperature protected from light by aluminum foil. The following specimens were tested:

- STe0: silica-based glass (control)
- Ste1: silica-based glass + 1% mol TeO2
- Ste5: silica-based glass + 5% mol TeO2

Specimens were heated sterilized for 3 hours at 100°C prior to biological experiments.

2.2.8.1 Cytocompatibility evaluation

- *Cells:* human bone marrow- derived stem cells (BMSCs) were cultivated in low-glucose Dulbecco's modified Eagle Medium (DMEM, Sigma-Aldrich) supplemented with 15% fetal bovine serum (FBS, Sigma) and 1% antibiotics (penicillin/streptomycin) at 37°C, 5% CO_2 atmosphere. Cells were cultivated until 80-90% confluence, detached by trypsin-EDTA solution, harvested and used for experiments.

- *Metabolic evaluation:* cells were directly seeded onto specimens' surface in a defined concentration ($3x10^4$ cells/specimen) and cultivated for 1-2-3 days. At each time points, the viability of the cells in direct contact with specimens were evaluated by the metabolic colorimetric Alamar blue assay (alamarBlue™, from Life Technologies) following Manufacturer's instructions. Briefly, supernatants were removed from each well containing cells and replaced with Alamar blue solution (10% v/v in fresh medium). Plates were incubated in the dark for 4 h and then 100 µl were removed, spotted into a new black 96-well plate and fluorescence signals were evaluated with a spectrophotometer (Spark®, Tecan Trading AG, CH) using the following set-up: fluorescence excitation wavelength 570 nm, fluorescence emission reading 590 nm.

- *ROS/RNS scavenge:* cells were seeded onto specimens' surface as prior described for the metabolic evaluation. At 1-2-3 days, cells were treated with 300 µM H_2O_2 for 3 hours to test tellurium antioxidant activity to scavenge the derived ROS and RNS species. The active species quantification was performed with the fluorescent OxiSelect™ assay (from Cell Biolabs) following Manufactures' instructions. Briefly, 50 µl of the test specimens' supernatants were collected and mixed with 50 µl of catalyst and 100 µl of the DCFH solution (both provided from the kit); after 45 minutes incubation the fluorescence signal was evaluated by spectrophotometer (Spark®, Tecan Trading AG, CH) using the following set-up: fluorescence excitation wavelength 480 nm, fluorescence emission reading 530 nm. Cells cultivated onto bioglasses without H_2O_2 stress were considered as control.

- *Osteogenesis*: cells were directly seeded onto specimens' surface in a defined concentration ($2x10^4$ cells/specimen) and cultivated for 7-14-21 days in the presence of osteogenic medium (low-glucose DMEM supplemented with 10% FBS, 10^{-7} M dexamethasone, 50 M β-glycerophosphate, 20 mM ascorbic acid). At each time point cells were stressed with 300 mM H_2O_2 for 3 hours as prior described; then, the supernatants were collected and the alkaline phosphatase (ALP) activity was measured to evaluate osteogenesis progression in the presence of inflammation. ALP activity was evaluated by a colorimetric assay (ab83369, from AbCam, UK) following Manufacturer's instructions: briefly, 80 µl of supernatants were collected from each sample and mixed with 50 µl of the *p*NPP solution and 10 µl of the ALP enzyme. After 60 minutes incubation, the reaction was stopped and the optical density was measured by spectrophotometer (Spark®, Tecan Trading AG, CH) using a 405 nm wavelength.

2.2.8.2 Antibacterial activity

- *Strains:* To test tellurium antibacterial activity, the orthopedic-related strains *Staphylococcus aureus* (*S. aureus*) and *Staphylococcus epidermidis* (*S. epidermidis*) were used. *S. aureus* was purchased from the American Type Culture Collection (ATCC, 43300) while *S. epidermidis* was clinically isolated from the Clinical Microbiology Unit of the Maggiore Hospital of Novara. Bacteria were cultivated onto Trypticase Soy Agar (TSA, Sigma-Aldrich) and incubated at 37°C until round single colonies were formed; then, 2-3 colonies were collected and spotted into 30 ml of Luria Bertani broth (LB, Sigma-Aldrich). Broth cultures were incubated overnight at 37°C in agitation (120 rpm in an orbital shaker), then bacteria concentration was adjusted until $1x10^5$ cells/ml by diluting in fresh media until optical density of 0.001 at 600 nm was reached as determined by spectrophotometer (Spark®, Tecan Trading AG, CH).

- *Biofilm formation: s*terile specimens were gently located into a 24 multiwell plate by sterile tweezers avoiding any surface damages. Each specimen was submerged with 1 ml of the $1x10^5$ cells/ml broth bacteria culture prepared as prior described; plate was incubated for 90 minutes in agitation (120 rpm) at 37°C to allows the separation between adherent biofilm cells and not-adherent floating planktonic cells (separation phase). Afterwards, supernatants containing planktonic cells were removed and replaced with 1 ml of fresh media to cultivate surface-adhered biofilm cells (growth phase). Biofilm were grown at 37°C for 1-2-3 days prior to evaluations.

- *Biofilm Metabolic evaluation: a*t each time-point, specimens were gently washed 3 times with PBS to remove non-adherent cells and then moved to a new 24 multiwell plate where bacteria metabolic activity was evaluated by the alamar blue assay as prior described for cells metabolic activity evaluation.

- *CFUs count:* to count the number of viable adhered colonies, after 3 days cultivation specimens were moved to tubes containing 1 ml of PBS and the biofilm was detached from specimens' surface by sonicator and vortex (30 seconds, 3 times each); Then, 100 µL of supernatant were collected from each well and used to perform six serial ten-fold dilutions, mixing 20 µL of bacterial suspension with 180 µL of sterile PBS. Twenty µL were then collected from each dilution, spotted onto plates containing LB agar medium, and incubated for 24 h at 37°C. Lastly, the CFU mL^{-1} were counted as follows:

$$CFU = [(number\ of\ colonies \times dilution\ factor)^{(serial\ dilution)}]$$

where:
number of colonies = countable single round colonies;
dilution factor = dilution made from the initial 1 mL suspension;
serial dilution = 1–6 ten-fold dilution areas where colonies were counted.

3. Results

In this chapter, the data and plots obtained by the different analyses outlined in chapter 2 are presented in order to characterize the different bioactive glass compositions from a physical, biological, chemical and morphological point of view.

3.1 Field-emission Scanning Electron Microscope and Electron Dispersive Spectroscopy

Scanning electron microscope equipped with an energy dispersive spectrometer (SEM/EDX) was used to identify and quantify the presence of tellurium. Analysis conditions were selected in the range 15–25 keV. Each measurement was repeated three times.

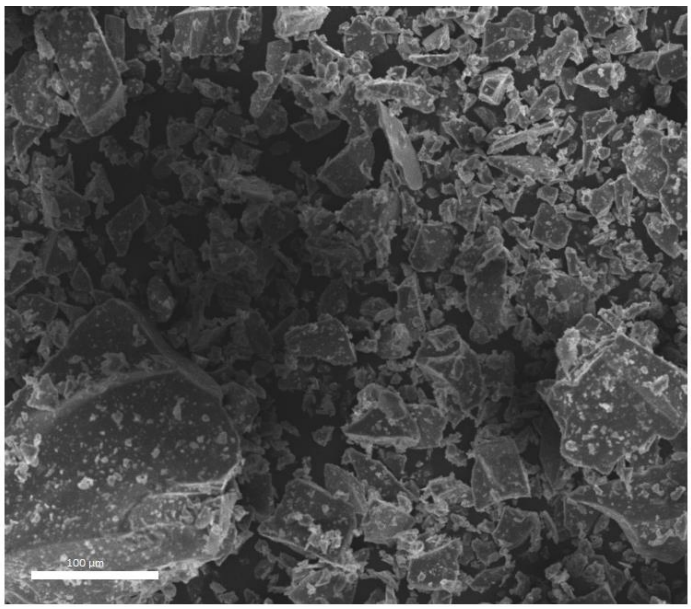

Figure 3.1: SEM micrographs of STe0 powders before immersion in SBF.

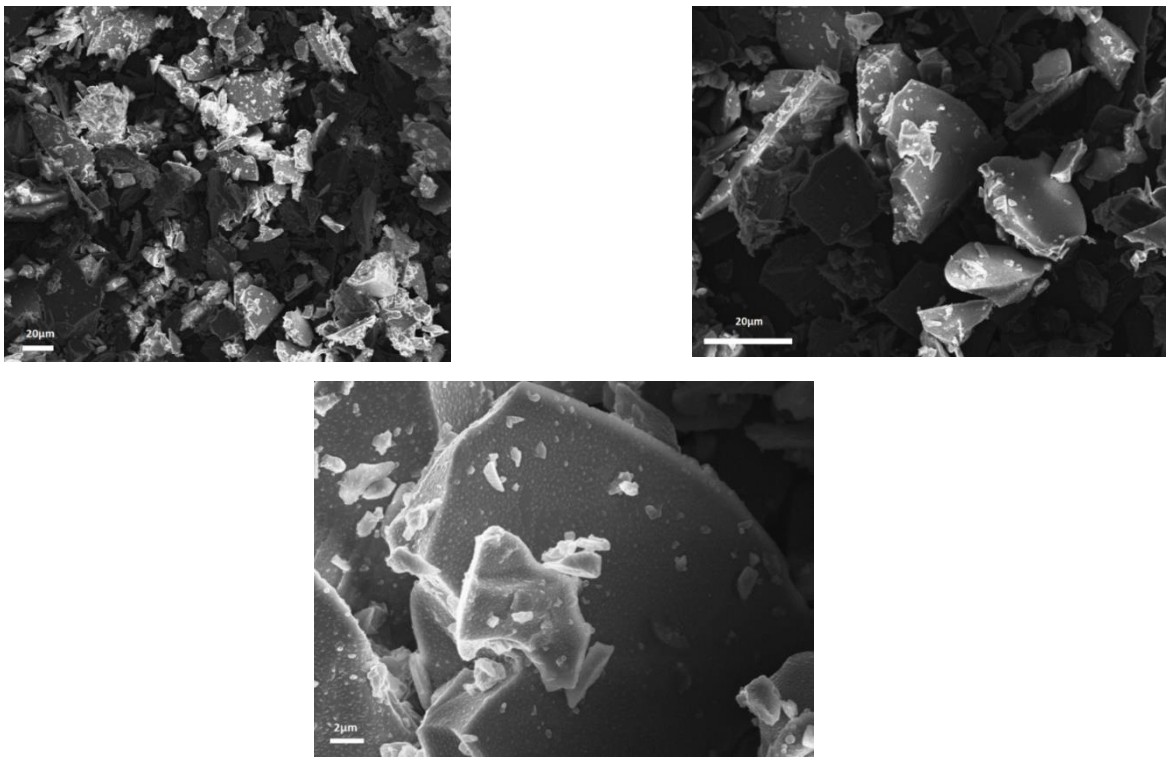

Figure 3.2: SEM micrographs of STe1 powders before immersion in SBF.

From FESEM analysis, it is clear that STe0 (**figure 3.1**), STe1 (**figure 3.2**) and STe5 (**figure 3.3**) powders were composed of various particles which exhibits irregular shape and a wide size distribution.

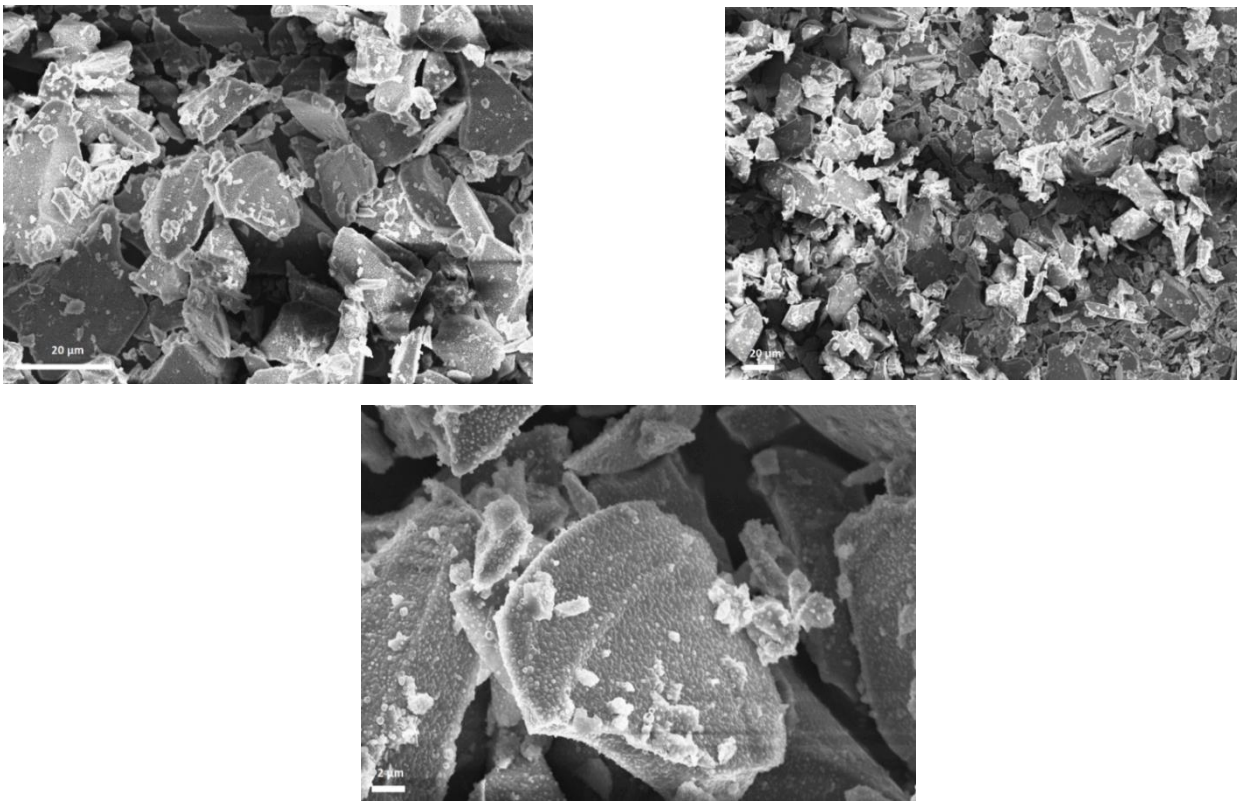

Figure 3.3: SEM micrographs of STe5 powders before immersion in SBF.

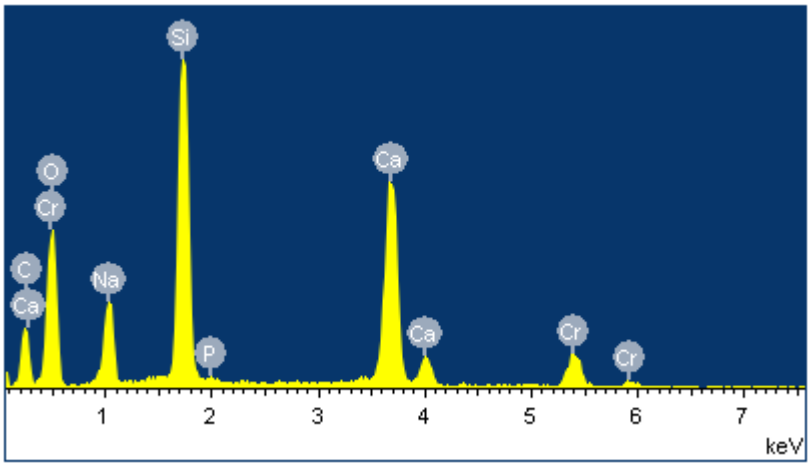

Figure 3.4: Elemental composition analysis of STe0 powders before immersion.

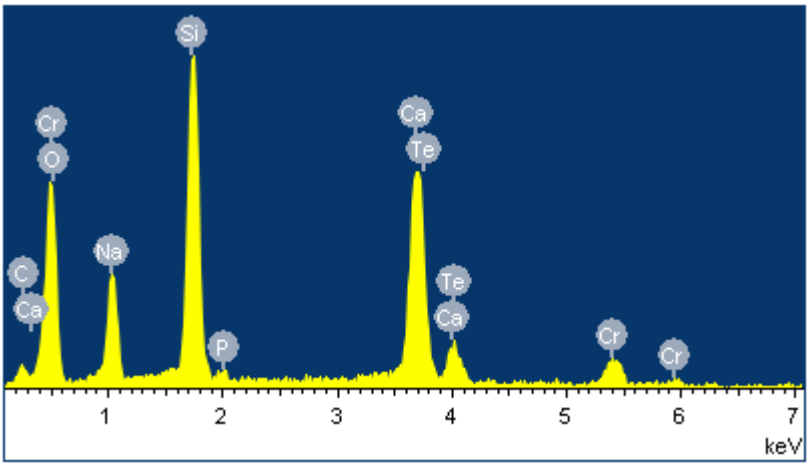

Figure 3.5: Elemental composition analysis of STe1 powders before immersion.

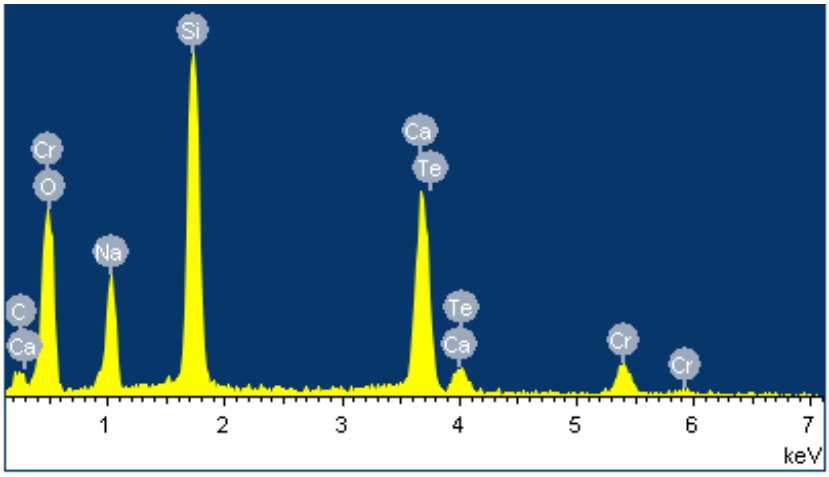

Figure 3.6: Elemental composition analysis of STe5 powders before immersion.

EDS analysis of STe0 (**table 3.1**), STe1 (**table 3.2**) and STe5 (**table 3.3**) revealed that the powder compositions closely resembled the theroetical ones (**tables 2.2-2.3**): sodium and calcium %at were slightly higher, whereas tellurium and silicon %at were lower. The peak in **figures 3.4-3.5-3.6**, referred to the chromium, is due to the metallization process necessary for FESEM analysis.

Table 3.1 EDS analysis of STe0 before immersion (%at: atomic percentage).

EDS	%at	average	st.dev.
Na	20,10	20,01	0,54
Si	44,36	44,82	0,60
P	0,61	0,72	0,12
Ca	34,94	37,45	0,45

Table 3.2 EDS analysis of STe1 before immersion (%at: atomic percentage).

EDS	%at	average	st.dev.
Na	19,29	18,1	1,28
Si	43,25	44,0	0,77
P	0,62	0,6	0,24
Ca	36,56	37,3	0,61
Te	0,29	0,1	0,17

Table 3.3 EDS analysis of STe5 before immersion (%at: atomic percentage).

EDS	**%at**	**average**	**st.dev.**
Na	19,43	19,0	0,38
Si	39,22	39,8	0,46
P	0,63	0,9	0,46
Ca	37,22	36,9	0,33
Te	3,5	3,4	0,08

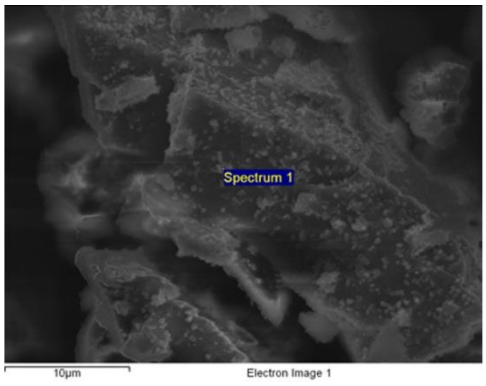

Element	Weight%	Atomic%
Na K	13.30	17.81
Si K	46.69	51.20
P K	1.05	1.04
Ca K	38.97	29.94
Totals	100.00	

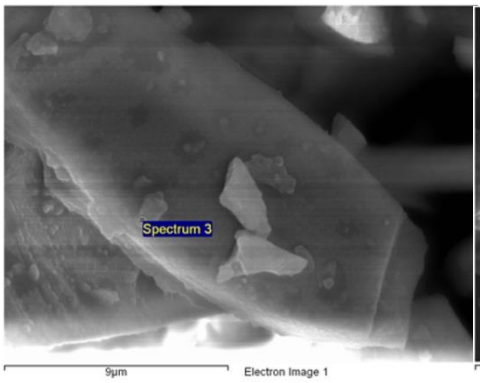

Element	Weight%	Atomic%
Na K	9.44	13.11
Si K	42.93	48.77
P K	0.87	0.90
Ca K	46.75	37.22
Totals	100.00	

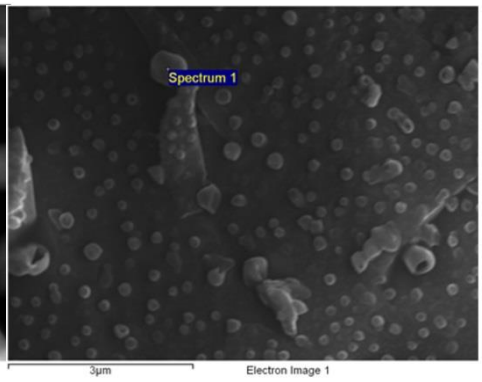

Element	Weight%	Atomic%
Na K	18.73	26.65
Si K	34.95	40.70
P K	1.04	1.10
Ca K	35.64	29.08
Te L	9.64	2.47
Totals	100.00	

Figure 3.7: SEM punctual micrographs of STe0, STe1 and STe5 (from left to right) powders before immersion in SBF and relative EDS analysis.

In all samples, two different zones were observed (**figure 3.7**): one with white "bubbles" richer in Na and the other richer in Si.

3.2 Bioactivity test: pH evolution

The pH evolution of the SBF (**figure 3.8**) and TRIS (**figure 3.9**) solutions after soaking STe0, STe1 and STe5 powders for 1 to 14 days are shown as function of time.

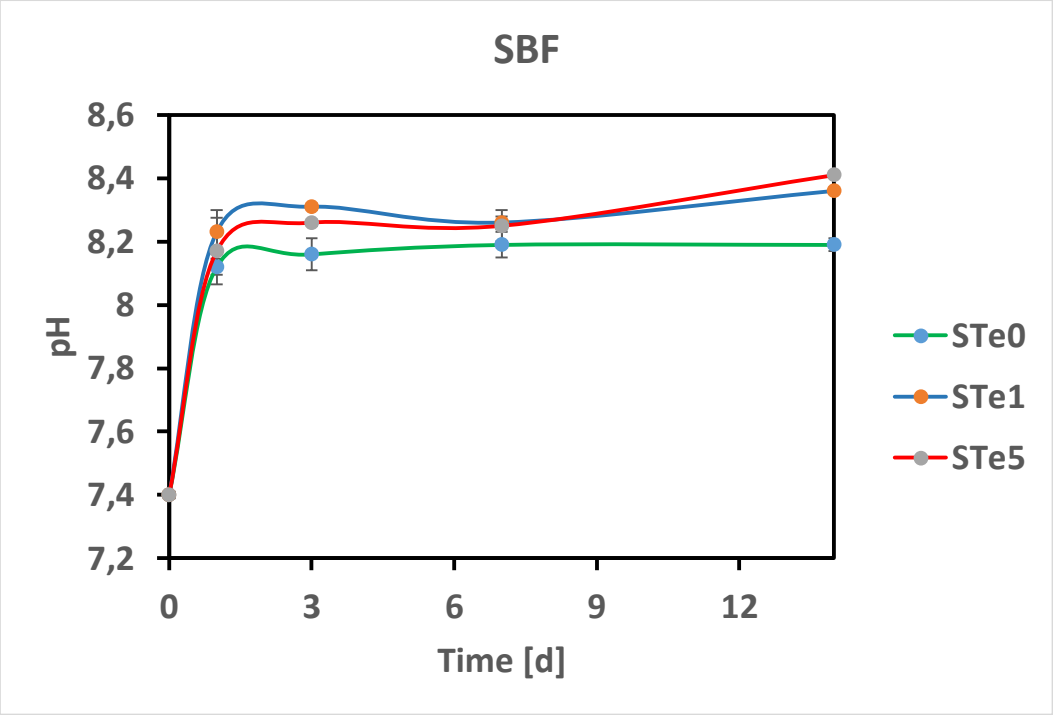

Figure 3.8: pH evolution of STe0, STe1 and STe5 compositions during immersion in SBF.

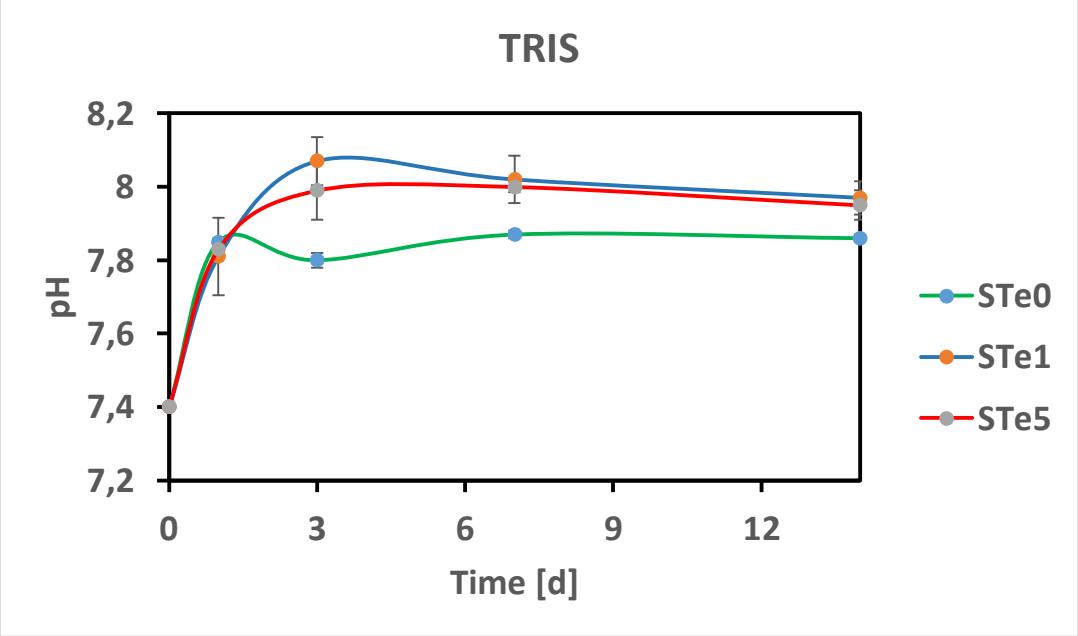

Figure 3.9: pH evolution of STe0, STe1 and STe5 compositions during immersion in TRIS.

The pH changes took obviously place after immersion in simulated body fluid (SBF) solution (**figure 3.8**); in fact, the pH starts to rise as compared to the initial pH of the SBF solution at 7.4. The greatest increase in pH were observed after 1 day of immersion for each samples from 7.4 to 8.15 and the maximum values can be seen at 14 days for each samples. Similarly, all glasses triggered a distinctive pH growth even in TRIS buffer (**figure 3.9**), but in this case, the pH gradually increases up to 7 days and then a slight decrease is observed. As seen with SBF (**figure 3.8**), the pH increase was more marked after 1 day, but the maximum value reached by all the samples in TRIS was lower than the one reached by the samples immersed in SBF. The maximum standard deviation of the pH measured was 0.21 for STe5 in SBF, whereas 0.58 for STe0 in TRIS. The pH values of SBF and TRIS were slightly higher for STe5 and STe1 respect STe0, in particular the highest values were reached by STe1. All compositions in SBF had a pH trend basically similar during the whole immersion period, except STe0 in TRIS, where trend was undergone a broad dip in the range from 3 to 7 days.

3.3 Differential Thermal Analysis

DTA curves were achieved for each glass composition before immersion (STe0, STe1 and STe5) and their characteristic temperatures were summarized in table (**table 3.4**).

Table 3.4 Temperatures of STe0, STe1 STe5 compositions as obtained using DTA

°C	STe0	STe1	STe5
T_g onset	591.52	575.29	567.19
T_g mid	611.12	607.11	589.76
T_g offset	625.59	616.53	597.69
T_{c1}	678.08	695.86	674,25
T_{c2}	727.13	724.74	671.82
T_{m1}	1279.65	1278.87	1257.49
T_{m2}	1285.77	1288.65	1263.37

All the plots of glasses showed six characteristic peaks: T_g onset, mid, offset glass transition temperatures, T_{c1} and T_{c2} crystallization temperatures and T_{m1} and T_{m2} melting temperatures. Since the glass transition may be a range rather than be a discrete point, $T_{g,mid}$ was assigned to glass transition point represented by the inflection of the DTA curve as its midpoint, while $T_{g,onset}$ is the lowest value (slope of the first tangent line before the inflection) and $T_{g,offset}$ is the end point (end of the slope).

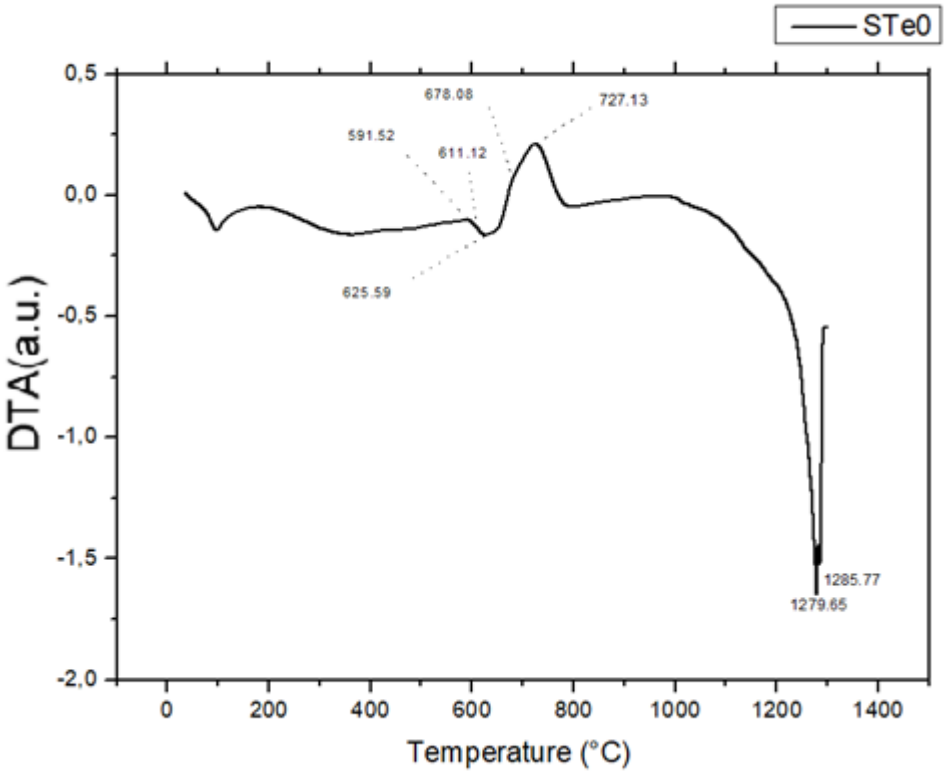

Figure 3.10: DTA analysis result of STe0 composition.

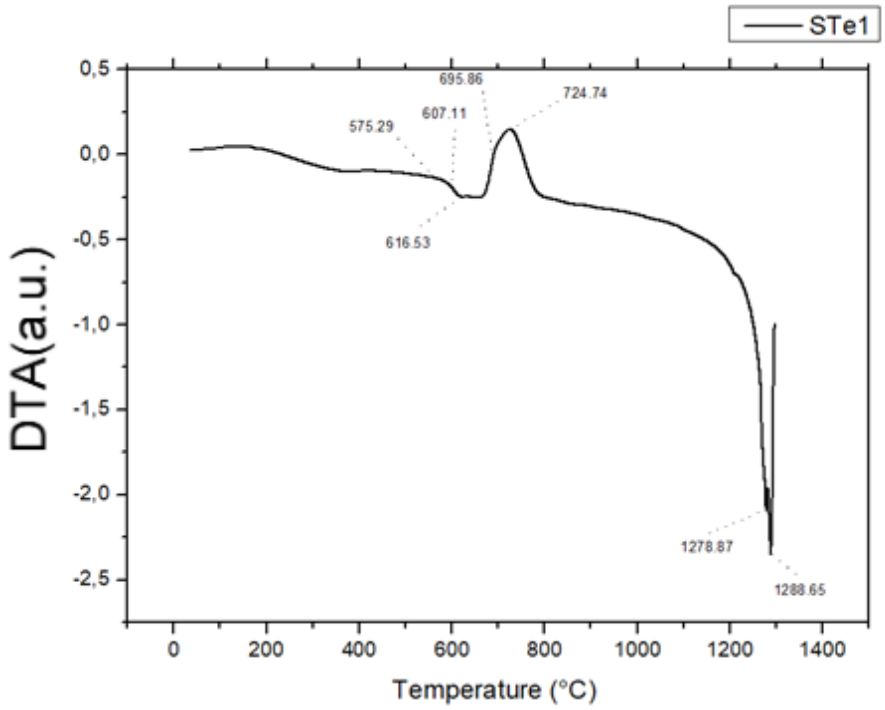

Figure 3.11: DTA analysis result of STe1 composition

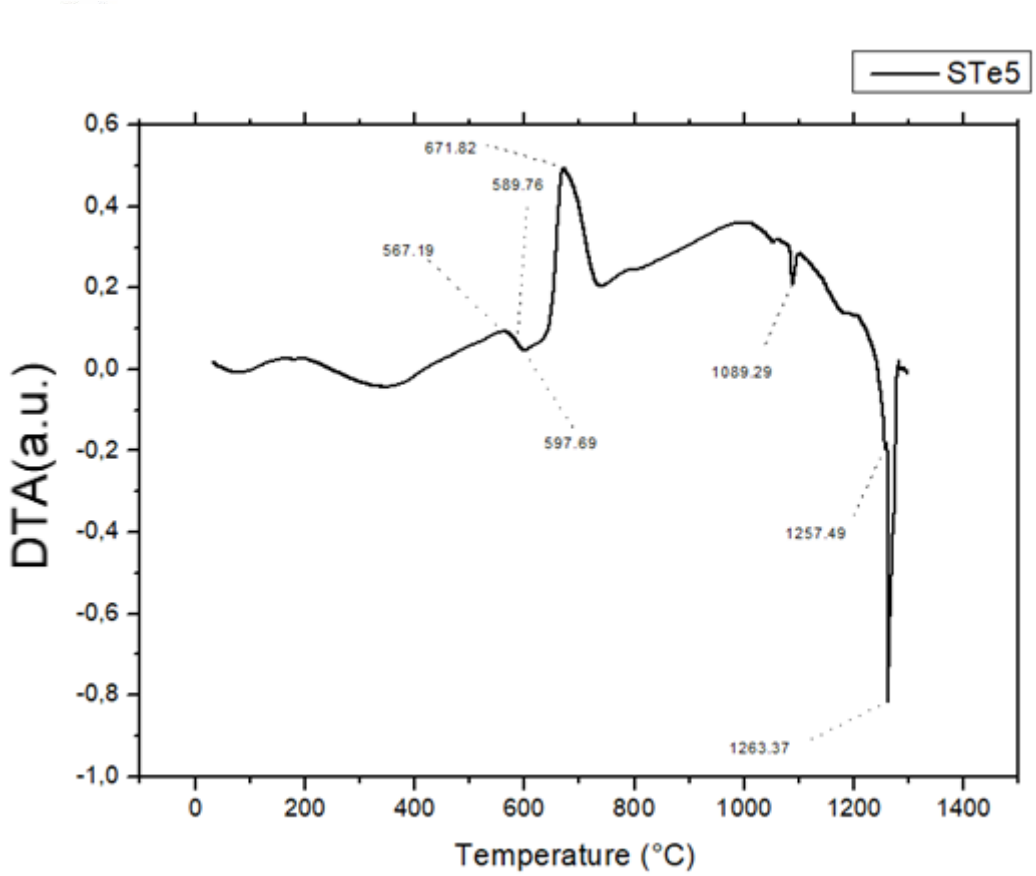

Figure 3.12: Thermal analysis result of STe5 composition.

Besides, the temperatures peaks T_{c1} and T_{c2} seen on each curves (**figure 3.10-3.11-3.12**) revealed the possible nucleation of two different crystalline phases for all samples. However, all DTA curves exhibit an endothermic peak T_{m1} and T_{m2} which is due to melting. Also in this case, the presence of a melting point involved melting of microcrystals found in crystallization processes. The difference between the three curves of samples is the value of T_{c2} for STe5 which differs by several degrees from STe0 and STe1 values. Overall, a shift of the characteristic temperatures toward lower values can be observed with increasing amounts of tellurium, especially for the glass STe5.

3.4 X-ray diffraction

X-ray diffraction was used to analyze the structure of the synthesized glasses. The obtained XRD patterns, before soaking in SBF and TRIS, have the characteristic amorphous halo between 25° and 35° as showed below (**figure 3.13-3.14-3.15**), any crystallization peak was observed, confirm the amorphous nature of the investigated materials.

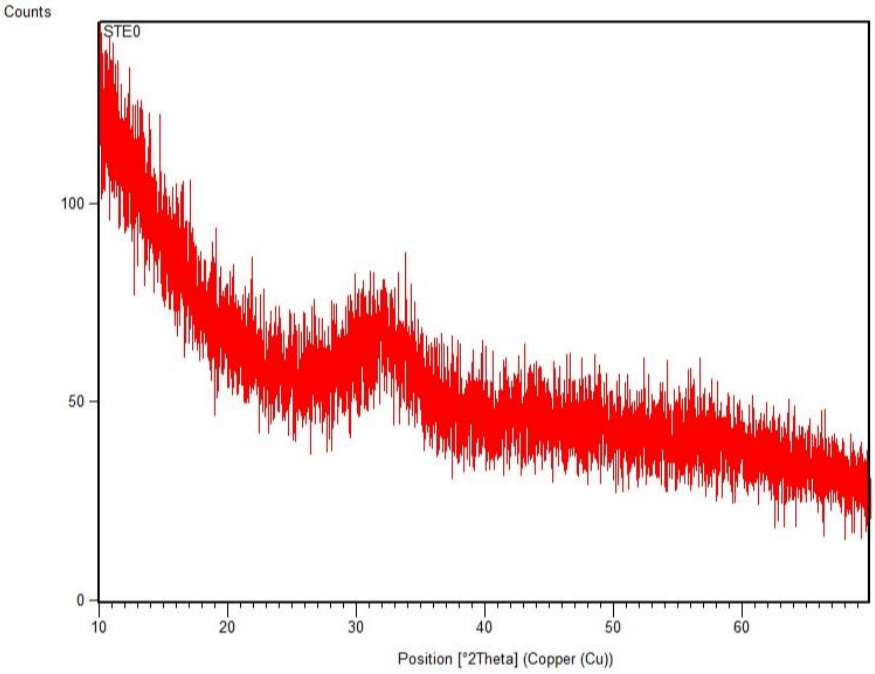

Figure 3.13: XRD pattern of the obtained STe0 composition.

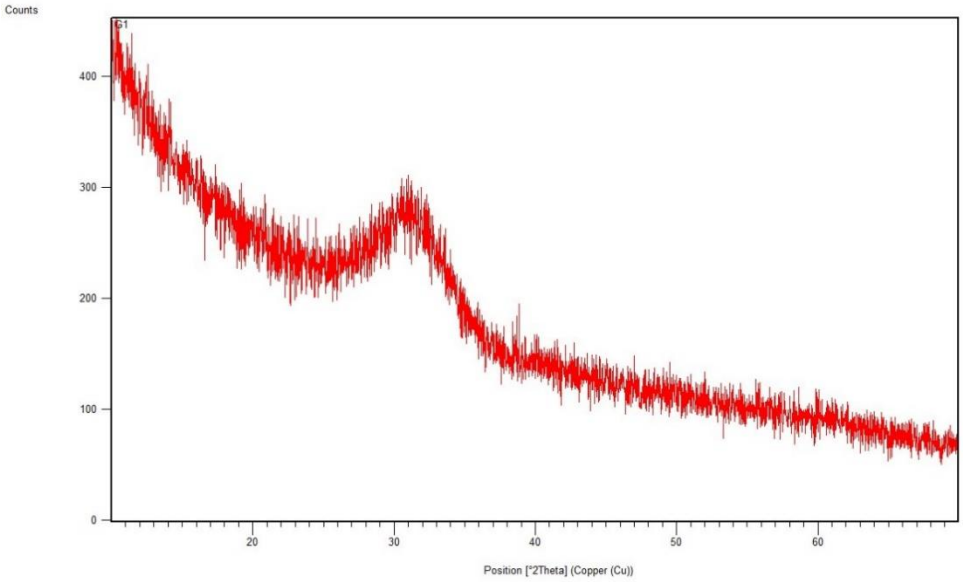

Figure 3.14: XRD pattern of the obtained STe1 composition.

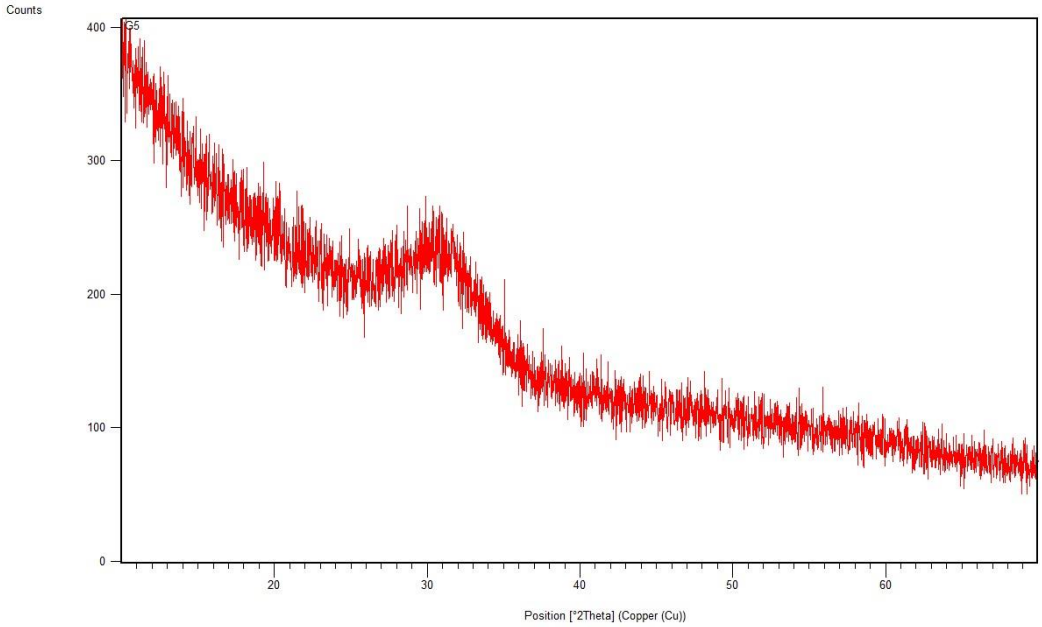

Figure 3.15: XRD pattern of the obtained STe5 composition.

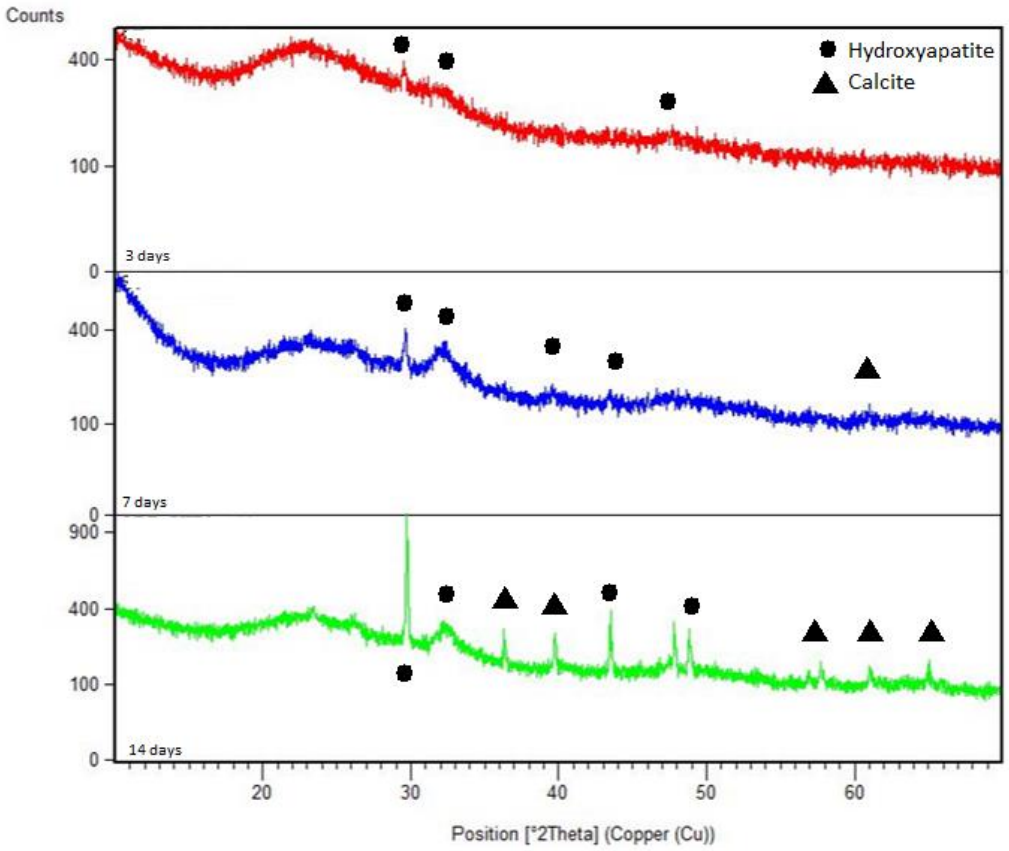

Figure 3.16: XRD patterns of the STe0 samples after immersing in SBF for 3, 7 and 14 days.

Figure 3.16 shows the XRD spectra of Ste0 after immersion in SBF for 14 days. The peaks located at 28.681° and 32.054° correspond to the hydroxyapatite, which already appeared after 3 days. Hydroxyapatite peaks became more evident after 7 days and new small peaks appeared at 39.673°, 46.679° and 49.498°. Additional peaks corresponding to calcite barely emerged at 36.039°, 42.244°, 56.678°, 57.517°, 61.527° and 65.796° after 7 days and increased in the crystallinity till 14 days.

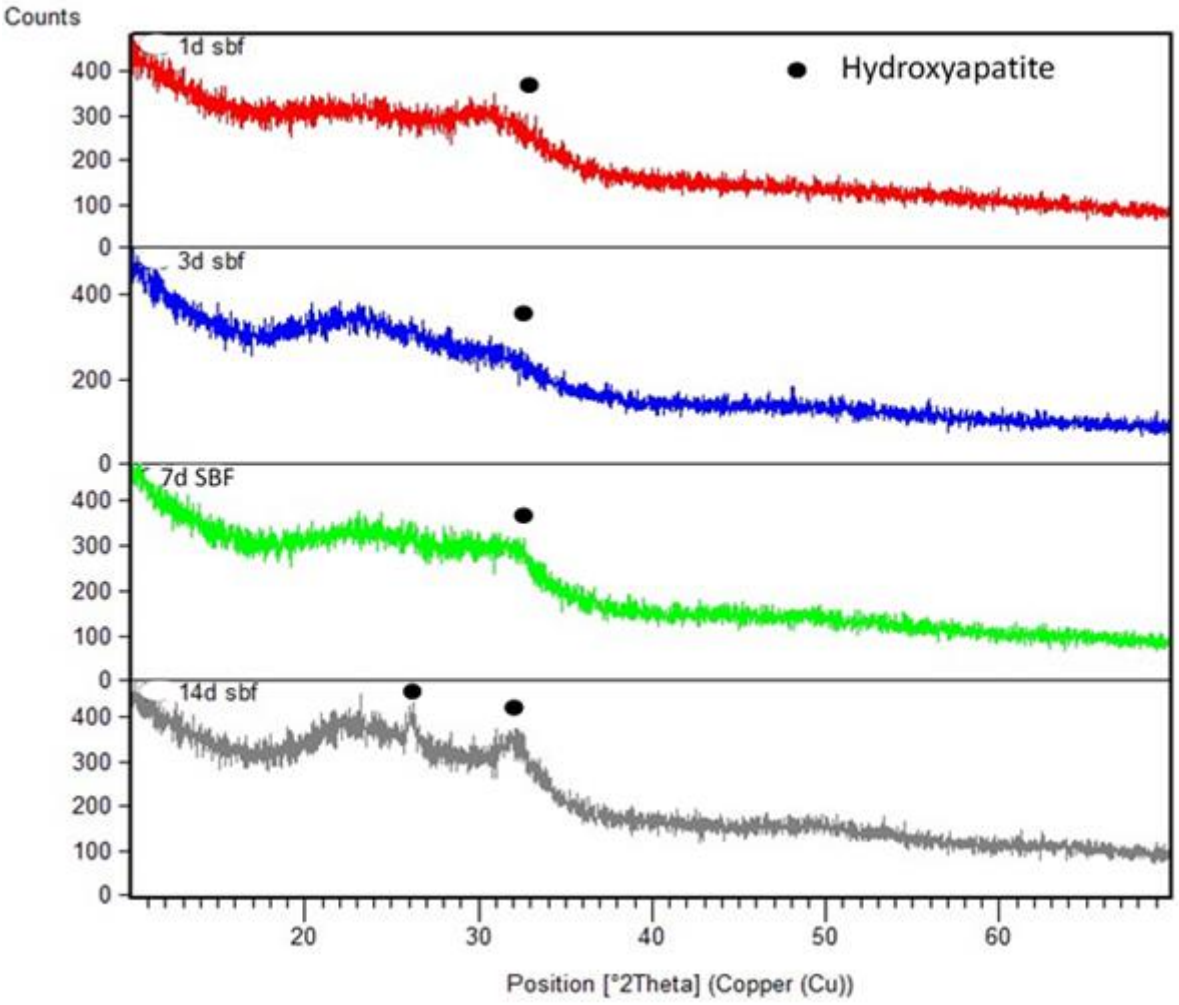

Figure 3.17: XRD patterns of the STe1 samples after immersing in SBF for 1, 3, 7 and 14 days.

In the case of STe1 (**figure 3.17**), a large peak ascribable to HAp at about 32.054° was observed after 1 day. This peak became more evident after 7 days of immersion and increases till 14 days. After 14 days, a slight and sharp peak corresponding again to hydroxyapatite was discernable at 25.879°. Regarding STe5 (**figure 3.18**) a large peak is barely visible after 1 days for STe5 [3.15]. Although, STe5 appeared to be less bioactive than ST0 and STe1.

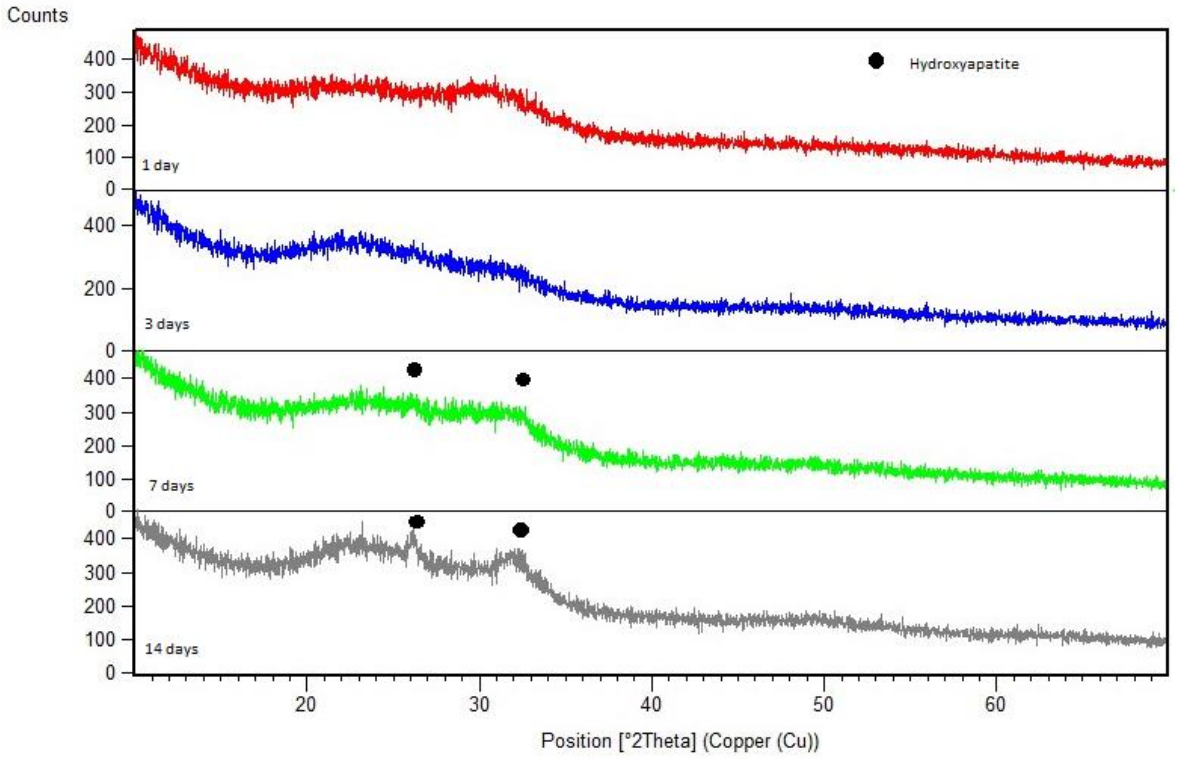

Figure 3.18: XRD patterns of the STe5 samples after immersing in SBF for 1, 3, 7 and 14 days.

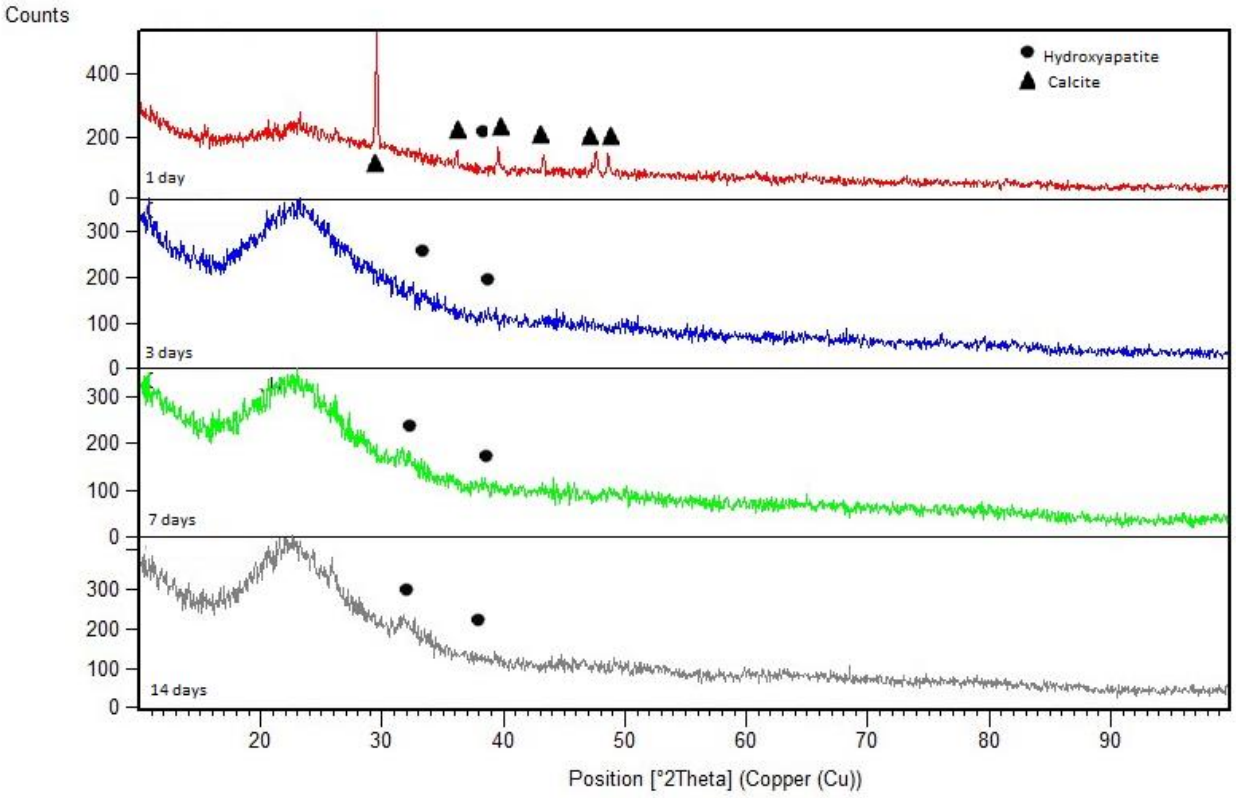

Figure 3.19: XRD patterns of the STe1 samples after immersing in TRIS for 1, 3, 7 and 14 days.

It is evident form the XRD pattern of STe1 (**figure 3.19**) in TRIS that peaks of calcite were found around 31.156°, 36.038°, 39.489°, 43.244°, 47.625° and 48.615°, whereas the peaks of hydroxyapatite were at 25.879° and 32.054°. All these peaks appeared after 1 day.

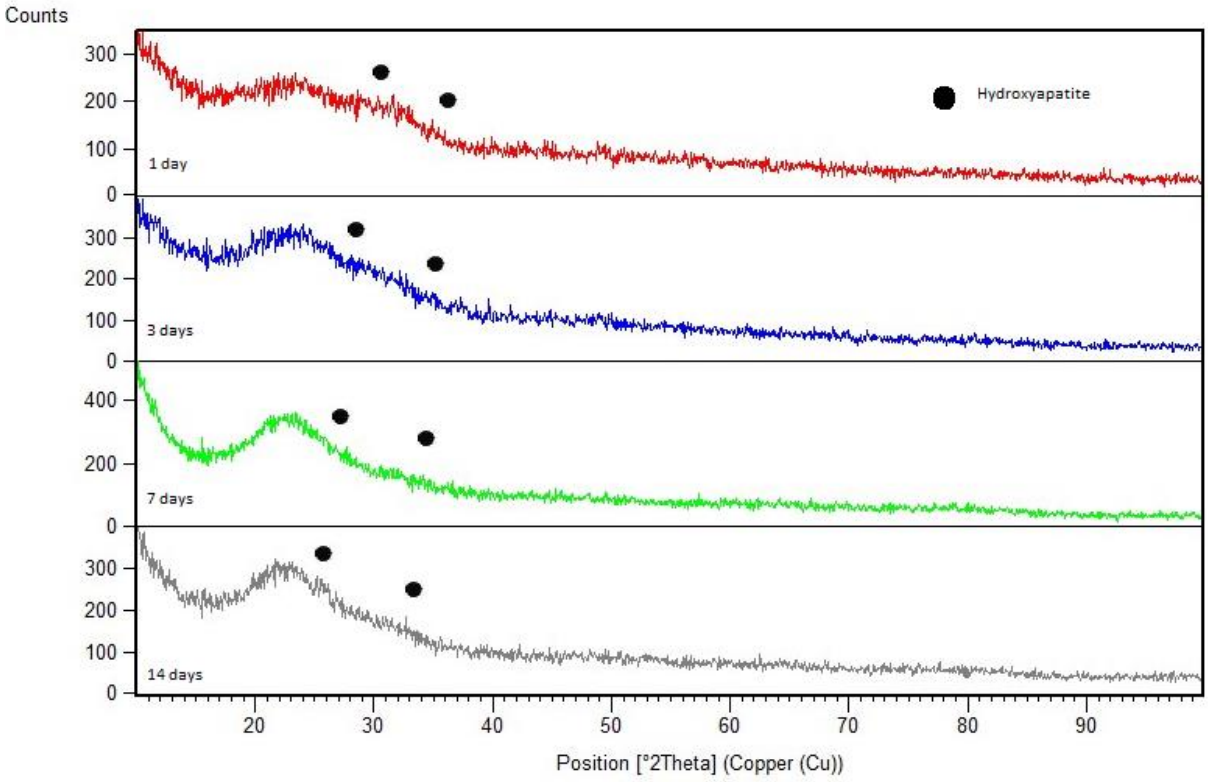

Figure 3.20: XRD patterns of the STe5 samples after immersing in TRIS for 1, 3, 7 and 14 days.

As for STe5 in TRIS (**figure 3.20**), it is clear that peaks appear as quick as the SBF one. Hydroxyapatite peaks can be observed at 25.879° and 32.054° after already 1 day of immersion.

3.5 Fourier Transform Infrared Spectroscope

As already mentioned, FTIR measurements have been intensively used in this work to study the functional groups in the glass compositions after and before immersion in TRIS and SBF solution. The FTIR curves of the bioactive glasses used as reference (before immersion) can be seen in **figure 3.21**. A broad peak at 707 cm^{-1} can be assigned to Si-O-Si bending vibration [186]. This peak is significantly more marked for STe5. The sharp peak positioned at 899 cm^{-1} was attributed to Si-O-Si stretching with non-bridging oxygen (Si-O-NBO) per SiO_4 tetrahedron groups [187]. Peaks at 850 cm^{-1} (for STe1 and STe5) and 870 cm^{-1} (for STe0) are assigned to carbonates adsorbed on the surface [188]. The shoulder band at 1010-1020 cm^{-1} could correspond to the asymmetric stretching mode of Si-O, while the band at 1350-1500 cm^{-1} to stretching mode of $\nu_3(CO_3^{2-})$ carbonate group [189] [188].

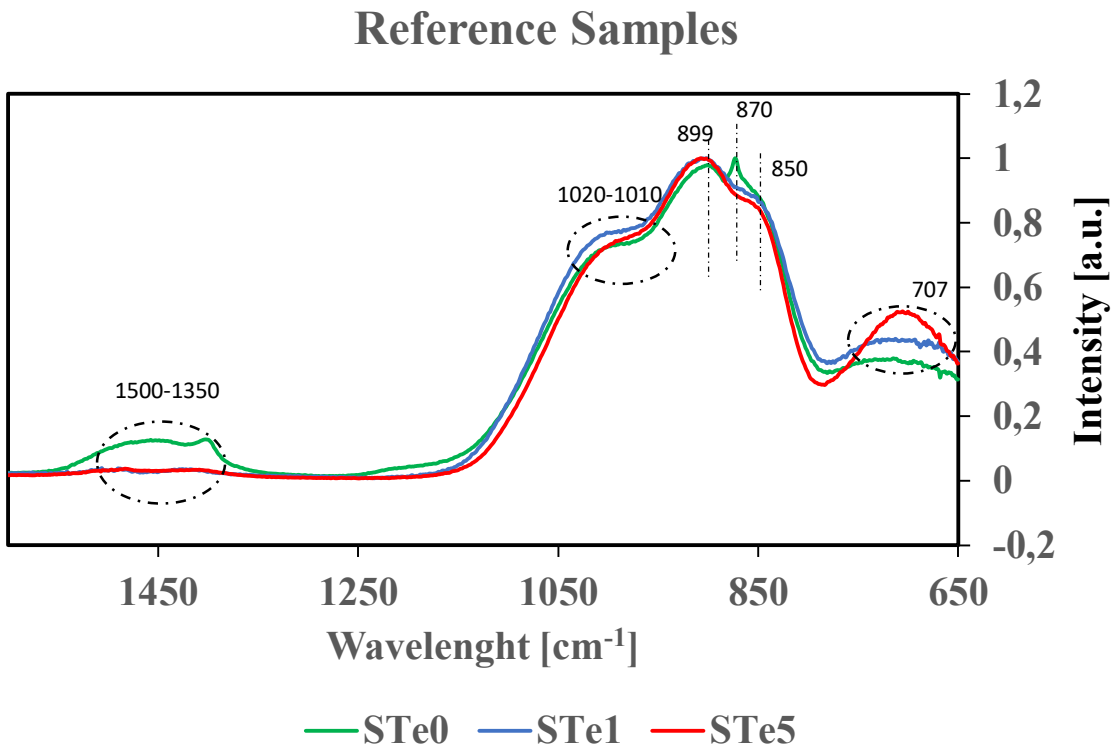

Figure 3.21: FTIR spectra of STe0, STe1 and STe5 reference samples.

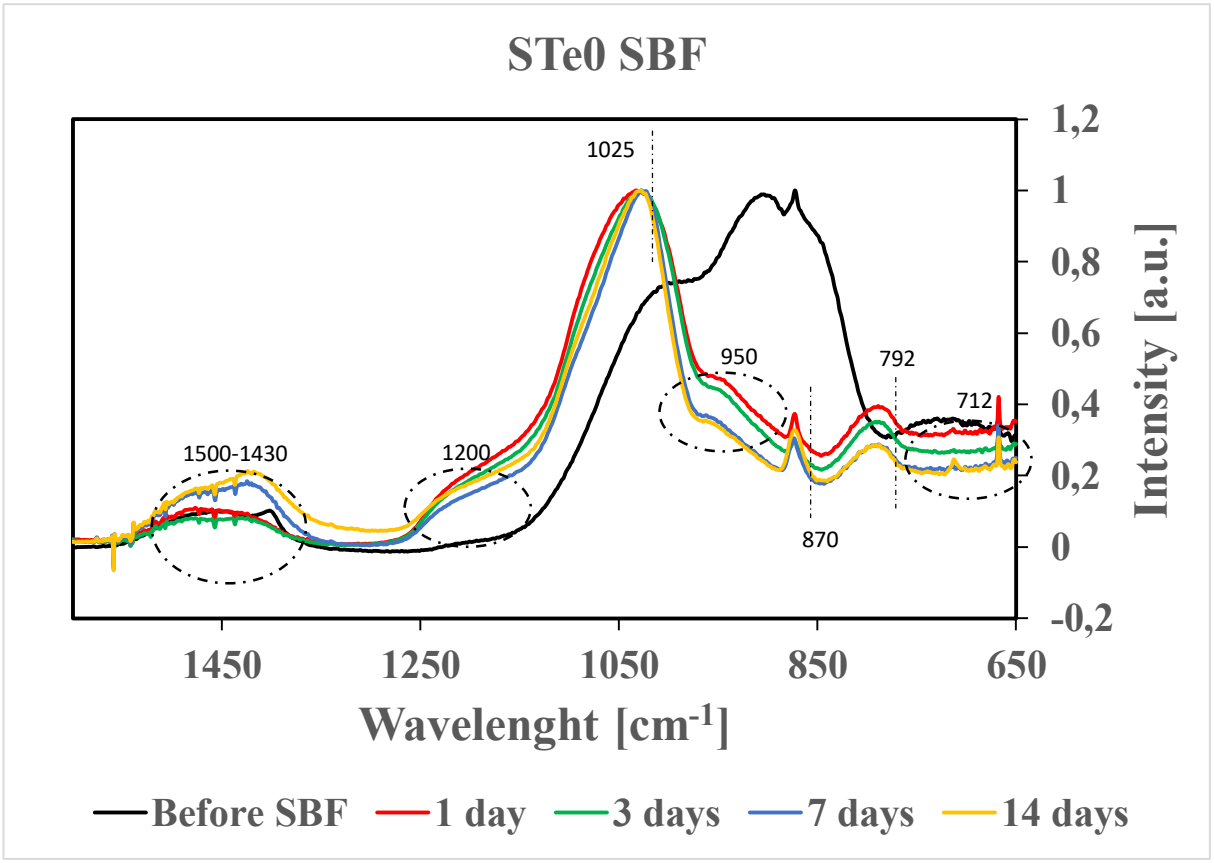

Figure 3.22: FTIR spectra of STe0 before and after soaking in SBF.

As regards STe0 after soaking in SBF (**figure 3.22**), a small characteristic band of calcite appears at 712 cm^{-1} [188]. The spectrum also shows the characteristic carbonated apatite band at 870 cm^{-1} [188]. The peak at 950 cm^{-1} is attributed to stretching of SiO_{NBO} due to the decrease contribute [188]. The wide peak at 1025 cm^{-1} is attributed to stretching mode of PO_4^{3-} group, whereas the band at 1200 cm^{-1} to vibration mode of Si-O-Si in the silica gel [188] [189]. Instead, the absorption of v_3 (CO_3) assigned to carbonate stretching mode at 1430-1500 cm^{-1} are due to the formation of a new HCA layer, whereas the small peak at 792 cm^{-1} is associated with the Si-O-Si vibration of 3D silica structure [188] [189].

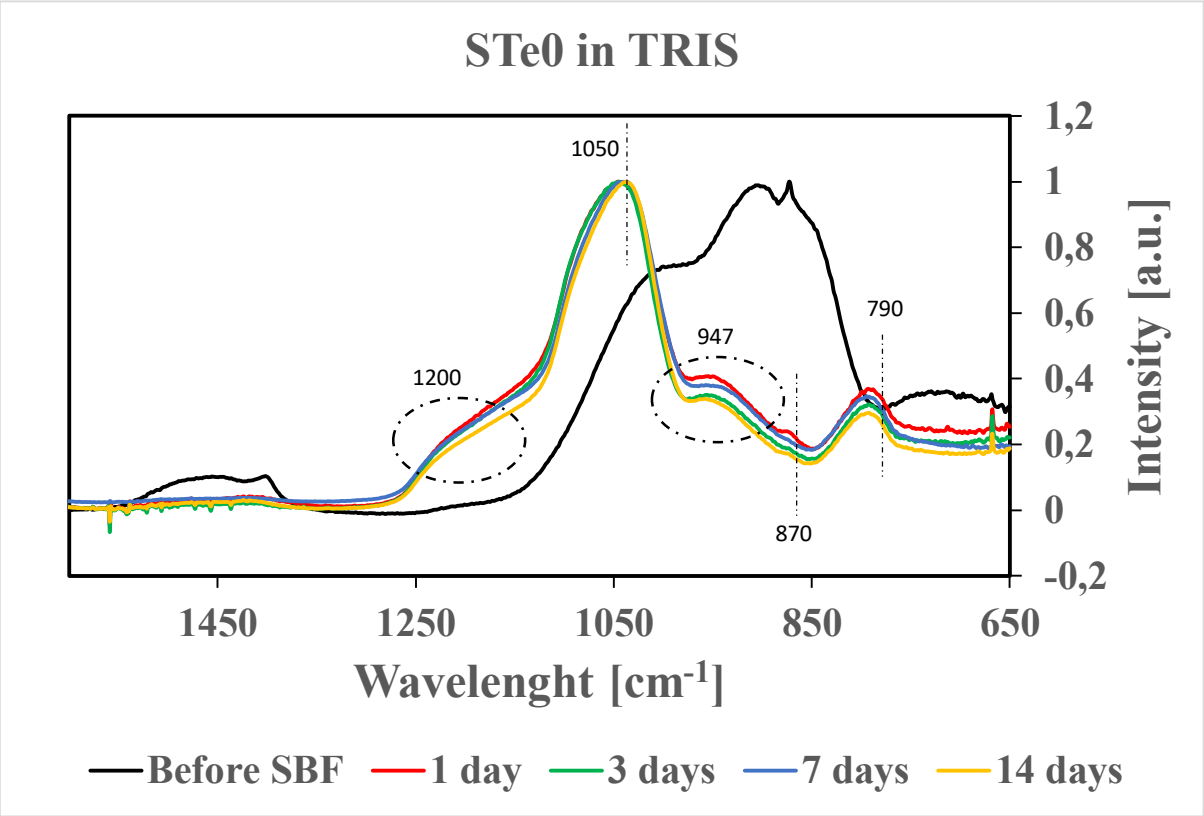

Figure 3.23: FTIR spectra of STe0 before and after soaking in TRIS.

However, regarding STe0 in TRIS (**figure 3.23**), the situation changes a little bit. The strongest absorption band at 1050 cm^{-1} can be related to P-O stretching mode of [PO_4^{-}] group, while the bands 790 cm^{-1}correspond to Si-O-Si vibration of 3D silica structure [188]. A small peak can be observed at 870 cm^{-1} and it is related to the carbonate apatite [188]. A barely visible peak at 712 cm^{-1} is attributed to the calcite [188]. Moreover, the small shoulder at 947 cm^{-1} corresponds to stretching SiO_{NBO} [188]. The soulder identified at 1200 cm^{-1} is referred to vibrational mode ν(Si-O-Si) in the silica gel [188].

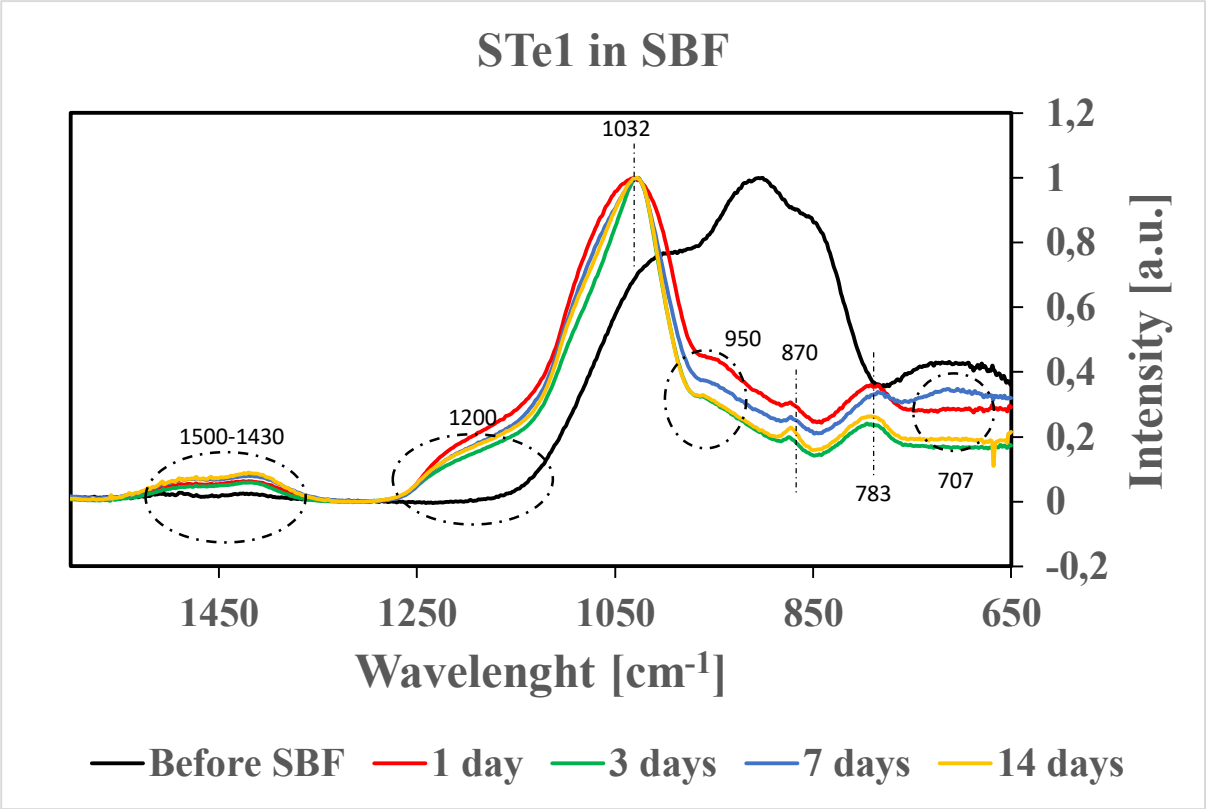

Figure 3.24: FTIR spectra of STe1 before and after soaking in SBF.

In the case of the STe1 in SBF (**figure 3.24**), the spectral curve appears similar to STe0 in SBF but differs in two respects: the small peak at 783 cm^{-1} is assigned to the Si-O-Si vibration 3D silica structure, whereas the band at 950 cm^{-1} and 707 cm^{-1} corresponds to stretching SiO_{NBO}, and to the Te-O vibration mode in the symmetric equatorial TeO4 groups and the contribute of the axial TeO4 units respectively [188] [190]. The spectra also show the presence of the stretching mode of C-O at around 1416 cm^{-1} and the asymmetric stretching mode of PO_4^{-3} at 1032 cm^{-1} [189]. Two small shoulders are identified: at 950 cm^{-1} attributed to stretching SiO_{NBO} and at 1200 cm^{-1} to vibrational mode ν(Si-O-Si) in the silica gel [188]. As well, it can be observed the doublet of carbonate species around 1500-1430 cm^{-1} [1] [189].

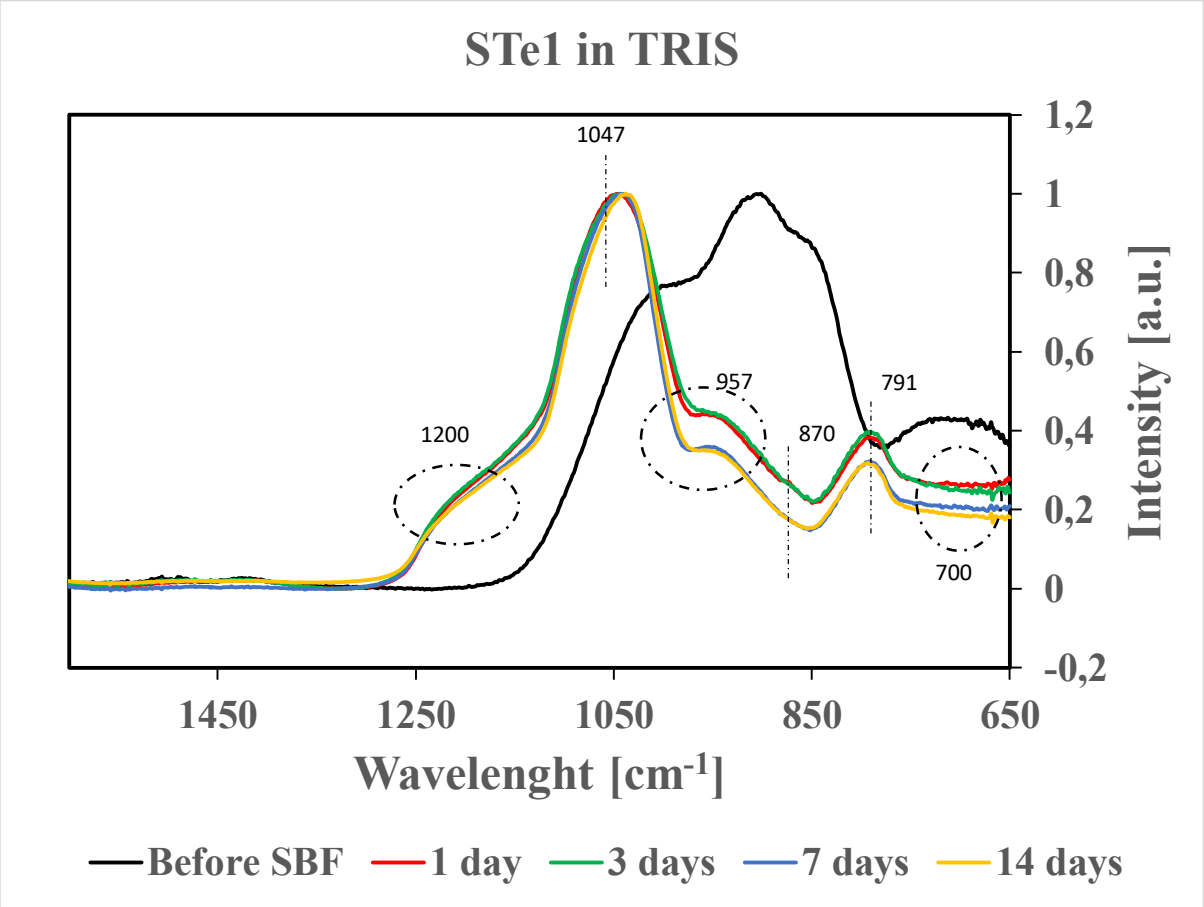

Figure 3.25: FTIR spectra of STe1 before and after soaking in TRIS.

However, for the STe1 in TRIS (**figure 3.25**), the decreasing of Si is due to stretching SiO_{NBO} and it is located at 957 cm^{-1}, while Si-O-Si vibration 3D silica structure is identified at around 791 cm^{-1} but that could be the other way around [188]. The highest peak at 1047 cm^{-1} corresponds to stretching mode of P-O [189]. The characteristic peak of Te-O vibration mode in the symmetric equatorial TeO4 groups and the contribute of the axial TeO4 units is positioned at lower frequency, 700 cm^{-1}, whereas the shoulder referred to the silica gel is positioned at 1200 cm^{-1} [188] [190]. The band of carbonated apatite is located at 870 cm^{-1} [188].

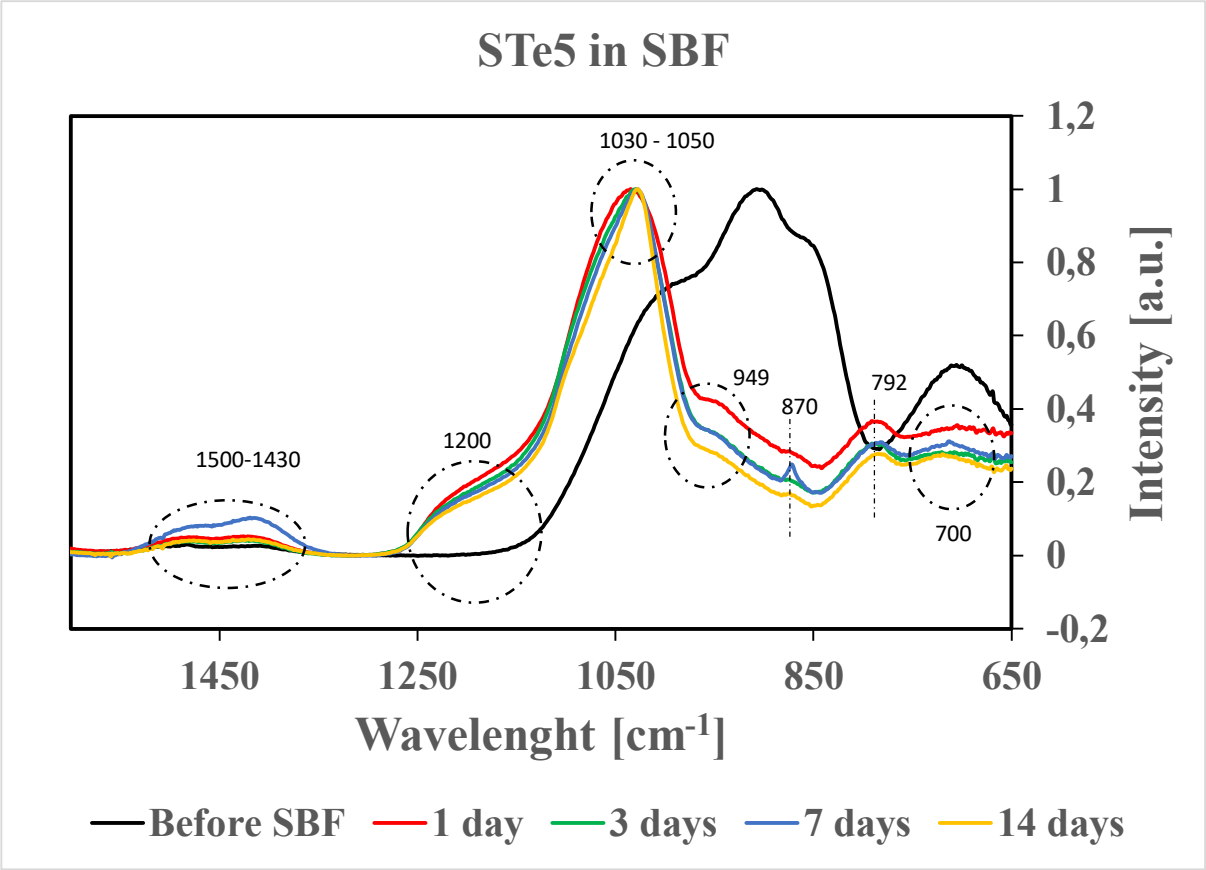

Figure 3.26: FTIR spectra of STe5 before and after soaking in SBF.

Then, on STe5 in SBF (**figure 3.26**) , symmetric stretching vibration vibration of Si–O– Si of non-bridging oxygen is assigned to the peaks 949, whereas 700 cm^{-1}can be attributed to the Te-O vibration mode in the symmetric equatorial TeO4 groups and the contribute of the axial TeO4 units [188] [190]. The peak at 870 indicates the formation of carbonate apatite, whereas peak at 783 cm^{-1} is related to asymmetric stretching of 3D Si-network [189]. The peak at 1200 cm^{-1} corresponds to vibrational mode ν(Si-O-Si) in the silica gel groups, as already seen before [188]. The magnitude of the doublet C-O and P-O peaks located between 1423-1422 cm^{-1} and 1032-1050 cm^{-1} increases relative as the immersion time is longer for all the samples [189].

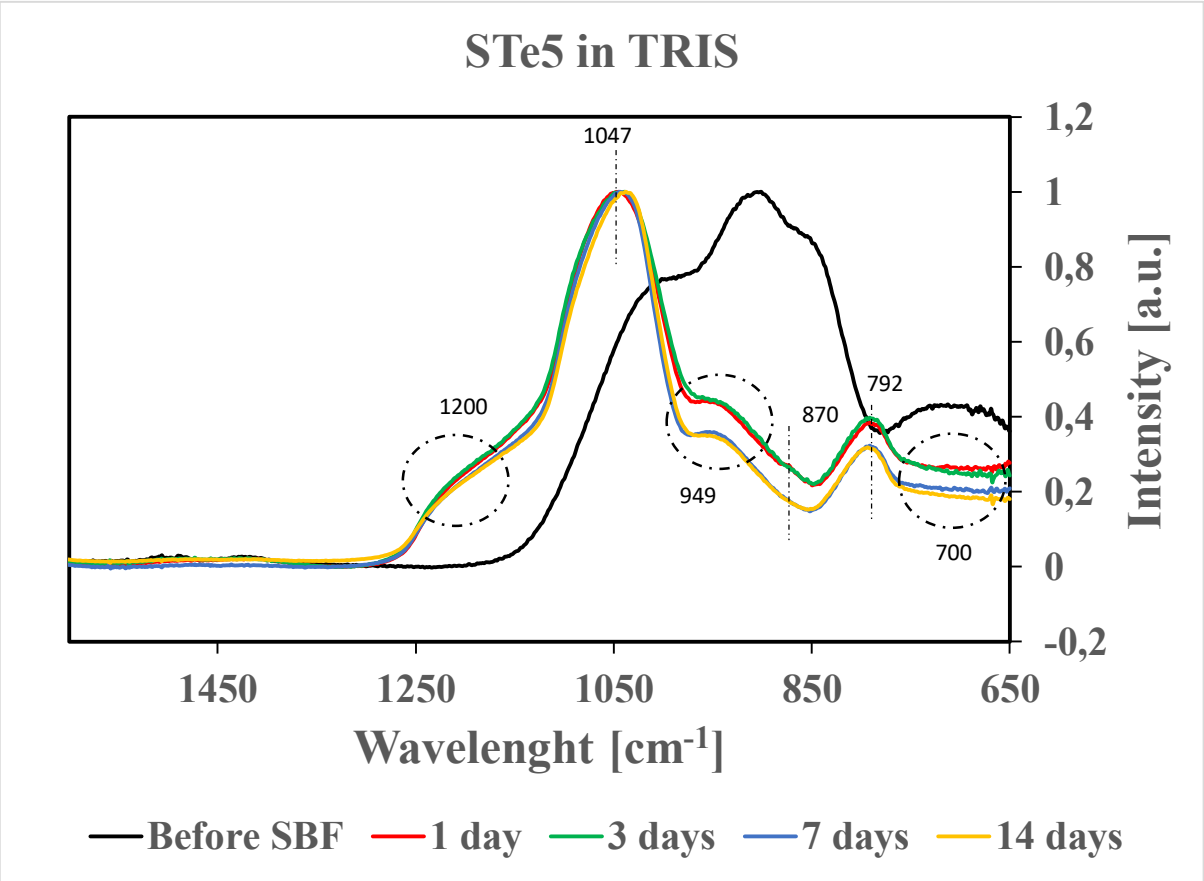

Figure 3.27: FTIR spectra of STe5 before and after soaking in TRIS.

And finally, STe5 immersed in TRIS (**figure 3.27**) exhibits a sharp and tall peak at 1047 cm^{-1} attributable to P-O stretching mode of [PO_4^-] group due to formation of calcium phosphate. The spectrum also reveals a shoulder at 1200 cm^{-1} referred to the vibrational mode ν(Si-O-Si) in the silica gel. A small but distinct peaks at 949 cm^{-1} can be assigned to stretching with non-bridging oxygen per SiO_4 tetrahedron groups [188]. Moreover, the peak at about 792 cm^{-1} is assigned to δ(Si-O-Si) 3D silica structure [188]. The weak band at 700 cm^{-1} can be attributed to Te-O vibration mode in the symmetric equatorial TeO4 groups and the contribute of the axial TeO4 units [190].

3.6 Inductively Coupled Plasma – Optical Emission Spectroscopy

In this section, the trends of ions released from STe0, STe1 and STe5 are showed (after immersion in SBF and TRIS at 37 °C for 1, 3, 7, and 14 days).

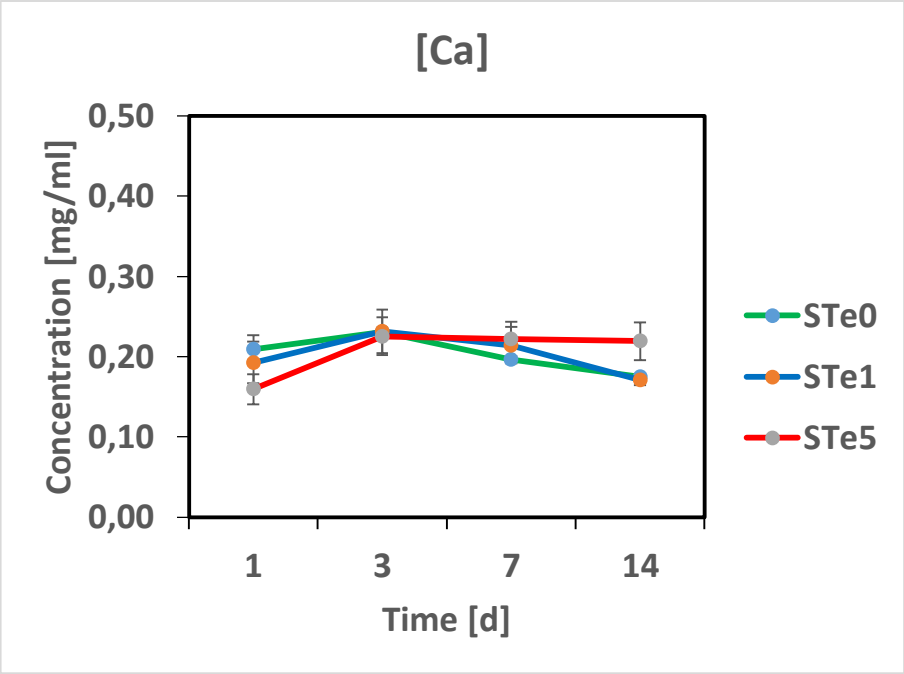

Figure 3.28: ICP analysis of the evolution of Ca concentration 100 ml SBF solution

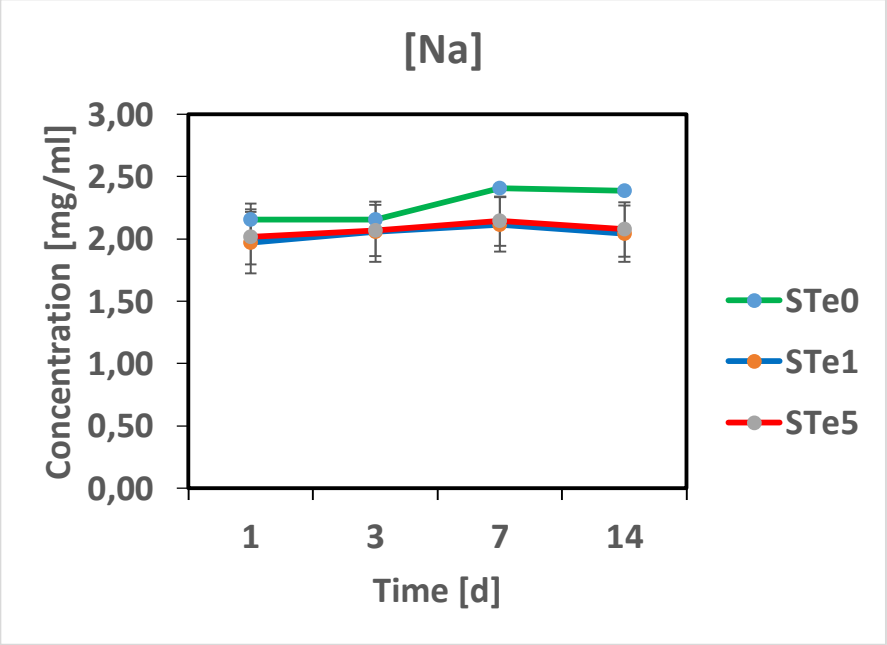

Figure 3.29: ICP analysis of the evolution of Na concentration 100 ml SBF solution.

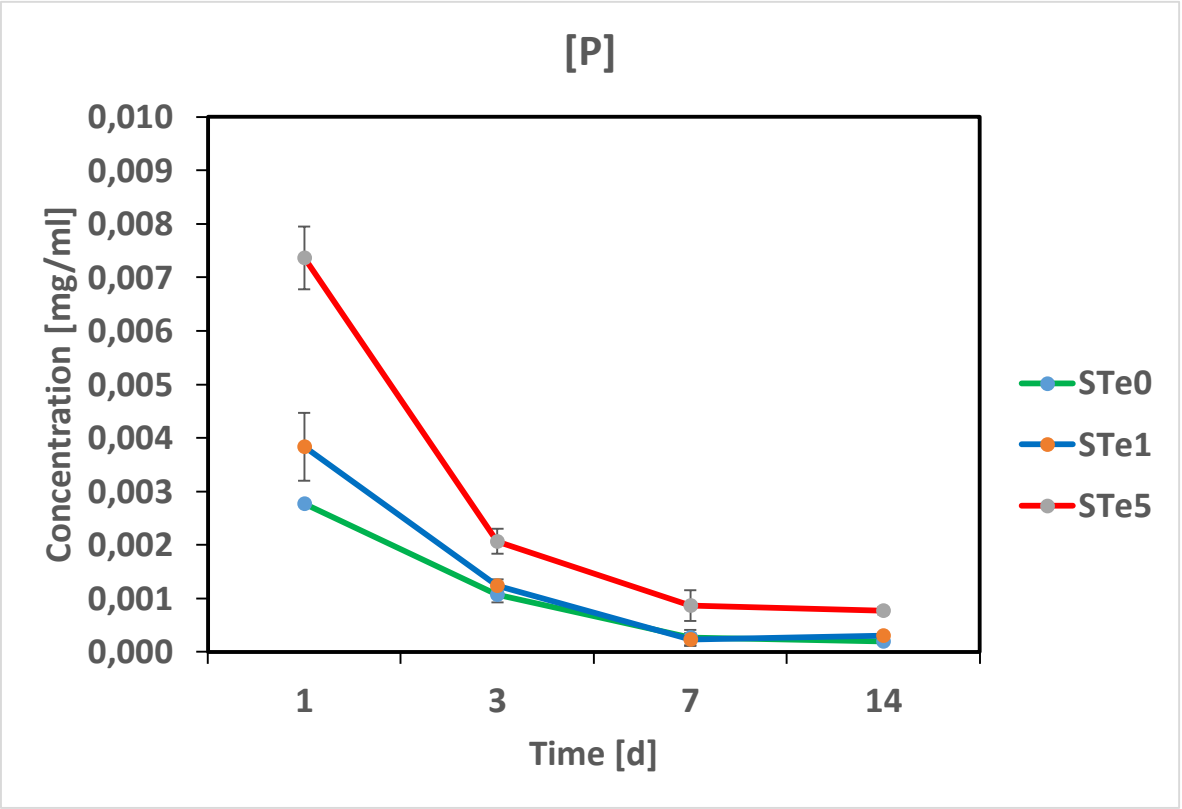

Figure 3.30: ICP analysis of the evolution of P concentration 100 ml SBF solution.

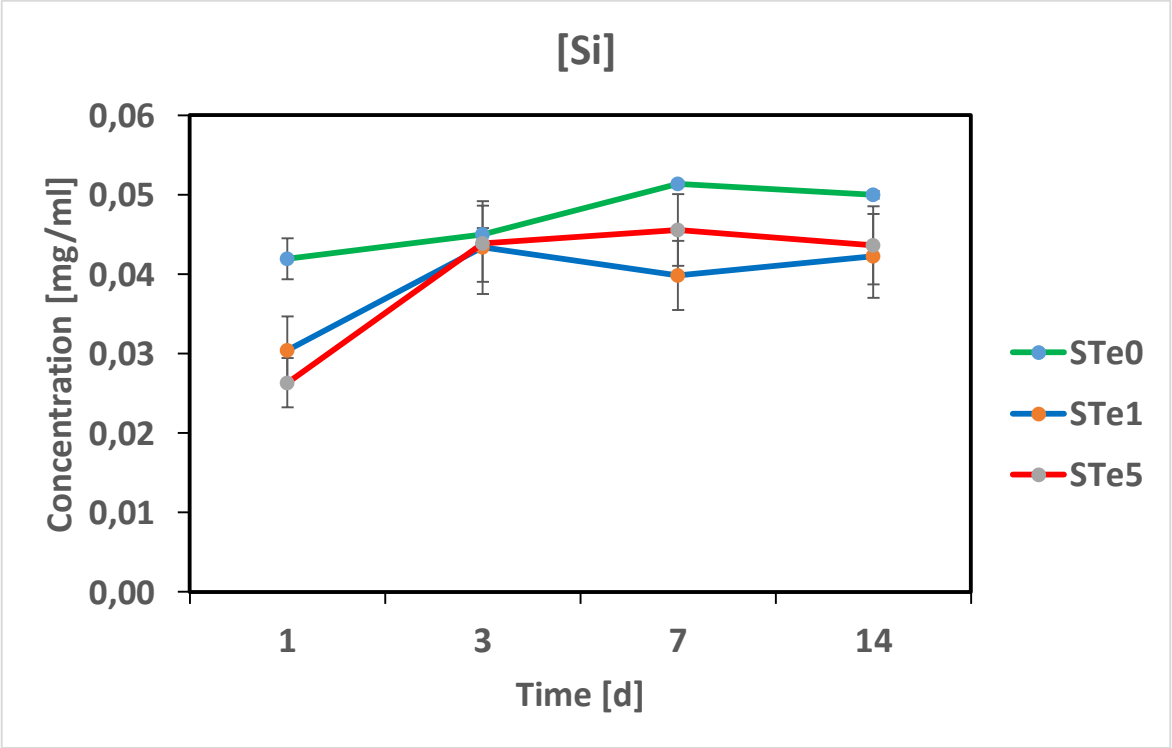

Figure 3.31: ICP analysis of the evolution of Si concentration 100 ml SBF solution.

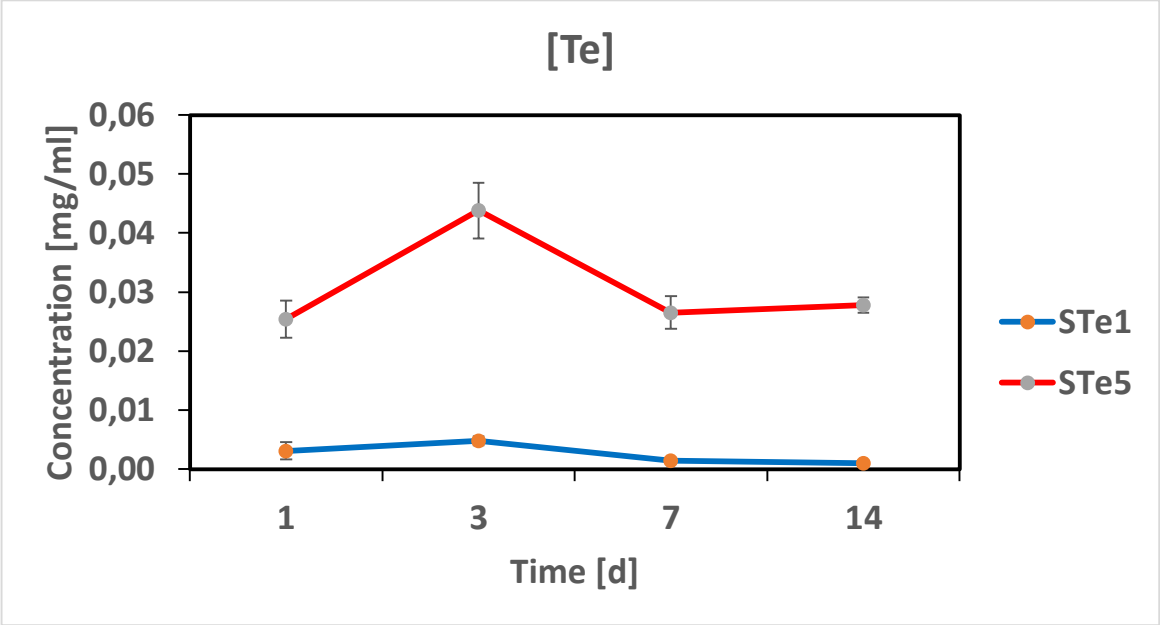

Figure 3.32: ICP analysis of the evolution of Te concentration 100 ml SBF solution.

The graph shows that the silicon concentrations (**figure 3.31**) in SBF generally increases with time for each samples. However, STe0 seems apparently to release more silicon than STe1 and STe5. On the contrary, phosphorous concentrations (**figure 3.30**) deacreses with time already from 1day immersion in SBF for each samples, evidencing the precipitation on glass surface. Although, after 7 days both the phosphorous and silicon releases are almost constant for each samples. However, calcium (**figure 3.28**) and sodium ion variations (**figure 3.29**) are not pronounced and no significant differences could be seen between STe0, STe1 and STe5 since samples are approximately constant over time. As opposed to the other ions, the change in the tellurium concentrations (**figure 3.32**) appears slightly different for STe1 and STe5. The Te concentration for STe5 starts to raise up to 3 days peaking in 3 days, after that, starts to deacrese up to 7 days, remained at similar level until the end of saoking period. For STe1, no pronounced differences in the dissolution of Te are observed.

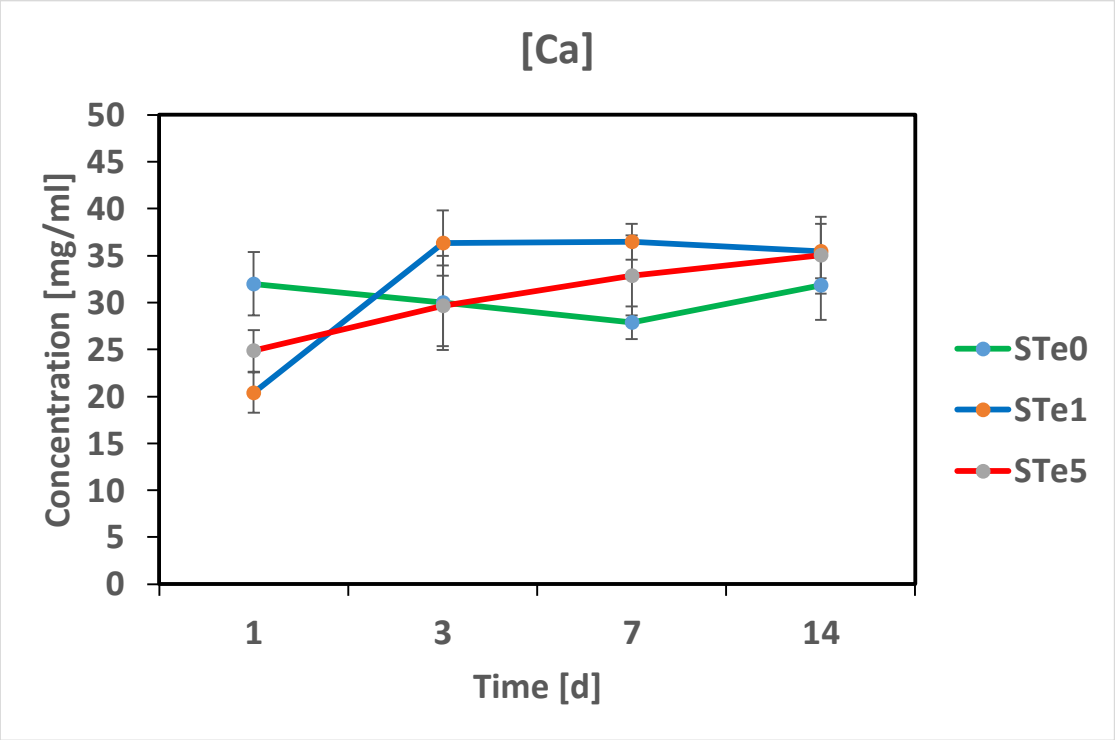

Figure 3.33: ICP analysis of the evolution of Ca concentration 100 ml TRIS solution.

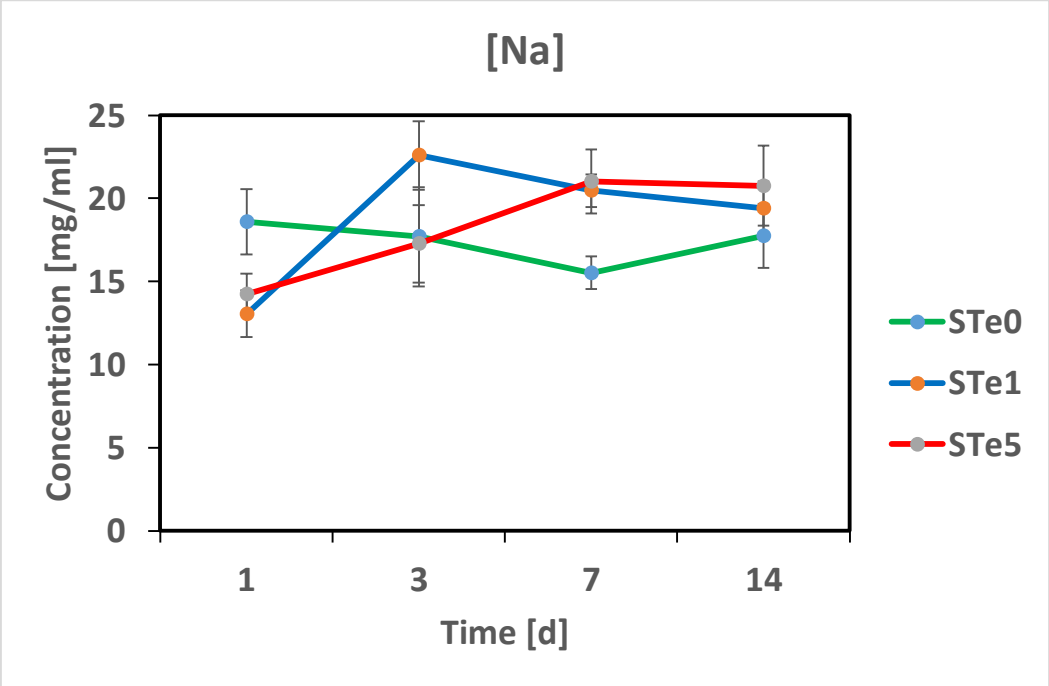

Figure 3.34: ICP analysis of the evolution of Na concentration 100 ml TRIS solution.

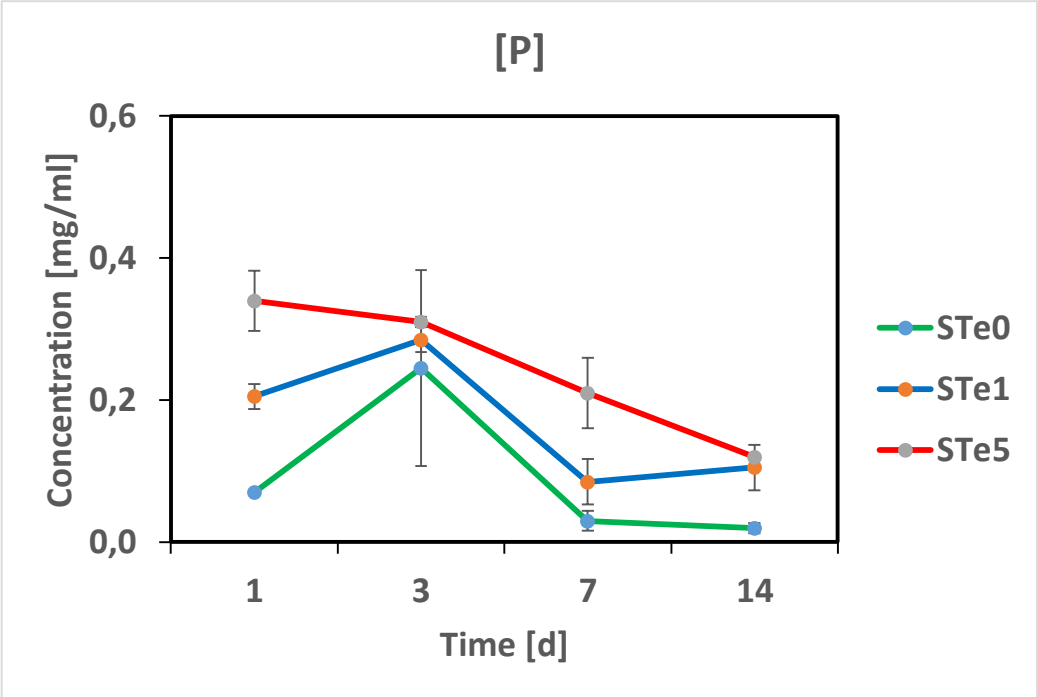

Figure 3.35: ICP analysis of the evolution of P concentration 100 ml TRIS solution.

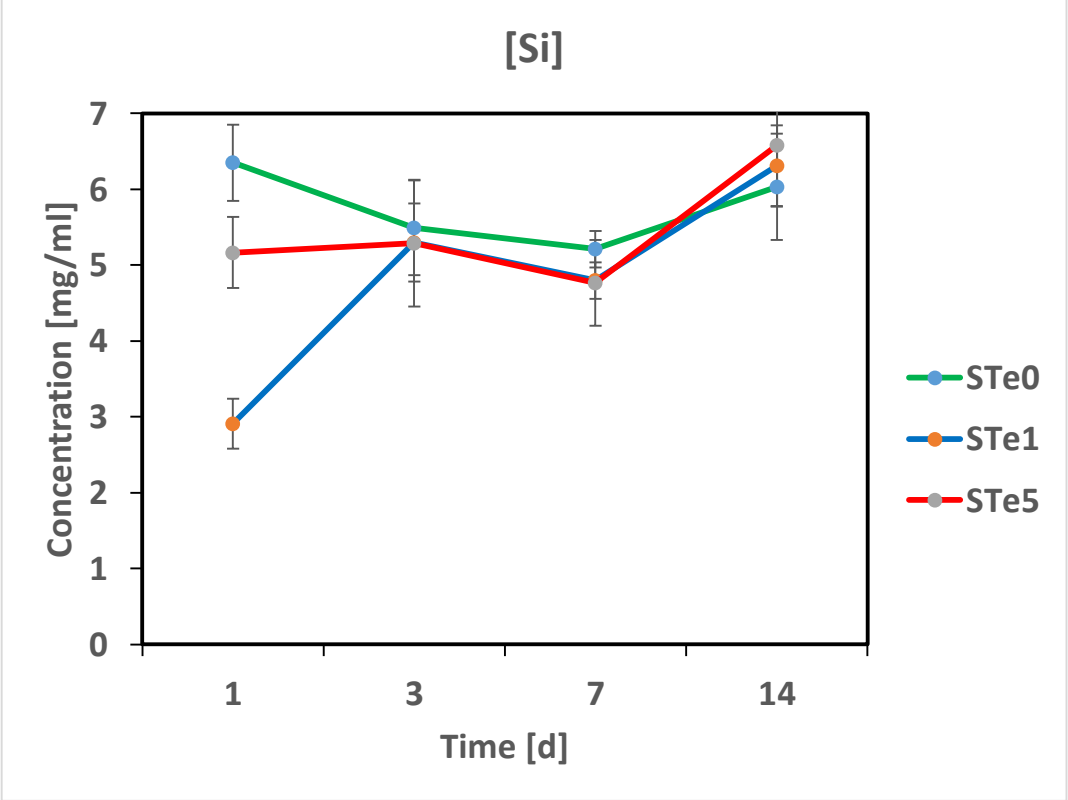

Figure 3.36: ICP analysis of the evolution of Si concentration 100 ml TRIS solution.

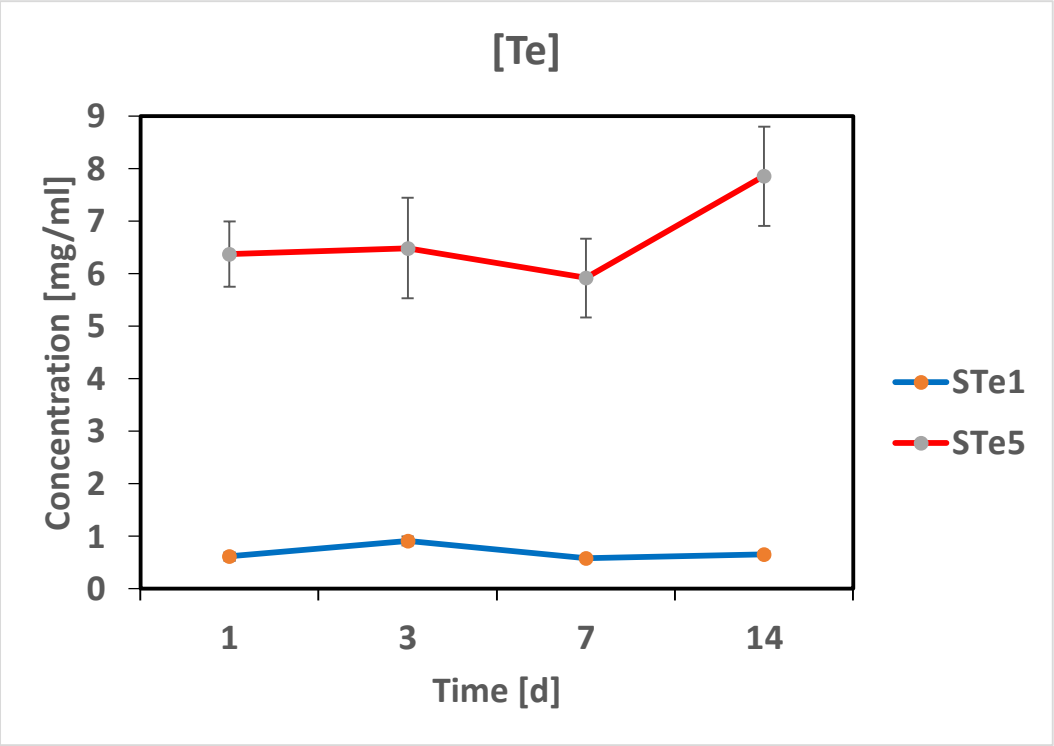

Figure 3.37: ICP analysis of the evolution of Te concentration 100 ml TRIS solution.

Ion release considerably changes considering TRIS buffer solutions from those observed in SBF. Calcium concentration (**figure 3.33**) increases over time for STe1 and STe5, showing a faster increasesfor STe1 than STe5 but remaining relatively costant after 3 days. STe0 first decrease up to 7 days though, then start to increase but far less pronounced than STe1 and STe5. Sodium (**figure 3.34**) showed a similar behavior as calcium for STe0. The concentration of sodium released into solution increases rapidly for STe1 up to 3 days of soaking. Then it decreases very slightly till 14 days, while for STe5 it increases more slowly than STe1 and after 7 days remains constant. The phosphorus concentration (**figure 3.35**) for STe5 decreases till the end of the immersion time, while for STe0 and STe1 P increase up to 3 days, then it decreases and remains apparently flat over time. The silicon concentration (**figure 3.36**) follows a complex trend. This trend seems to form an inflection for STe1 and STe5, so rise up to 3 days. An apparently plateu is reached, and then it starts to arise again after 7 days. In contrast, an initially decrease is observed for STe0, while the trend changes after 7 days and likely arises till 14 days. The tellurium level (**figure 3.37**) doesn't really change during the soaking period for STe1 but it drops considerably after 7 days for STe5.

3.7 Raman spectroscopy

Raman spectroscopy is able to monitor vibrational modes of functional groups as well as FTIR, since these techniques are complementary, as previously noted in chapter 2. The Raman spectra of samples before and after the immersion in SBF and TRIS are shown below.

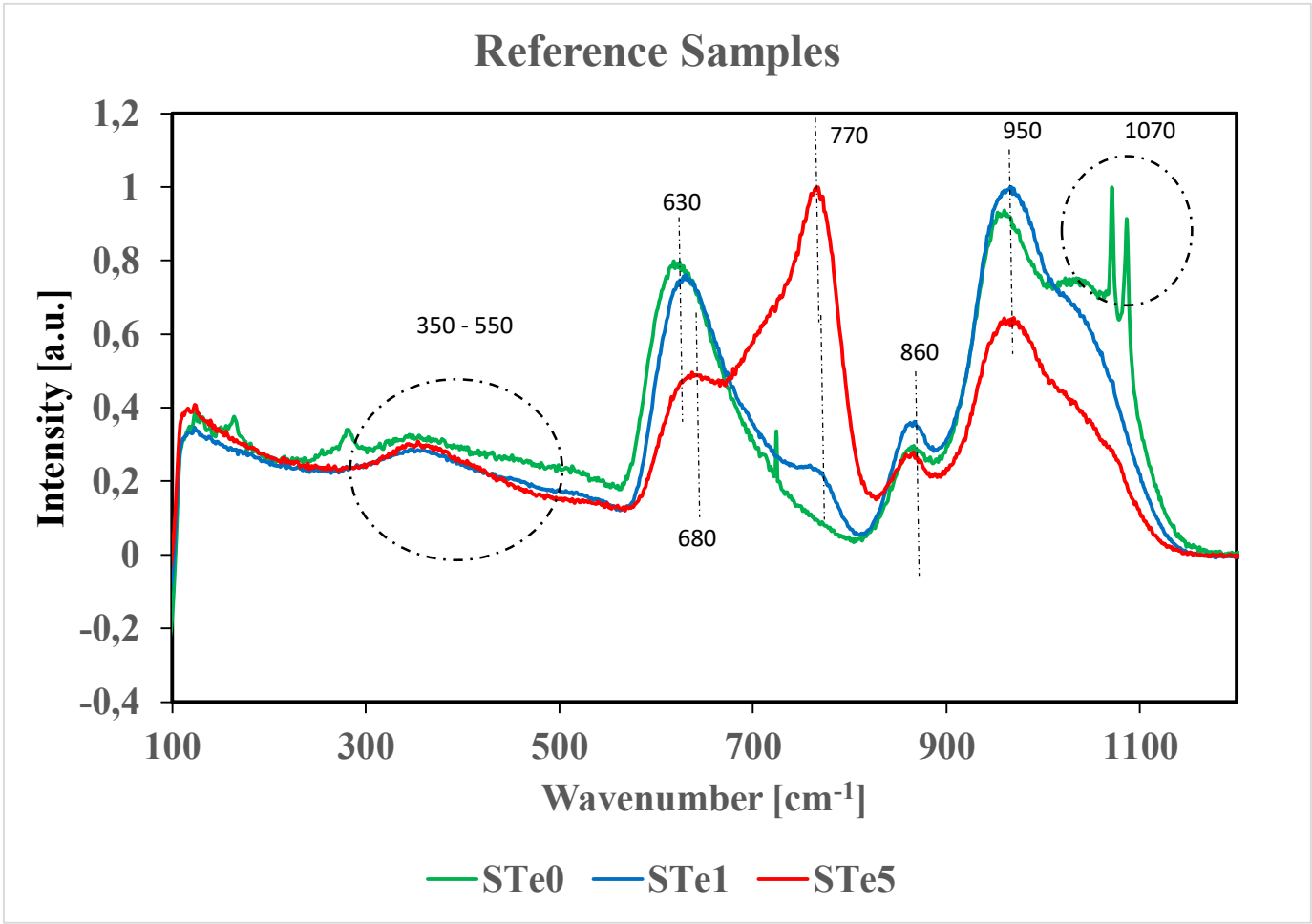

Figure 3.38: Raman spectra of reference samples.

Reference samples (**figure 3.38**) were first investigated. Beginning with low wavenumbers, a broad band in the 550–350 cm-1 range can be assigned to siliceous bulk vibrational modes for each samples [191]. Bands at 630 and 860 cm^{-1} indicates the presence of Si-O units, four non-bridging oxygen in symmetric stretching vibration, while the band 950 cm^{-1} is related to a symmetrical stretching of PO_4 group [192]. These bands are less evident for STe5, but it is possible to see a shoulder at 680 cm^{-1} related to asymmetric stretching vibrational Te-O bond of $[TeO_4]^{4-}$ [193]. Moreover, at 770 cm^{-1}, there is a peak referred to bending vibrational Te-O bond of $[TeO_3]^{2-}$ [193]. These peaks confirm the presence of tellurium in STe5, while it seems to be weaker in STe1. Lastly, a sharp peak doublet located at 1070 cm^{-1} can be assigned to carbonates adsorbed, but it appears only in STe0 [192].

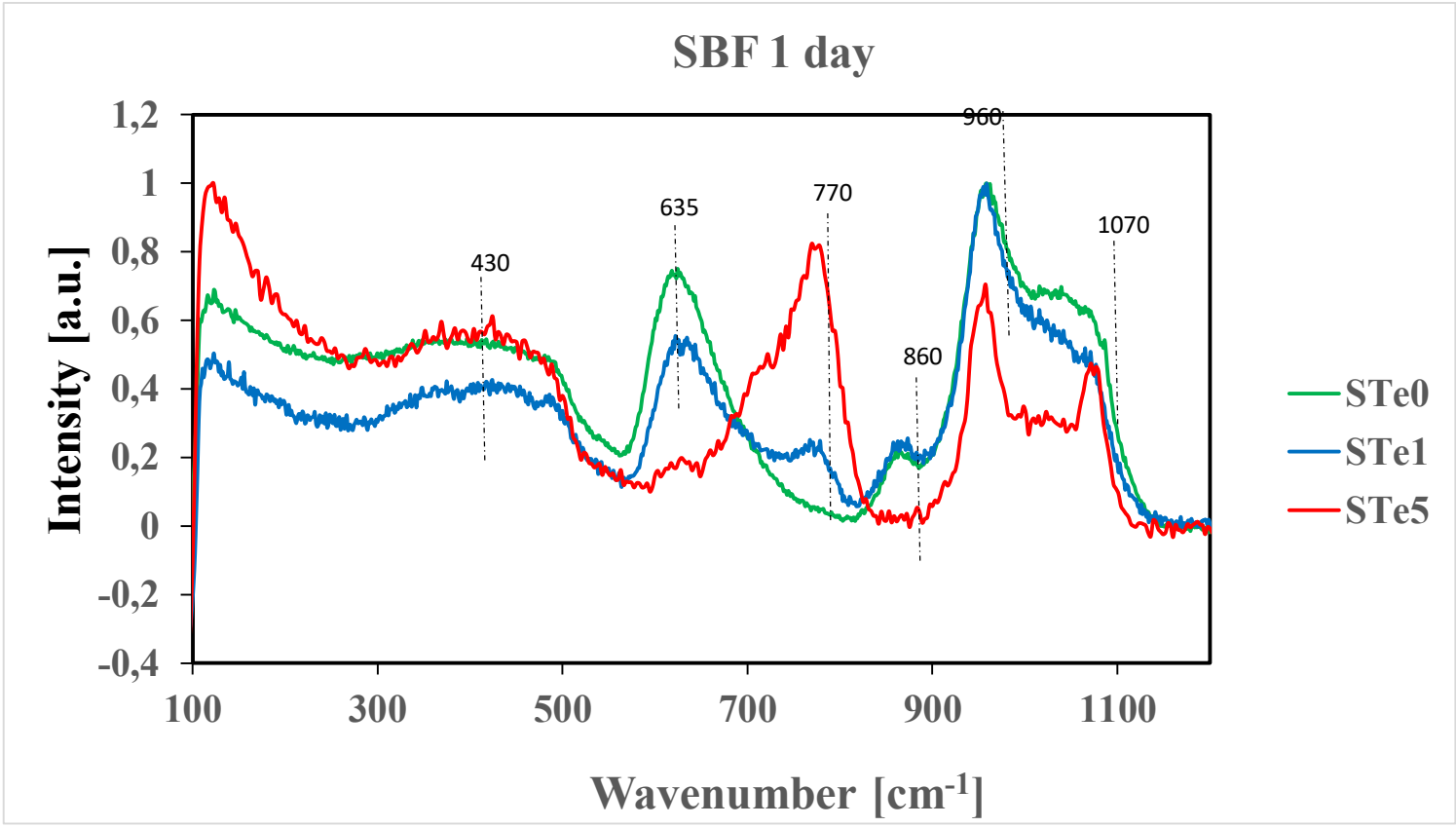

Figure 3.39: Raman spectra of STe0, STe1 and STe5 samples after 1 day of immersion in SBF.

In all the samples after immersion in the SBF for 1 day (**figure 3.39**), it can be seen the peak of P – O bending group centered at 430 cm^{-1} [191]. The intensity of the absorption bands at 635 cm^{-1} is related to Si-O-Si vibration groups decreases and products a shift to 580 cm^{-1} during immersion time from 1 day (**figure 3.39**) to 14 days (**figure 3.40**) for STe0 and STe1 [192]. That peak is not very noticeable for STe5. The band around 770 cm^{-1} is identified as bending vibrational Te-O bond of $[TeO_3]^{2-}$ and it remained visible till the last day of immersion [193]. Additionally, vibration (Si–O) of Si–OH groups is positioned at 976 cm^{-1} but it appeared only after 14 days. The Si – O – Si stretching mode of tetrahedral silicate units is also barely visible in the band located at 865 cm^{-1} after 1 day in SBF (**figure 3.39**) for STe0 and STe1, but it disappears on 14 days (**figure 3.40**) [194]. The peak at 960 cm^{-1} is assigned to the symmetric stretching of the orthophosphate group [194]. This peak was present in all the glasses spectra and became thinner from 1 day to 14 days.

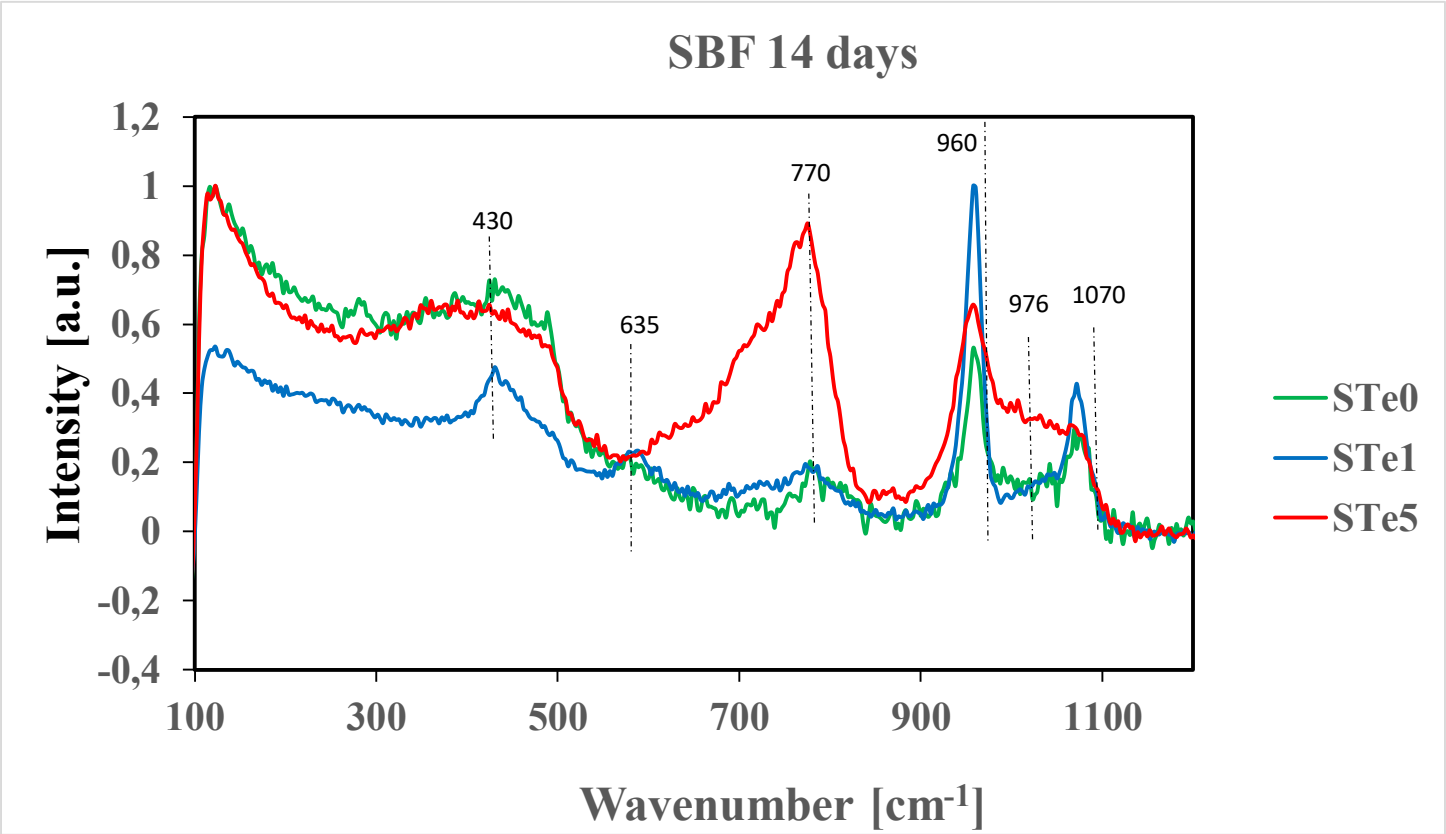

Figure 3.40: Raman spectra of STe0, STe1 and STe5 samples after 14 days of immersion in SBF.

The presence in the spectrum of a band at 1073 cm^{-1} is attributed to carbonate species [194]. This band is more evident and sharp for STe5 at 1 day and hard to determine by visual inspection for STe1 and STe0, however it became clearer for STe0 and STe1 after 14 days.

The figure shows the FTIR spectra of the samples soaking in TRIS after 1 (**figure 3.41**) and 14 days (**figure 3.42**) respectively.

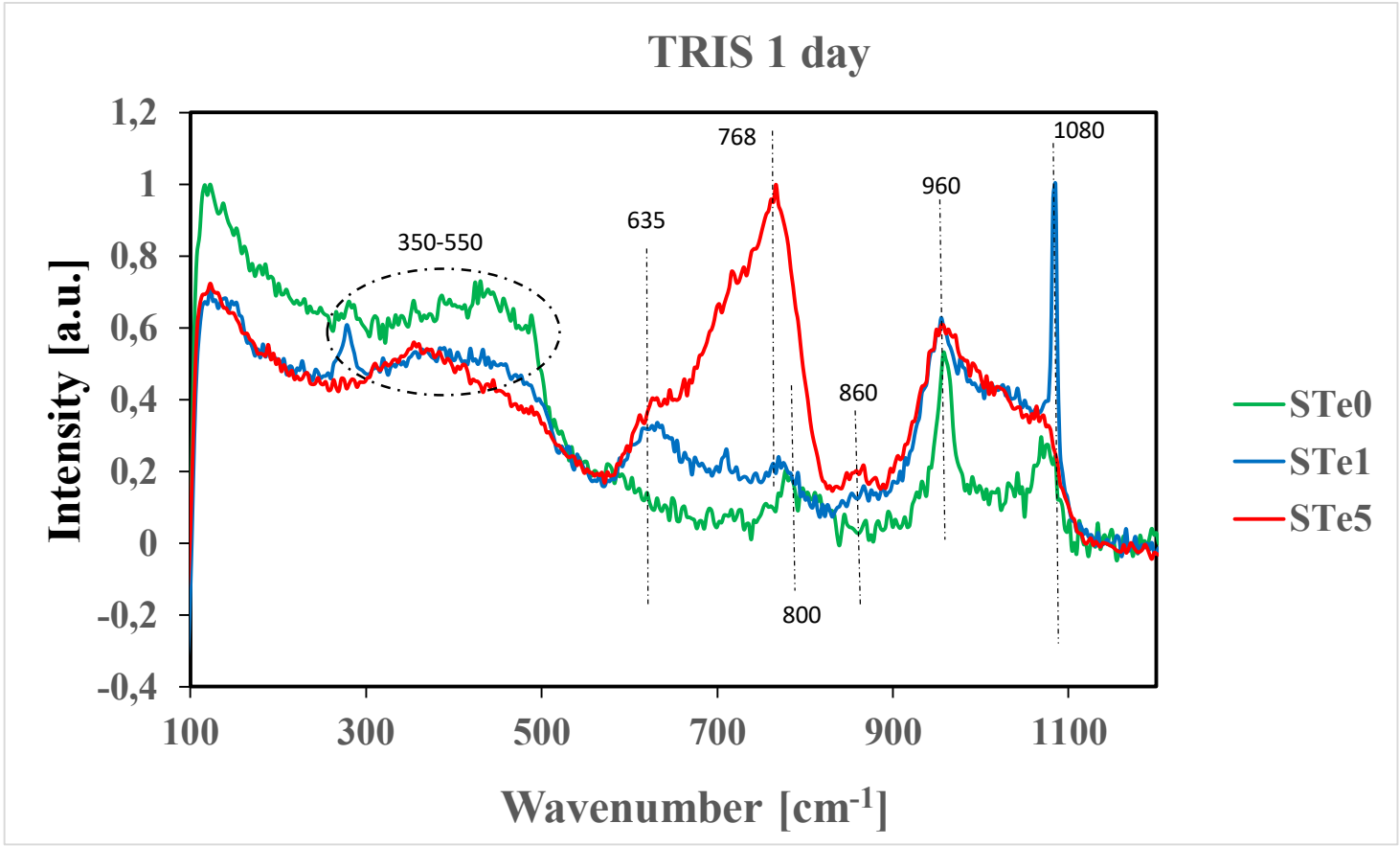

Figure 3.41: Raman spectra of STe0, STe1 and STe5 samples after 1 day of immersion in TRIS.

The spectrum of the samples immersed in TRIS after 1 day (**figure 3.41**) is dominated by a large peak at 768 cm^{-1} attributed to bending vibrational Te-O bond of $[TeO_3]^{2-}$ for STe5 and a shrinked peak at 1080 cm^{-1} to ν_{CO} vibrational mode of ionic carbonate species for STe1 [193] [191]. It should be noted that the tellurium peak undergoes a shift from 768 to 777 cm^{-1} after 14 days [193]. There is another one band less evident located at 860 cm^{-1}. This band could be related to monomers SiO_4 after 1 day [192]. The band about 800 cm^{-1} for STe 0 can be assigned to υ(SiOH) vibrations. A broad band for each samples is also observed at 955-957 cm^{-1} corresponding to the symmetric stretching of the orthophosphate [194]. This band gets sharper after 14 days (**figure 3.42**) for all samples. In addition, there is a characteristic peak of apatite at the low Raman bands between 355- 500 cm^{-1} [191].

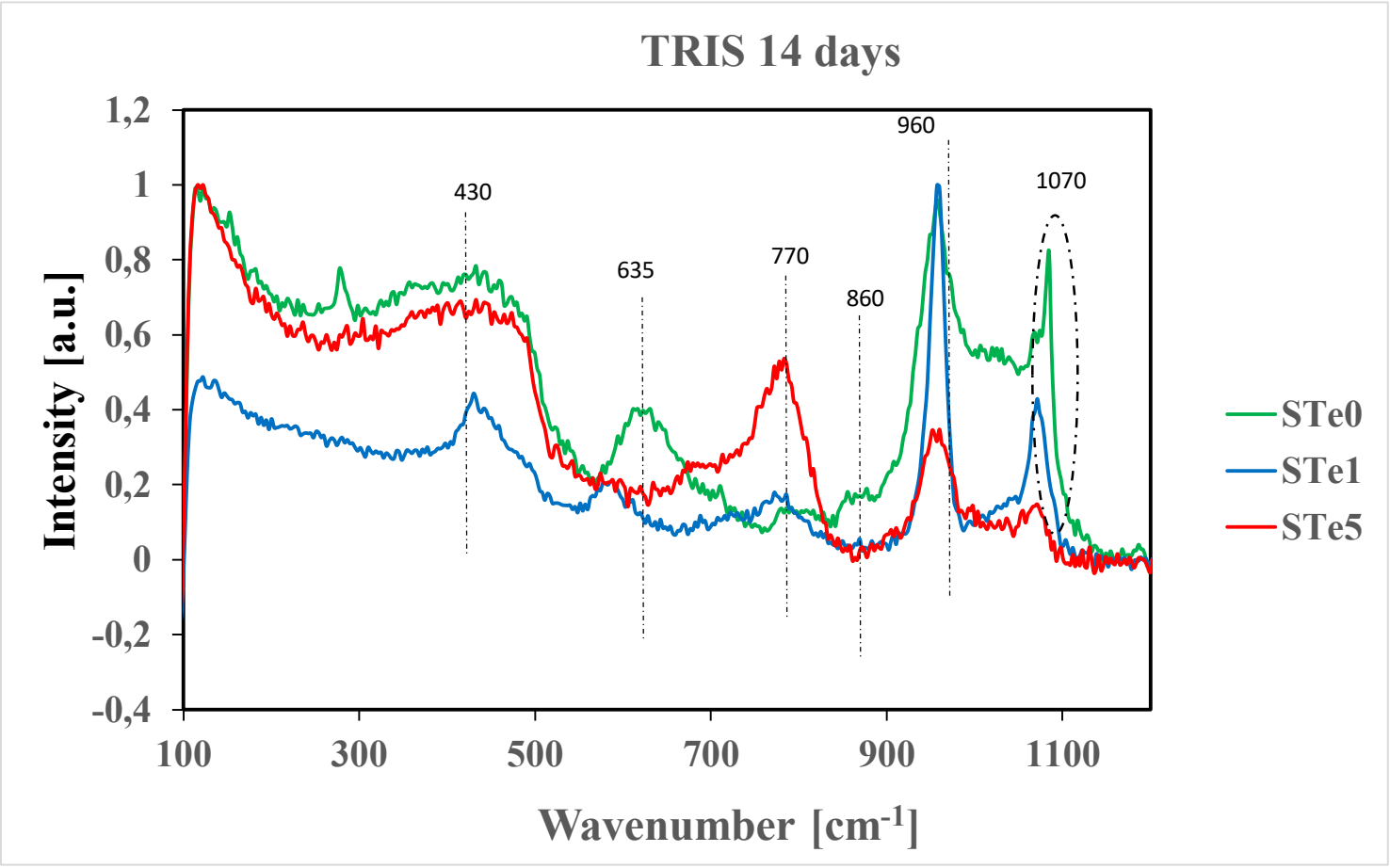

Figure 3.43: Raman spectra of STe0, STe1 and STe5 samples after 14 days of immersion in TRIS.

As already seen in SBF, the band at 430 are attributed to ν_4^P bending mode in **figure 3.43** [191]. The silicon-oxygen symmetric stretching vibration is located at 635 cm^{-1} for STe1, while the tetrahedral silicate units vibration at 860 cm^{-1} for STe1 and STe5 [191]. The bands located at 430 and 635 cm^{-1} become more pronounced after 14 days for all the samples. Besides, the bands 860 cm^{-1} disappear for all the samples after 14 days [191]. In addition, **figure 3.43** has features centered at about 770 cm^{-1} assigned to bending vibrational Te-O bond of [TeO3]2-and at 960 cm^{-1} assigned to PO_4 group [191]. The spectra (**figure 3.39**) also shows the narrowing of the band at 1070 cm^{-1} corresponding to the carbonates adsorbed [192].

3.8 Cell Culture Test

3.8.1 Cytocompatibility

Tellurium-doped specimens in vitro cytocompatibility results are summarized in **Figure 3.44.**

In general, tellurium insertion did not increased specimens' toxicity; in fact, results were comparable between tellurium-doped specimens (STe1 and STe5) and untreated controls (STe0, $p>0.05$).

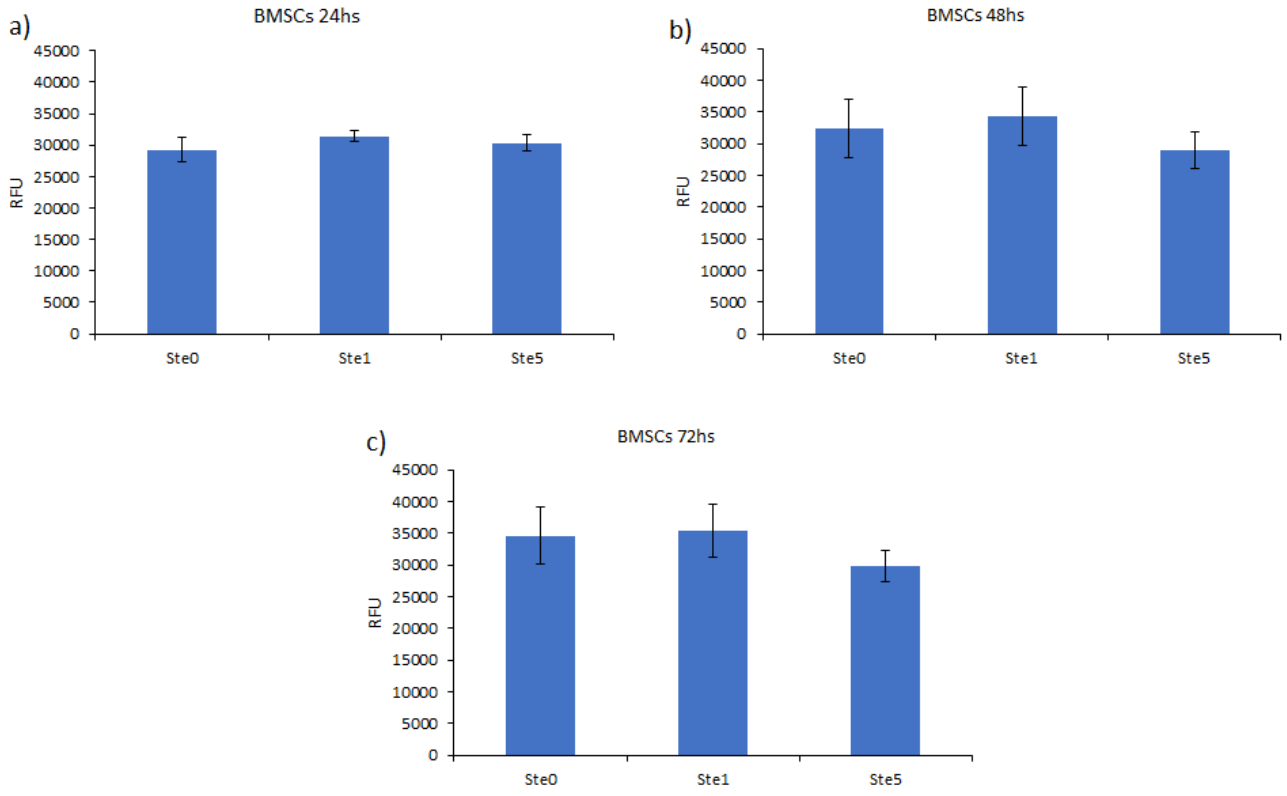

Figure 3.44: Human bone marrow- derived stem cells (BMSCs) metabolic activity after 24 (a), 48 (b) and 72 (c) hours direct cultivation onto specimens' surface.

3.8.2 ROS/RNS scavenge

Tellurium-doped specimens' in vitro ability to protect cells from inflammation results are summarized in **Figure 3.45**.

In general, tellurium insertion was effective in protecting cells from apoptosis induced by the H_2O_2 treatment. In fact, while in the untreated controls STe0 specimens' cells viability was significantly reduced after the H_2O_2 treatment ($p<0.05$, indicated by *), the tellurium doped ones (STe1-STe5) preserved cells metabolic activity.

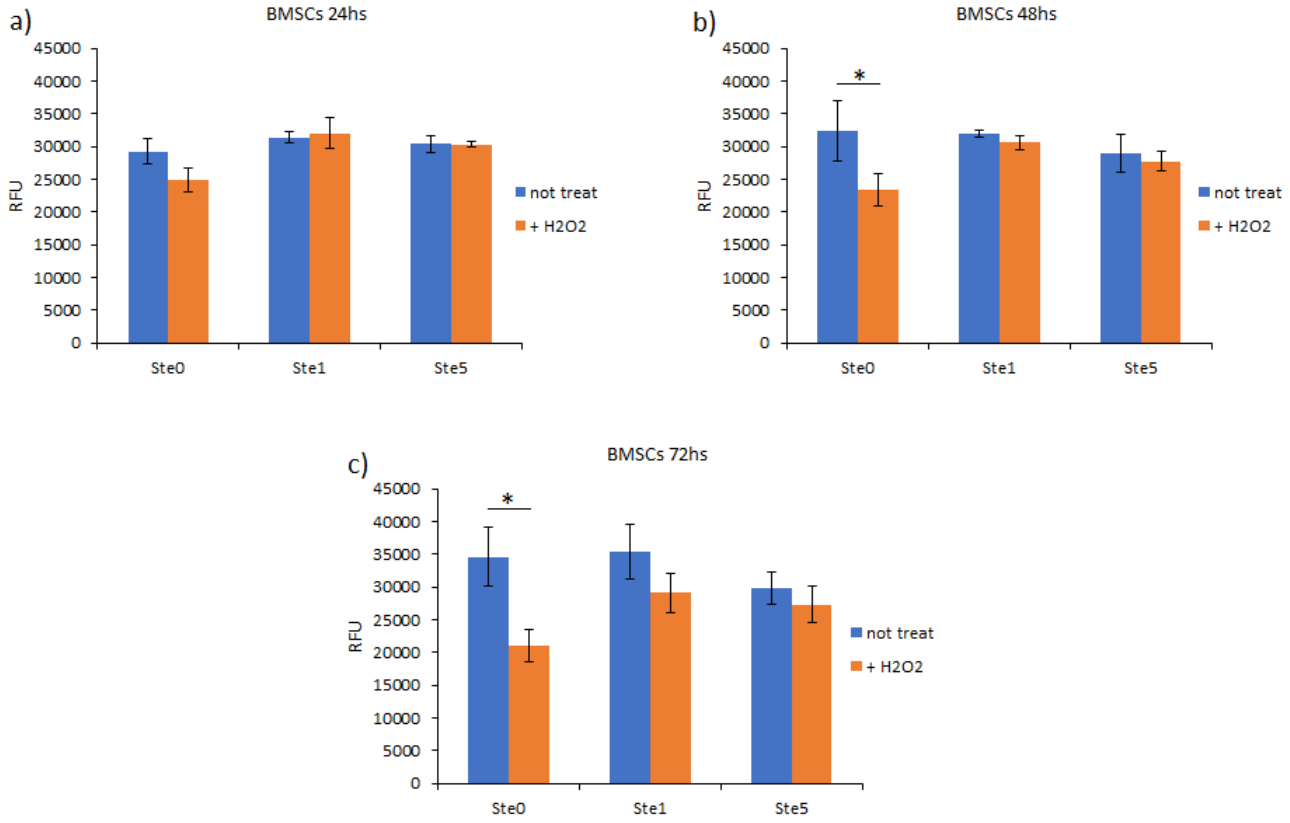

Figure 3.45: Human bone marrow- derived stem cells (BMSCs) metabolic activity after 24 (a), 48 (b) and 72 (c) hours direct cultivation onto specimens' surface with (+ H_2O_2) and without hydrogen peroxide treatment. While in the untreated controls STe0 specimens' cells viability was significantly reduced after 48 and 72 hours H_2O_2 treatment ($p<0.05$, indicated by *), the tellurium doped ones (STe1-STe5) preserved cells metabolic activity.

3.8.3 Antibacterial activity

Tellurium-doped specimens antibacterial results are summarized in **Figures 3.46 and 3.47**, for *S. aureus* and *S. epidermidis* respectively.

The tellurium insertion bestowed to bioglass a strong ability to inhibit biofilm formation, even if in a dose-dependent manner.

In fact, STe1 and STe5 resulted as significant in terms of biofilm metabolic reduction in comparison with the untreated STe0 (considered as control).

However, the effect was dose-dependent as STe5 was significant in comparison with Ste1 after 48 and 72 hours (b, c, $p<0.05$ indicated by the §).

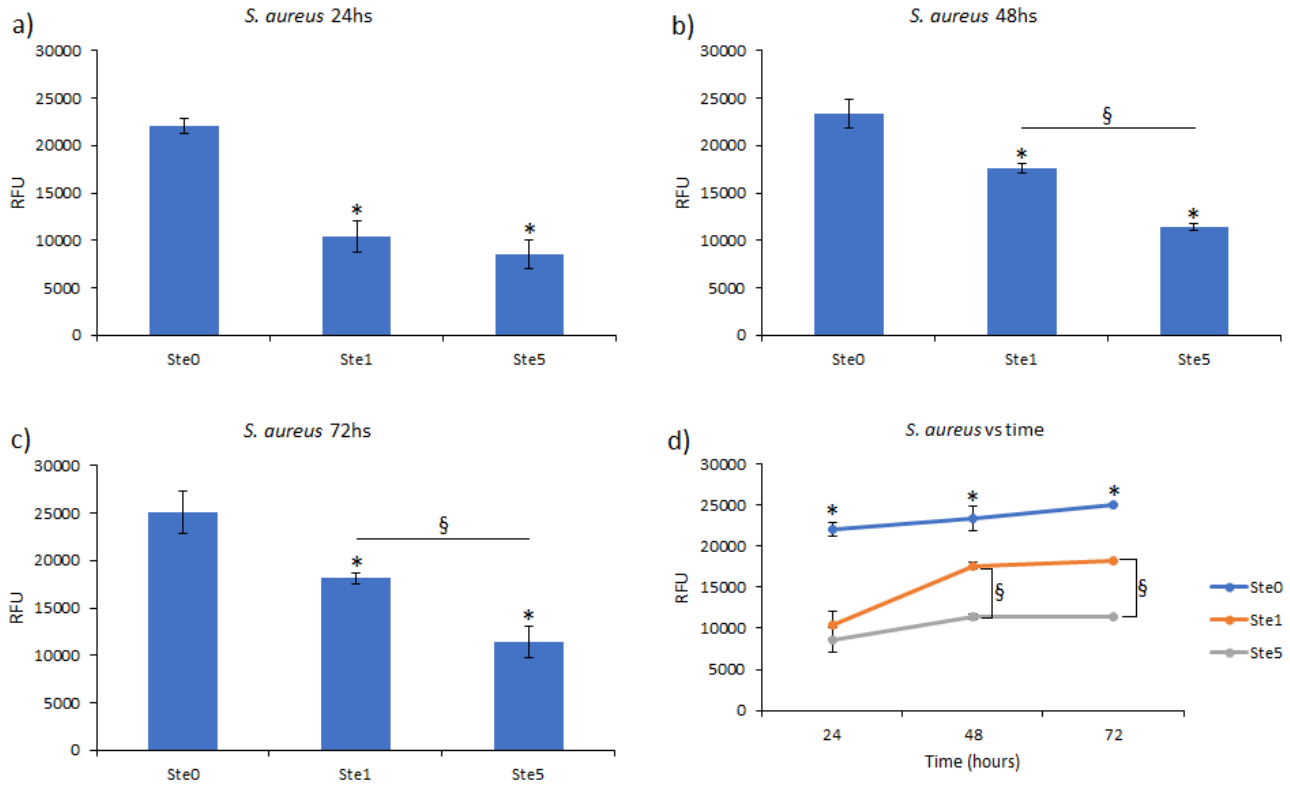

Figure 3.46: S. aureus biofilm metabolic activity evaluation. Tellurium insertion (STe1 and STe5) determined a significant reduction of bacteria viability at each 24 (a), 48 (b) and 72 (c) hours time-point in comparison with untreated control STe0 ($p<0.05$, indicated by the *). The antibacterial activity was maintained during the 3-days test as summarized in (c). However, the effect was dose-dependent as STe5 was significant in comparison with STe1 after 48 and 72 hours (b, c, $p<0.05$ indicated by the §).

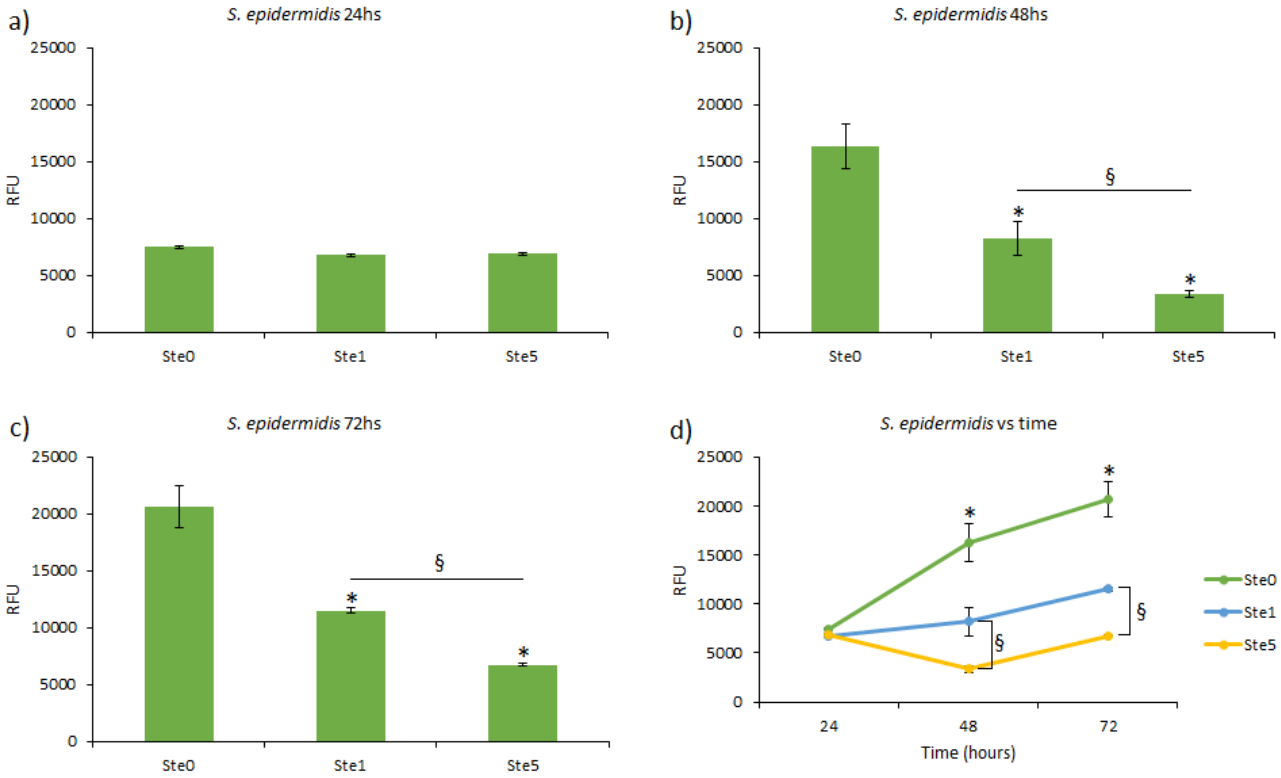

Figure 3.47: S. epidermidis biofilm metabolic activity evaluation. Tellurium insertion (STe1 and STe5) determined a significant reduction of bacteria viability after 48 (b) and 72 (c) hours time-point in comparison with untreated control Ste0 ($p<0.05$, indicated by the *). The antibacterial activity was maintained after 48 hs as summarized in (c). However, the effect was dose-dependent as STe5 was significant in comparison with STe1 after 48 and 72 hours (b, c, $p<0.05$ indicated by the §).

4. Discussion

4.1 Field-emission Scanning Electron Microscope and Electron Dispersive Spectroscopy

The morphology of powders did not change significantly among the three compositions before immersion in SBF. The presence of the tellurium was confirmed by EDX analysis even if calcium has very close peaks to tellurium, making an accurate interpretation of the results very difficult.

4.2 Bioactivity test: pH evolution

Regarding the pH evaluation results, it may be concluded that the pH variation, when powders are immersed in SBF, is due to ion exchange. The pH of the solution deprotonates the glass surface, building a negative charge on the particle surface. The sodium and calcium contained on the surface samples quickly leach into solution, exchanging with hydrogen ions leading to an increase of the pH, at the beginning of the SBF soaking (**figure 4.1**). This process leaves the silicate glass open to attack by water and as a results, it slowly releases soluble silica, exposing silanol groups on the surface (**figure 4.2**). Then silanol groups condensation occurs (**figure 4.3**). A supersaturated alkaline solution of calcium and phosphate is now formed and it is the perfect environment for the deposition of crystalline hydroxyapatite [195]. Lastly, the ion exchange is established between the solution and the silica layer.

$$Si - O - Na + H_2O \rightarrow \equiv Si - OH + OH^- + Na^+$$

Figure 4.1: Interchange of sodium (or calcium) and hydronium

$$Si - O - Si + H_2O \rightarrow Si - OH + OH - Si$$

Figure 4.2: Formation of silanol groups

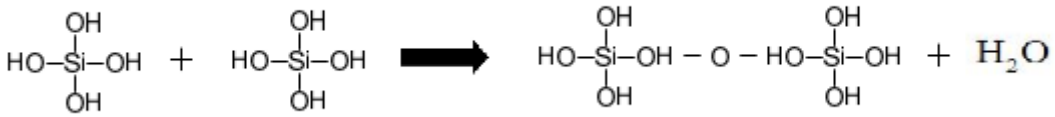

Figure 4.3: Silica-gel polymerization

Monitoring this factor is a requirement in order to ensure biocompatibility as grow fast and change of the pH can affect cells behavior, damaging it irreparably. In order to achieve this in the best possible conditions, the pH was measured every two days and it was realized that the pH stabilized its values after just one day because of the hydroxyapatite formation. This same experiment was replicated with TRIS-buffer, obtaining different results; the pH of the solution increased over time as the samples degraded up to reach the value equal to 8, slightly lower than one obtained for SBF. Both SBF and TRIS favors the precipitation of hydroxyapatite (HAp). Nevertheless, the TRIS could represent a valuable alternative to the standard SBF because the dissolving process of glass is much more evident in TRIS rather than SBF. It might be beneficial in order to better observe the samples evolution.
Despite, the results are statistically similar for TRIS and SBF, SBF reaches supersaturation as the presence of sodium and calcium in the solution and in the glass, causing a pH increase too fast. Consequently, the TRIS is preferable to use when the glass dissolution is analyzed in evaluating the ion amounts and how pH changes as a results of this. The ability of a glass to induce HAp formation can be checked appropriately using both SBF and TRIS as an effect of glass surface dissolution. It is also worth mentioning that pH of STe1 and STe5 samples increase more rapidly and reach greater values than STe0. Apparently, tellurium-containing samples exhibits a better solubility. The following equation could be described the pH beahviour in SBF and TRIS, even if it is only a very rough indication:

$$y = 7.4 + a(1 - e^{-bx}) + c(1 - e^{-dx})$$

Equation 4.1: pH beahviour in SBF and TRIS for each sample [196]

where a, b, c and d are costant (depending on the curve), y is the term referred to the pH value, while x to the time. This behavior is not confirmed for STe0 in TRIS.

4.3 Differential Thermal Analysis

DTA analysis was carried out not only for assessing the characteristic temperatures for each composition (**table 3.3**), but also for understanding how temperature changes in function of the tellurium content. In addition to the main and evident crystallization point, DTA has focused attention on some small peaks related to the crystallization point at 678.08°C, 695.86°C, 674.25°C for STe0, STe1 and STe5 respectively. These peaks form as a sort of hump and could be merely indicating that the characterized material has more than one crystalline phase. This may be further confirmed by the presence of two peaks more marked at 1285.77°C, 1278.87°C and 1257.49°C at the melting point for STe0, STe1 and STe5 respectively, even if it is not very clear.
Another result of great interest is the influence of the tellurium on the temperature points. It is clear how an increased tellurium content leads to a reduction of all characteristic temperature points. Tellurium oxide is a glass former as silica but tellurium glasses have lower melting temperature in comparison to silica glasses [197]. Therefore, the heat should be transferred so much faster on tellurium-containing sample, such that mass reaches its characteristic points first.

4.4 X-ray diffraction

It is clear from the **figures 3.10-3.11-3.12** reported in the chapter 3 that samples have no long range structure or order but a short range order of SiO_4 tetrahedron. In fact, while samples are diffracted, X-rays are scattered in many directions leading to a large bump instead of high intensity narrower peaks.

Analysis carried out on samples after immersion in SBF and TRIS showed the existence of crystalline peaks on XRD pattern. These peaks can be attributed to deposition of hydroxyapatite and calcite. Hydroxyapatite crystal appear to grow after 1 day for all the samples in SBF (**figure 3.13-14-15**). These peaks are more intense and marked in STe0 than in STe1 and, above all, in STe5 (**figure 3.14-3.15**). There are also some small and broad peak on XRD pattern but this is most probably due to the presence of finer crystals of HAp. The calcium carbonate phase is a HAp precursor, therefore calcite may precipitate before in STe0 in SBF (**figure 3.13**). Similarly, the peaks of hydroxyapatite are identified for STe1 and STe5 in TRIS after 1 day (**figure 3.16**). The intensity of peaks is very small compared to the SBF ones. Nucleation and growth of HAp appears less relevant in TRIS as sodium and calcium leach out only from the glasses. Overall, the tellurium-containing samples shows less and marked crystals of HAp compared to the STe0 whether in SBF and TRIS. In this scenario, it can be assumed that STe1 and STe5 have a thinner layer of HAp than STe0.

4.5 Fourier transform infrared spectroscopy

First of all, the FTIR have provided additional information about the silica network. The band belongs to the P-O stretching mode of $[PO_4^-]$ group and the vibrational $v_2(CO_3^2)$ are a result of hydroxyapatite formation on the surface of powders as the days passed. Therefore, the bioactivity can be confirmed because those peaks are evident for each composition.

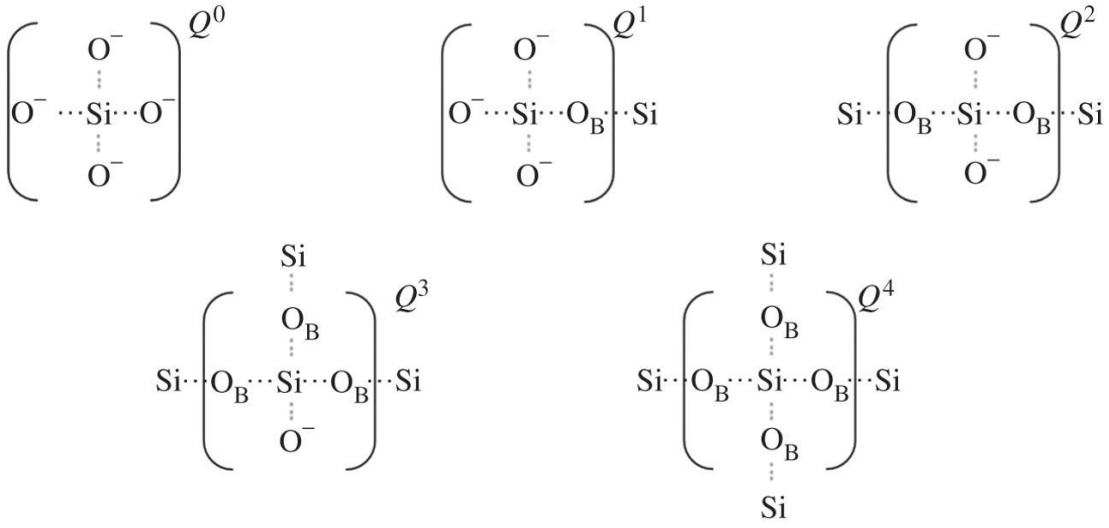

Figure 4.3: Q structures describe Si network connectivity in glasses. O_B represents a network-forming bridging oxygen bond (Si–O–Si) [198].

Before the immersion, the dominant band can be assigned to Si-O-Si vibrations from the silica network at first, but the phosphate bands become dominant over time after immersion. On the contrary, the bands related to SiO non-bridging oxygens atoms (**figure 4.3**), appears due to the ion exchange in the glass network, leaching of sodium and calcium. However, the stretching with non-bridging oxygen (Si-O-NBO) per SiO_4 tetrahedron groups (described as Q_3^{Si} in **figure 4.3**) confirmed that glass network kept its amorphous form. Consequently, no additional sharp or split peaks were detected in FTIR curves after immersion, as already confirmed by XRD analysis.

The presence of carbonate peak at 1416-1423 cm^{-1} is identified as a calcium carbonate in deposition on apatite layer and subsequently forms the hydroxycarbonateapatite layer whose presence play a key role in the formation of apatite structure and morphology. This carbonate apatite can be attributed to B-type carbonate, that should be distinguished from A-type carbonate [199]. The main difference lies on the mode of substitution: a direct of substitution of OH^- with CO^{2-}_3 is defined as A-type carbonate, whereas PO_4^{3-} substituting a tetrahedral group with CO_3^{2-} is defined as B-type carbonate. Some parameters of glass can change depending on the type of carbonate [199]. Besides, this peak appears only after immersion in SBF and not in TRIS for STe1 and STe5, whereas it already occurs for STe0 before immersion. As already seen for Raman, it could be related to the natural carbonation of the sample.

FTIR bands were not affected by the silica amount despite it was a little bit different for each composition. The same applies to the phosphate, whose quantity remains constant for each composition. Tellurium bands were found from FTIR analysis for STe1 and STe5. As reported from this article, addition of modifiers Na_2O and CaO leads to an openness of the glass structure through transformation of TeO_4 units to TeO_3 ones [147]. As a result, network connectivity decreases with disintegration of TeO_4 rings.

Table 4.1 HAp and HCAp peaks detected in the FTIR spectra of STe0, STe1 and STe5

Assignement	Position (cm^{-1}) and Shape	Day of appearance	Remarks
$\nu_2(CO_3^{2-}$)characteristic carbonated apatite	Small peak at 870	1 day for all samples	Not very intense for all samples
PO_4^{-3} asymmetrical stretching mode	Intense broad band at 1029-1032	1 day for all samples	Intense for all samples
V_3 assigned to B-type carbonate substitues phosphate ion (PO_4 group incorporated CO_3 groups, B-Type Hap is formed)	Broad band at 1416-1424	1 day for STe0 3 days for STe1 7 days for STe5	Less intense for STe1 and almost absent for STe5

4.6 Inductively coupled plasma - optical emission spectroscopy

The behaviour of each sample in TRIS and SBF was investigated in order to quantify total released ion amounts and obtain a dissolution leaching profile. From the results of analysis, Na, Si, Ca, P and Te release was confirmed in each solution after 1, 3, 7 and 14 days. Regarding the experiment conducted in SBF, Si dissolution effects on glass, in fact, the range of values is in the order of 0,03 to 0,05 mg_{ion}/ml_{sample} (**figure 3.28**). As a SiO_2 former, the release of Si from STe0, STe1 and STe5 is very low.

Despite the lower concentration of phosphorous in each composition, its release can be observed even if in negligible quantities (**figure 3.27**). As regards sodium and calcium, the ion exchange process between samples and SBF are such that the glass will be in equilibrium with the new solution, and there won't be an abrupt loss to the glass when the dilution is made. Therefore, it is difficult to identify a change in the amount of sodium and calcium release.
Tellurium release is accomplished despite its small amount. Overall, phosphorous and tellurium have lesser order of magnitude (**figure 3.27-3.29**) than other ions because they appear in minute quantities, while sodium (**figure 3.26**) seems to be released in greater concentration, between 2 to 1 mg_{ion}/ml_{sample}
The supersaturation does not occur in TRIS immersed solutions, therefore it is possible to observe a more significant change in Ca and Na concentrations than in SBF solutions. Only for STe 5, there was a certain fall. However, the remaining ions in TRIS have a behavior quite similar to those found in the SBF solutions for each composition. Only the amounts released are different. Phosphorous has one or two orders of magnitude lower than other ions because it is present in lesser amount in the glass compositions. A significant difference in tellurium release can be seen between STe1 and STe5, increasing an order of magnitude. In any case, weight leakage for each ion in TRIS and SBF changes non-linearly.

4.7 Raman spectroscopy

In Raman spectra, a shift indicates the chemical bond length of molecules, therefore it is necessary to understand what they represent and implies. No relevant frequency shifts of the bands were reported on Raman curves from each samples. Silicon oxide depolarized the scattered light depending on the number of symmetries of the molecule that are maintained throughout the oscillation (**figure 4.4**).

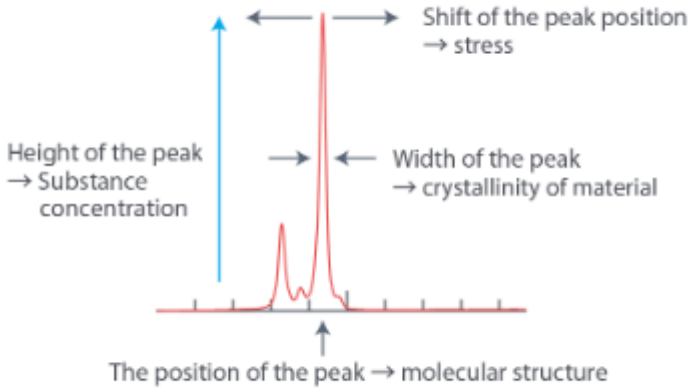

Figure 4.4: Raman peaks corresponding to a particular crystal structure and molecular vibration [200].

However, the bands referred to SiO modes at 635 and 860 cm $^{-1}$ (**figure 3.35-3.36-3.7-3.8-3.39**) shows that the content of Si should not be change a lot in silica network for each composition. These peaks should decrease until they completely disappear after immersion for each sample. The increase of Si-O-NBO groups in the network helps the ion exchange with solutions, leading to a more rapid formation of hydroxyapatite layer. It must be pointed out that phosphorous band at 952-955 cm^{-1} translate to 960-957 cm^{-1} after 14 days and this can be due to the reactions between P and SBF or TRIS solutions. This peak is relatively high, despite the phosphorus concentration, because the P release doesn't change much during the immersion time. The P amount appears higher for STe0 and STe1 than STe5 in both SBF and TRIS.

The peak at 1073 cm^{-1} for STe0 reference sample may be attributed to the carbonation of the sample. STe0 was prepared much earlier than else samples, therefore samples may be carbonated due to the atmosphere. As regards sample after immersion, it is difficult to say why the carbonates due to precipitation of carbonated HAp, appear intense for STe5 after 1 day in SBF, while they disappear after 14 days. The same goes for STe1 in TRIS. Furthermore, the band at 430 cm^{-1} after immersion in TRIS and SBF confirms the formation of hydroxyapatite, since it is not visible in the reference, but only after 1 day. **Figures 3.36, 3.37, 3.38 and 3.39** show that the growth of HAp is higher in STe0 than STe1 and STe5, as reported above.

A study suggests that phosphate component starts as an amorphous phase and gradually changes to a crystalline phase. Moreover, the most striking finding concerns the presence of a tellurium band. Tellurium oxide should be work as a glass former as illustrated by the band at 680 and 770 cm^{-1}. It is easy to observe how high is this band for STe5, whereas it doesn't appear for

STe0. Raman spectroscopy has not been able to consolidate if the glass former TeO_2 has a denser atomic packing efficiency and reduced medium-range order.

4.8 Cell Culture Test

Cells viability analysis showed no significant changes in viability among samples. Tellurium doping (STe1-STe5) did not introduced toxic effects as the metabolism of cells cultivated onto doped specimens was comparable to that obtained onto control ones (STe0, $p>0.05$).

The antibacterial effect is clearly dose-dependent as STe5 is significant more antibacterial in comparison with Ste1 after 48 and 72 hours. Therefore, tellurium-doped specimens have provided to be good antibacterial agents. The toxic effect could be related to tellurium dioxide. It has a low solubility at physiological pH leading to an oxidation of different ions compound called oxyanions: tellurite (TeO_3^{2-}) and tellurate (TeO_4^{2-}) [201]. These oxyanions are probably responsible for the observed antibacterial effects, since the toxicity of tellurium is still not sufficiently understood. Looking at the literature, the tellurite toxicity can be explained in two mechanisms:

- replacing the sulfur group in a number of amino acids creating non-functional proteins [202]

- oxidizing the glutathione reservoir of the cells leading to the generation of excessive amounts of reactive oxygen species (ROS) [202]

Tellurium oxyanions are able to trigger the generation of ROS reacting with intracellular thiols (RSH), especially with glutathione (GSH), as already seen in chapter 1.10.4. Oxyanions reduction generates superoxide radicals resulting in oxidative stress (**figure 4.5**). It is worth noting that the tellurium insertion in the bioactive glass promote the ability to hinder biofilm formation in a dose-dependent manner.

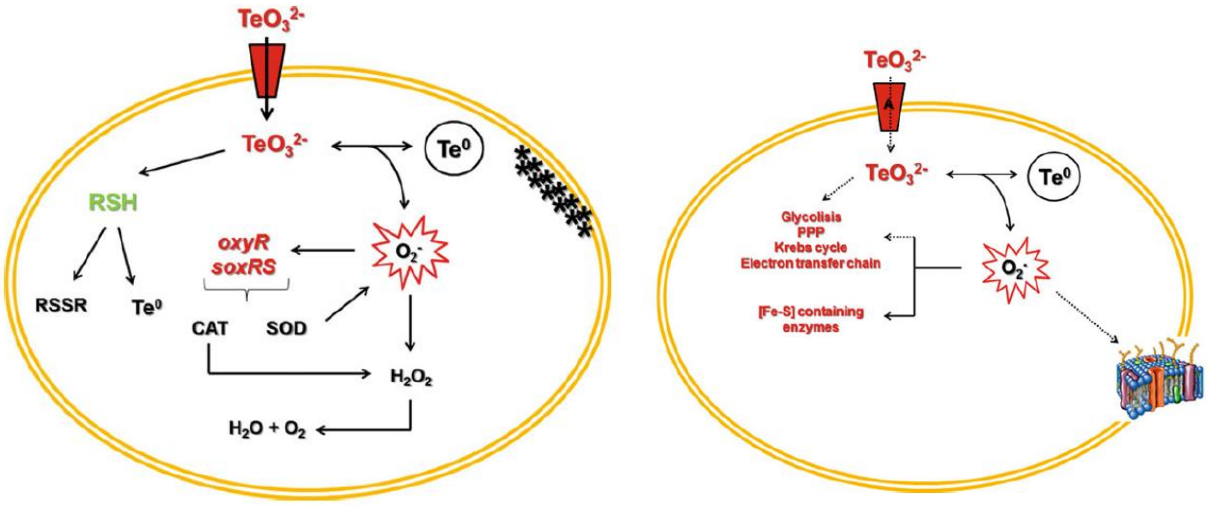

Figure 4.5: Current models for tellurite toxicity [203].

However, there are tellurite-sensitive and tellurite-resistant organisms [203]. Some bacteria are able to resist the attacks of these oxyanions thought direct extrusion of the toxicant. TeO_3^{2-} is reduced to the insoluble elemental form Te^0 which accumulates as black deposits. Then, it is converted to volatile methylated forms and easily eliminated from the cell, generating the classic garlic-like odor.

In addition, analysis conducted on ROS evaluation, tellurium has proved as promising agents for antioxidant therapeutics. Tellurium may be better neucleophiles than classical antioxidants since it can also inhibit peroxidation even if the mechanism is not yet clear. These antioxidative effects may be due to the ability of tellurium compounds to act as radical trapping agents, and the capacity of the organotellurium compound to mimic the action of the GPx-enzymes [138].

5. Conclusions

The primary purpose of this dissertation is to develop a novel bioactive glass doped with tellurium and investigate its morphology, bioactivity, physical/chemical and structural properties. Tellurium was chosen because its potential biological role in health has been suggested in literature, including the antibacterial and antioxidant effects, although the exact mechanism is still not clear. Three different compositions were fabricated by melt-derived route with different molar fraction of tellurium: STe0, STe1 and STe5, 0 mol%, 1 mol%, 5 mol% respectively. Overall, the compositions of the bioactive glass were inspired by 45S5 Bioglass®. The particles obtained in order to perform examinations were sieved below 25 μm.

First of all, detailed experimental analyses on characteristic temperatures were carried in order to determine the crystallization, glass transition and melting point of the materials. The investigated DTA curves demonstrated that as the concentration of tellurium increased, the characteristic temperatures slightly reduced. This decrease might be related to tellurium introduction and by weakening network.

Then, the morphology of the powders was investigated by FESEM. Results showed a heterogeneous distribution of particles. The size of these particles ranged between 20 and 2 μm. In addition, the EDS spectrum was obtained for each sample in order to confirm the composition of the theoretical ones. As observed, the analysis determined that STe0, STe1 and STe5 were mainly composed by silica, calcium and sodium, with a small atomic percentage of phosphorous and tellurium. Overall, the composition collected were quite close from the theoretical ones.

In vitro studies were conducted on all composition by soaking in TRIS and SBF to evaluate the bioactivity and the ion released from glasses. The first step consisted in the pH analysis evolution over time. It was observed that the pH of each composition increased as function of time from 1 day to 14 days. The starting value was 7.4 reaching 8.4 and 8.1 in SBF and TRIS respectively. The pH increases are in agreement with the well-known mechanism of ion exchange between sodium and calcium in the samples and hydronium in the SBF/TRIS solution. In addition, this was accompanied by glass dissolution, where a fast release of phosphorous was observed in TRIS and SBF. On average, other ion leached out more slowly and controlled than phosphorous. It was difficult to assess the release of ions in SBF because the super saturation of the solutions occurred. Overall, ion release was higher for STe0 compared to the STe5 and ST1 one with a corresponding elevation in pH. The high sodium and calcium concentrations likely de-polymerizes the Si–O–Si network resulting in a highly soluble glass as confirmed in EDS.

The X-ray diffraction was used for determining microstructure of the glasses by measuring the angles and intensities of diffracted beams, before and after immersion in SBF. The XRD patterns collected from as prepared powders showed an amorphous structure thus confirming their glassy nature. After immersion in SBF, crystalline peaks confirmed the formation of a hydroxyapatite layer on the surface of each samples. Some peaks related to calcite were found on the powder surface of each sample, as well. They might be precursors of hydroxyapatite. The presence of tellurium oxide did not affect intensely the bioactivity of the glass if compared with the parent composition.

FTIR helped to study the functional groups present in the samples before and after soaking in TRIS and SBF. As expected, all reference present vibration of bridging and non-bridging oxygen of silica network. But even carbonates adsorbed on the surface was found at 850-870 cm^{-1} and 1550-1350 cm^{-1}. The most important bands where the hydroxyapatite appeared after

immersion for all samples was at 870 and 1025 cm^{-1}. They appeared after 1 day in accordance with the results from XRD and FESEM. FTIR also demonstrated that tellurium acted as former since its characteristic band were located at 775 e 660 cm^{-1}.

RAMAN spectroscopy provided complementary results to FTIR. The bands of interest for the silica bridging and non-bridging oxygen bulk vibrational modes were at 350-500, 635 and 860 cm^{-1}. In addition to silica features, it is possible to observe intense bands corresponding to the formation of hydroxyapatite or phosphate like species at 430 and 950 cm^{-1}. Also in this analysis, tellurium bands can be observed at 680 and 770 cm^{-1}. These bands were attributed asymmetric stretching vibrational Te-O bond of $[TeO_4]^{4-}$ and bending vibrational Te-O bond of $[TeO_3]^{2-}$ respectively. The Si, Na, Ca, P and Te concentration in solution released by each sample were analyzed by ICP-OES. On the basis of the above mentioned results, bioactivity was confirmed by the formation of hydroxyapatite on the surface of glasses as seen in XRD, FTIR and RAMAN, whereas pH evaluation demonstrated the presence of the steps which lead to the formation of hydroxyapatite. RAMAN and ICP analyses should be repeated to verify if results are reproducible.

The research went beyond the material characterization by focusing on culture cell tests: in particular, on antibacterial effect, cytocompatibility and ROS evaluation. Assessment of the action of the bioactive glass against bacterial and ROS was tested on human bone marrow-derived stem cells were cultivated in low-glucose Dulbecco's modified Eagle Medium (DMEM, Sigma-Aldrich) supplemented with 15% fetal bovine serum (FBS, Sigma) and 1% antibiotics (penicillin/streptomycin) at 37°C, 5% CO_2 atmosphere. The data obtained from the cytocompatibility analysis conducted after 24, 48, and 72 hours illustrated that neither STe0, nor tellurium content, time negatively affected the cells. Moreover, cells were treated with 300 M H_2O_2 for 3 hours at 1-2-3 days in order to test tellurium antioxidant impact. STe1 and STe5 exhibited a greater antioxidant activity than STe0, in fact the cells viability was significantly reduced after 48 and 72 hours H_2O_2 treatment on STe0, while STe1 and STe5 reported an optimal defense system against stress oxidation. Tellurium antibacterial activity was performed using the orthopedic-related strains *Staphylococcus aureus* (*S. aureus*) and *Staphylococcus epidermidis* (*S. epidermidis*). Sterile samples were gently located into a 24 multiwell plate by sterile tweezers avoiding any surface damages. Each specimen was submerged with 1 ml of the $1x10^5$ cells/ml broth bacteria culture. The study allowed to conclude that STe1 and ST5 had an antibacterial activity. Tellurium determined a significant reduction of bacterial viability after 48 and 72 hours in comparison with untreated control STe0. The effect was dose dependent as STe5 was significant in comparison with STe1.

In conclusion, this work has been able to get a preliminary set of results concerning a new class of melt-derived silica-based bioactive glasses doped with tellurium. The obtained data motivate future studies with improved set up and new analysis. The glasses developed in this work show interesting properties as a new class of biomaterials, due to their bioactivity, antibacterial properties, antioxidant ability and an affinity for cells.
This bioactive glass may provide a comprehensive improvement in the research of bioactive glasses. Therefore, in-depth comprehensions are required by pursuing past developments and studying the present situation and future forecast based on the actual bioactive glass market. The following list should include future works and suggest how to overcome the limitations that this work cannot do at present:

- The study provided an in-depth analysis of the bioactive glass powders, but it would recommend trying to form a bulk compact and then repeated the same tests on them, making a comparision with those ones reported in the literature. In addition, new

material characteriziations should be performed: study of roughness to improve the fatigue resistance and corrosion; wettability to understand interactions occuring between a liquid media and the bioactive glass; zeta potential of bioactive glass particles.

- Comprehensive analysis of all mechanical properties should be provided to determine the opportunities existing to apply material as a coating, scaffold, etc. in different biomedical fields: density, hardness, bending strength, fracture toughness and Young's modulus.

- Extensive analysis of the tellurium activity should be conducted for a better understanding of its effect and to constantly fine-tune its amount.

Bibliography

[1] E. Vernè, *Dispense del corso 'Biomateriali,* 2016.

[2] S. H. Wemple, «Refractive-index behavior of amorphous semiconductors and glasses,» *Physical Review,* vol. B 7.8, p. 3767, 1973.

[3] [Online]. Available: http://www.benbest.com/cryonics/?C=N;O=D. [Consultato il giorno 14 Gennaio 2019].

[4] K. A. L. M. Souquet J.L., Theory and Applications of Amorphous Solid for Electrochemical Cells, vol. vol 217, Boston: Springer, 1990.

[5] R. e. a. Fulchiron, «A simple method for tuning the glass transition process in inorganic phosphate glasses,» *Scientific reports,* n. 5, p. 8369, 2015.

[6] M. B. C. H. a. G. Z. Yoshioka, «Crystallization of indomethacin from the amorphous state below and above its glass transition temperature,» *Journal of pharmaceutical sciences,* n. 83.12, pp. 1700-1705, 1994.

[7] P. G. a. F. H. S. Debenedetti, «Supercooled liquids and the glass transition,» *Nature,* n. 410.6825, p. 259, 2001.

[8] A. Q. Tool, «Relation between inelastic deformability and thermal expansion of glass in its annealing range,» *Journal of the American Ceramic society,* n. 29.9, pp. 240-253, 1946.

[9] L. a. F. P. Hui, «Structural study of local order in quenched lead under high pressures,» *Chemical physics,* n. 304.3, pp. 261-271, 2004.

[10] M. B. a. J. T. Z. Tang, «Thermodynamic behavior of glass-forming metallic supercooled liquids,» *Physica B: Condensed Matter,* n. 426, pp. 1-5, 2013.

[11] D. a. J. P. G. Chandler, «Dynamics on the way to forming glass: Bubbles in space-time,» *Annual review of physical chemistry,* n. 61, pp. 191-217, 2010.

[12] M. Haldimann, «Fracture strength of structural glass elements,» THESIS_LIB. EPFL, 2006.

[13] Amgreen, «Wikipedia,» 13 October 2010. [Online]. Available: https://it.m.wikipedia.org/wiki/File:Brittle_v_ductile_stress-strain_behaviour.png. [Consultato il giorno 15 12 2018].

[14] F. C. Roesler, «Brittle fractures near equilibrium,» in *Proceedings of the Physical society*, 1956, p. 981.

[15] N. P. a. R. H. D. Bansal, Handbook of glass properties, Elsevier, 2013.

[16] S. M. Wiederhorn, «Influence of water vapor on crack propagation in soda-lime glass,» *Journal of the American Ceramic Society,* n. 50.8, pp. 407-414, 1967.

[17] A. a. J. D. M. Makishima, «Calculation of bulk modulus, shear modulus and Poisson's ratio of glass,» *Journal of Non-crystalline solids,* n. 17.2, pp. 147-157, 1975.

[18] [Online]. Available: https://www.fose1.plymouth.ac.uk/fatiguefracture/tutorials/FractureMechanics/Griffith/GriffTheory1.htm . [Consultato il giorno 16 Gen 2019].

[19] R. a. I. A. Sakin, «Statistical analysis of bending fatigue life data using Weibull distribution in glass-fiber reinforced polyester composites,» *Materials & Design,* n. 29.6, pp. 1170-1181, 2008.

[20] C. A. Klein, «Characteristic strength, Weibull modulus, and failure probability of fused silica glass,» *Optical Engineering,* n. 48.11, 2009.

[21] J. M. e. a. Brader, «Glass rheology: From mode-coupling theory to a dynamical yield criterion,» *Proceedings of the National Academy of Sciences,* n. 106.36, pp. 15186-15191, 2009.

[22] K. Tippins, «Slide Player,» [Online]. Available: https://slideplayer.com/slide/3496538/. [Consultato il giorno 10 12 2018].

[23] P. A. a. G. B. M. O'Connell, «Arrhenius-type temperature dependence of the segmental relaxation below Tg,» *The Journal of chemical physics,* n. 110.22, pp. 11054-11060, 1999.

[24] D. L. Griscom, «Optical properties and structure of defects in silica glass,» *Journal of the Ceramic Society of Japan ,* n. 99.1154, pp. 923-942, 1991.

[25] W. S. a. R. J. S. Rodney, «Index of refraction of fused quartz glass for ultraviolet, visible, and infrared wavelengths,» *JOSA,* n. 44.9, pp. 677-679, 1954.

[26] J. H. K. a. T. A. Uozumi, «Fraunhofer diffraction by Koch fractals,» *Journal of modern optics,* n. 37.6, pp. 1011-1031, 1990.

[27] J. M. Stevels, «The electrical properties of glass,» in *Electrical Conductivity*, Berlin, Springer, 1957, pp. 350-391.

[28] D. J. D. S. S. a. R. T. H. Monk, «Determination of the etching kinetics for the hydrofluoric acid/silicon dioxide system,» *Journal of the Electrochemical Society ,* n. 140.8, pp. 2339-2346, 1993.

[29] J. J. a. J. V. W. Mazer, «Dissolution kinetics of silica glass as a function of pH between 40 and 85 C,» *Journal of non-crystalline solids,* n. 170.1, pp. 32-45, 1994.

[30] K. Chase, «Slide Player,» [Online]. Available: https://slideplayer.com/slide/10797189/. [Consultato il giorno 28 11 2018].

[31] P. Meyers, «Behavior of silica in ion exchange and other systems,» *IWC,* n. 99, p. 64, 1999.

[32] G. R. R. a. S. B. Lérondel, «Roughness of the porous silicon dissolution interface,» *Journal of applied physics,* n. 81.9, pp. 6171-6178, 1997.

[33] E. J.-M. B. a. F. L. Grinenval, «A Novel Approach to Prepare Well-Defined Silica-Supported Polyoxometalate Species by Reaction with a Chlorinated Support,» *Journal of Inorganic Chemistry ,* n. 2013, 2013.

[34] S. e. a. Takeda, «Surface OH group governing wettability of commercial glasses,» *Journal of non-crystalline solids,* n. 249.1, pp. 41-46, 1999.

[35] J. Jackle, «Models of the glass transition,» *Reports on Progress in Physics,* n. 49.2, p. 171, 1986.

[36] J. H. a. E. A. D. Gibbs, «Nature of the glass transition and the glassy state,» *The Journal of Chemical Physics,* n. 28.3, pp. 373-383, 1958.

[37] M. I. Ojovan, «Viscosity and glass transition in amorphous oxides,» *Advances in Condensed Matter Physics,* n. 2008, 2008.

[38] A. A. Abu-Sehly, «Kinetics of the glass transition in As22S78 chalcogenide glass: Activation energy and fragility index,» *Materials Chemistry and Physics,* n. 125.3, pp. 672-677, 2011.

[39] R. e. a. Böhmer, «Nonexponential relaxations in strong and fragile glass formers,» *The Journal of chemical physics,* n. 99.5, pp. 4201-4209, 1993.

[40] M. I. a. W. E. L. Ojovan, «Immobilization of radioactive wastes in glass,» *An introduction to nuclear waste immobilisation,* n. 2, pp. 245-282, 2005.

[41] W. Zachariasen, «The atomic arrangement in glass,» *J. Am. Chem. Soc.,* n. 54, p. 3841, 1932.

[42] G. a. H. D. W. De Leede, «Evaluation of glass formation criteria,» *Journal of non-crystalline solids,* n. 104.1, pp. 45-51, 1988.

[43] A. K. Varshneya, Fundamentals of inorganic glasses, Elsevier, 2013.

[44] A. Dietzel, «Glasstruktur und Glaseigenschaften,» *Glastechn. Ber,* n. 22, pp. 41-50, 1948.

[45] W. Vogel, «Historical Development of Glass Chemistry,» in *Glass Chemistry*, Berlin, Springer, 1994, pp. 1-21.

[46] N. A. R. a. I. M. Boubata, «Thermodynamic and relative approach to compute glass-forming ability of oxides,» *Bulletin of Materials Science,* n. 36.3, pp. 457-460, 2013.

[47] S. D. Stookey, «Catalyzed crystallization of glass in theory and practice,» *Industrial & Engineering Chemistry,* n. 51.7, pp. 805-808, 1959.

[48] D. R. Uhlmann, «A kinetic treatment of glass formation,» *Journal of Non-Crystalline Solids,* n. 7.4, pp. 337-348, 1972.

[49] R. J. M. R. a. M. R. Casasola, «Glass–ceramic glazes for ceramic tiles: a review,» *Journal of Materials Science,* n. 47.2, pp. 553-582, 2012.

[50] E. D. Zanotto, «Surface crystallization kinetics in soda-lime-silica glasses,» *Journal of Non-Crystalline Solids,* n. 129.1-3, pp. 183-190, 1991.

[51] J. W. Cahn, «Phase separation by spinodal decomposition in isotropic systems,» *The Journal of Chemical Physics,* n. 42.1, pp. 93-99, 1965.

[52] C.-w. C. Hsieh, *Effect of molecular structure on the viscoelastic properties of cellulose acetate in a ternary system,* 2010.

[53] W. D. H. B. a. J. H. S. HALLER, «Miscibility Gaps in Alkali-Silicate Binaries—Data and Thermodynamic Interpretation,» *Journal of the American Ceramic Society ,* n. 57.3 , pp. 120-126, 1974.

[54] A. L. Johnson, «Process fo melting glass,» *U.S. Patent ,* pp. 606-825, 21 Sep. 1971.

[55] T. a. D. A. B. Barrow, «Melting of glass,» *U.S. Patent,* pp. 715,319, 6 Apr. 2004.

[56] C. J. a. G. W. S. Brinker, «Sol→ gel→ glass: I. Gelation and gel structure,» *Journal of Non-Crystalline Solids,* n. 70.3, pp. 301-322, 1985.

[57] L. L. a. J. K. W. Hench, «The sol-gel process,» *Chemical reviews,* n. 90.1, pp. 33-72, 1990.

[58] W. a. L. L. H. Cao, «Bioactive materials,» *Ceramics international ,* n. 22.6, pp. 493-507, 1996.

[59] V. Schwitters, «Virginia Schwitters,» 15 February 2017. [Online]. Available: https://virginiaschwitters.wordpress.com/2017/02/15/evolution-of-the-prosthetic/. [Consultato il giorno 13 Nov 2018].

[60] L. L. a. J. M. P. Hench, «Third-generation biomedical materials,» *Science,* n. 295.5557 , pp. 1014-1017, 2002.

[61] V. L. E. Z. G. Cogliano, Perspectives on Biologically Based Cancer Risk Assessment, USA: Springer, 2012.

[62] M. e. a. Kusdemir, «Evaluation of cytotoxic effects of six self-etching adhesives with direct and indirect contact tests,» *Dental materials journal,* n. 30.6, pp. 799-805, 2011.

[63] R. e. a. Bonnet, «The strong inhibition of triosephosphate isomerase by the natural β-carbolines may explain their neurotoxic actions,» *Neuroscience,* n. 127.2, pp. 443-453, 2004.

[64] I. S. H. Z. H. T. S. S. K. T. Y. T. Kokubo T, «Ca,P-rich layer formed on high-strength bioactive glass-ceramic A-W,» *J Biomed Mater Res,* n. 24, p. 331–43, 1990.

[65] G. G. Nahas, «The pharmacology of tris (hydroxymethyl) aminomethane (THAM),» *Pharmacological reviews,* n. 14.3, pp. 447-472, 1962.

[66] J. S. K. S. a. A. B. G. Nourmohammadi, «Bone-like apatite layer formation on the new resin-modified glass-ionomer cement,» *Journal of Materials Science: Materials in Medicine,* n. 19.12, p. 3507, 2008.

[67] A. a. N. R. Srinivasan, «Surface characteristics, corrosion resistance and MG63 osteoblast-like cells attachment behaviour of nano SiO 2–ZrO 2 coated 316L stainless steel,» *RSC Advances,* n. 5.33, pp. 26007-26016, 2015.

[68] K. Hoffmeier, «Wikipedia,» 15 March 2007. [Online]. Available: https://en.wikipedia.org/wiki/Tris. [Consultato il giorno 13 Dic 2018].

[69] A. e. a. Pizzoferrato, «Cell culture methods for testing biocompatibility,» *Clinical materials,* n. 15.3, pp. 173-190, 1994.

[70] D. A. M. F. a. S. V. N. Raftos, «Exocytosis of a complement component C3-like protein by tunicate hemocytes,» *Developmental & Comparative Immunology,* n. 28.3, pp. 181-190, 2004.

[71] T. L. e. a. Riss, Cell viability assays, 2016.

[72] K. a. H. H. Apel, «Reactive oxygen species: metabolism, oxidative stress, and signal transduction,» *Annu. Rev. Plant Biol.,* n. 55, pp. 373-399, 2004.

[73] K. e. a. Reilly, «Oxidative stress responses during cassava post-harvest physiological deterioration,» *Plant molecular biology,* n. 53.5 , pp. 669-685, 2003.

[74] J. A. J. J. H. a. R. J. T. Lemire, «Antimicrobial activity of metals: mechanisms, molecular targets and applications,» *Nature Reviews Microbiology,* n. 11.6 , p. 371, 2013.

[75] G. M. J. A. B. a. T. L. Garrity, «Class II. Betaproteobacteria class. nov.,» in *Bergey's manual® of systematic bacteriology*, Boston, Springer, 2005, pp. 575-922.

[76] M. T. J. M. M. a. J. P. Madigan, *Brock biology of microorganisms,* vol. Vol. 11, Upper Saddle River: Prentice hall, 1997.

[77] Z. a. P. J. S. Guo, «Metals in medicine,» *Angewandte Chemie International Edition,* n. 38.11, pp. 1512-1531, 1999.

[78] K. Barbusiński, «Fenton reaction-controversy concerning the chemistry,» *Ecological Chemistry and Engineering,* n. 16.3 , pp. 347-358, 2009.

[79] J. S. e. a. Fernandes, «Multifunctional bioactive glass and glass-ceramic biomaterials with antibacterial properties for repair and regeneration of bone tissue,» *Acta biomaterialia,* n. 59, pp. 2-11, 2017.

[80] I. a. K. Ő. Sóvágó, «Metal ion selectivity of oligopeptides,» *Dalton Transactions,* n. 32, pp. 3841-3854, 2006.

[81] C. A. T. M. T. a. K. G. S. Impellitteri, «The speciation of silver nanoparticles in antimicrobial fabric before and after exposure to a hypochlorite/detergent solution,» *Journal of environmental quality,* n. 38.4, pp. 1528-1530, 2009.

[82] F. S. F. a. C. V.-B. Baino, «Bioactive glass-based materials with hierarchical porosity for medical applications: Review of recent advances,» *Acta biomaterialia ,* n. 42, pp. 18-32, 2016.

[83] W. a. M. Y. Suchanek, «Processing and properties of hydroxyapatite-based biomaterials for use as hard tissue replacement implants,» *Journal of Materials Research,* n. 13.1, pp. 94-117, 1998.

[84] T. e. a. Leventouri, «Crystal structure studies of human dental apatite as a function of age,» *International journal of biomaterials,* n. 2009 , 2009 .

[85] M. H. e. a. Uddin, Biomimetic fabrication of apatite related biomaterials, InTech, 2010.

[86] L. L. Hench, «Chronology of bioactive glass development and clinical application,» *New Journal of Glass and Ceramics,* n. 3.02, p. 67, 2013.

[87] C. C. a. S. C. L. Della Santina, «Ceravital reconstruction of canal wall down mastoidectomy: long-term results,» *Archives of Otolaryngology–Head & Neck Surgery,* n. 132.6, pp. 617-623, 2006.

[88] J. R. Jones, «Review of bioactive glass: from Hench to hybrids,» *Acta biomaterialia,* n. 9.1, pp. 4457-4486, 2013.

[89] L. L. Hench, «The story of Bioglass®,» *Journal of Materials Science: Materials in Medicine,* n. 17.11, pp. 967-978, 2006.

[90] J. R. a. L. L. H. Jones, «Biomaterials: bioceramics,» in *Encyclopedia of medical devices and instrumentation*, 2006.

[91] G. e. a. Kaur, «Review and the state of the art: sol–gel and melt quenched bioactive glasses for tissue engineering,» *Journal of Biomedical Materials Research Part B: Applied Biomaterials,* n. 104.6, pp. 1248-1275, 2016.

[92] T. e. a. Kokubo, «Chemical reaction of bioactive glass and glass-ceramics with a simulated body fluid,» *Journal of Materials science: Materials in medicine,* n. 3.2, pp. 79-83, 1992.

[93] F.-X. e. a. Huber, «Evaluation of a novel nanocrystalline hydroxyapatite paste and a solid hydroxyapatite ceramic for the treatment of critical size bone defects (CSD) in rabbits,» *Journal of Materials Science: Materials in Medicine,* n. 19.1, pp. 33-38, 2008.

[94] E. e. a. Verné, «Bioverit® I base glass/Ti particulate biocomposite:“in situ” vacuum plasma spray deposition,» *Journal of the European Ceramic Society,* n. 20.4, pp. 473-479, 2000.

[95] J. C. e. a. Vogt, «Free Bioverit® II implants coated with a nanoporous silica layer in a mouse ear model—A Histological Study,» *Journal of biomaterials applications,* n. 24.2, pp. 175-191, 2009.

[96] M. a. E. D. Z. Montazerian, «History and trends of bioactive glass-ceramics,» *Journal of Biomedical Materials Research Part A,* n. 104.5, pp. 1231-1249, 2016.

[97] G. e. a. Brunelli, «PERIOGLASS AND ITS OSTEOGENIC POTENTIAL,» *European Journal of Inflammation,* n. 10.1, pp. 43-47, 2012.

[98] I. P. S. a. J. F. Saarenpää, «BAG S53P4 putty as bone graft substitute–a rabbit model,» *Biomedical Glasses,* n. 3.1, pp. 30-40, 2017.

[99] Z. e. a. Qiu, «Ionic dissolution products of NovaBone® promote osteoblastic proliferation via influences on the cell cycle,» *Journal of International Medical Research,* n. 37.3, pp. 737-745, 2009.

[100] N. Koporcic, «Born Globals in Interactive Branding Environment: A case of the BonAlive,» in *3rd Business & Management Conference*, Lisbon, 2016.

[101] A. e. a. Mahato, «Applications of DifferenBioactive Glass and Glass-Ceramic Materials for Osteoconductivity and Osteoinductivity,» *Transactions of the Indian Ceramic Society,* n. 76.3, pp. 149-158, 2017.

[102] V. A. Dubok, «Bioceramics—yesterday, today, tomorrow,» *Powder Metallurgy and Metal Ceramics,* n. 39.7-8, pp. 381-394, 2000.

[103] «Technavio,» Nov 2017. [Online]. Available: https://www.technavio.com/report/global-bioactive-glass-market.

[104] Technavio, «Global Bioactive Glass market 2015-2019,» 2015.

[105] F. S. H. a. S. K. Baino, «Bioactive glasses: where are we and where are we going?,» *Journal of functional biomaterials,* n. 9.1, p. 25, 2018.

[106] L. L. a. J. R. J. Hench, «Bioactive glasses: frontiers and challenges,» *Frontiers in bioengineering and biotechnology,* n. 3, p. 194, 2015.

[107] «NaijaLi,» 23 July 2018. [Online]. Available: http://naijali.ml/2018/07/23/global-bioactive-glass-market-forecast-company-trend-type-and-applications-upto-2023/. [Consultato il giorno 15 11 2018].

[108] M. Rizzotto, Metal complexes as antimicrobial agents, IntechOpen, 2012.

[109] P. D. S. a. M. A. Pravina, «Calcium and its role in human body,» *J. Res. Pharm. Biomed. Sci,* n. 4.2, pp. 659-668, 2013.

[110] V. J. P. C. a. A. R. B. Mouriño, «Metallic ions as therapeutic agents in tissue engineering scaffolds: an overview of their biological applications and strategies for new developments,» *Journal of the Royal Society Interface,* n. 9.68, pp. 401-419, 2011.

[111] J. H. J. G. H. a. R. J. B. De Baaij, «Magnesium in man: implications for health and disease,» *Physiological reviews,* n. 95.1, pp. 1-46, 2015.

[112] S. M. a. R. A. F. Payne, «The critical role of iron in host-bacterial interactions,» *The Journal of clinical investigation,* n. 61.6, pp. 1428-1440, 1978.

[113] G. e. a. Liu, «Applications and potential toxicity of magnetic iron oxide nanoparticles,» *Small,* n. 9.9-10, pp. 1533-1545, 2013.

[114] N. W. Solomons, «Biochemical, metabolic, and clinical role of copper in human nutrition,» *Journal of the American College of Nutrition,* n. 4.1, pp. 83-105, 1985.

[115] J. L. a. L. C. C. Hobman, «Bacterial antimicrobial metal ion resistance,» *Journal of medical microbiology,* n. 64 , pp. 471-497, 2015.

[116] C. K. e. a. Sen, «Copper induced vascular endothelial growth factor expression and wound healing,» *American Journal of Physiology-Heart and Circulatory Physiology,* 2002.

[117] M. Hambidge, «Human zinc deficiency,» *The Journal of nutrition,* n. 130.5, pp. 1344-1349, 2000.

[118] D. K. P. C. a. S. K. Bhowmik, «A potential medicinal importance of zinc in human health and chronic,» *Int J Pharm,* n. 1.1, pp. 05-11, 2010.

[119] C. T. e. a. Chasapis, «Zinc and human health: an update,» *Archives of toxicology,* n. 86.4, pp. 521-534, 2012.

[120] K. S. T. a. A. K. S. Czarnek, «Selected aspects of the action of cobalt ions in the human body,» *Central-European journal of immunology,* n. 40.2, p. 236, 2015.

[121] A. S. a. H. A. C. Gordon, «The endocrine system and hemopoiesis,» *Annals of the New York Academy of Sciences,* n. 48.7, pp. 615-640, 1947.

[122] T. R. e. a. Vrabec, «Impact of local tumor relapse on patient survival after cobalt 60 plaque radiotherapy.,» *Ophthalmology,* n. 98.6, pp. 984-988, 1991.

[123] A. B. Lansdown, «Silver in health care: antimicrobial effects and safety in use,» *Biofunctional textiles and the skin,* vol. 33, pp. 17-34, 2006.

[124] B. Leyland-Jones, «Treatment of cancer-related hypercalcemia: the role of gallium nitrate,» *Seminars in oncology,* vol. 30, pp. 13-19, 2003.

[125] C. J. Palestro, «The current role of gallium imaging in infection,» *Seminars in nuclear medicine,* vol. 24, pp. 128-141, 1994.

[126] K. e. a. Aihara, «Zinc, copper, manganese, and selenium metabolism in thyroid disease,» *The American journal of clinical nutrition,* n. 40.1, pp. 26-35, 1984.

[127] M. a. P. S. C. Irshad, «Oxidant-antioxidant system: role and significance in human body,» *Indian Journal of Experimental Biology,* vol. 40, pp. 1233-1239, 2002.

[128] R. M. e. a. Walter, «Copper, zinc, manganese, and magnesium status and complications of diabetes mellitus,» *Diabetes care ,* n. 14.11 , pp. 1050-1056, 1991.

[129] L. e. a. Wielopolski, «Application of XRF to measure strontium in human bone in vivo,» Upton, 1982.

[130] S. G. e. a. Dahl, «Incorporation and distribution of strontium in bone,» *Bone,* n. 28.4, pp. 446-453, 2001.

[131] A. R. a. L. K. Byrne, «Vanadium in foods and in human body fluids and tissues,» *Science of the total environment,* n. 10.1, pp. 17-30, 1978.

[132] D. Rehder, «Vanadium. Its role for humans,» *Interrelations between essential metal ions and human diseases,* pp. 139-169, 2013.

[133] L. a. R. S. Dinca, «Boron in human nutrition and its regulations use,» *Journal of Nutritional Therapeutics,* n. 2.1 , pp. 22-29, 2013.

[134] I. R. Scorei, «Boron compounds in the breast cancer cells chemoprevention and chemotherapy,» *Breast Cancer-Current and Alternative Therapeutic Modalities.*

[135] A. N. S. G. a. A. R. B. Hoppe, «A review of the biological response to ionic dissolution products from bioactive glasses and glass-ceramics,» *Biomaterials,* n. 32.11 , pp. 2757-2774, 2011.

[136] R. Jugdaohsingh, «Silicon and bone health,» *The journal of nutrition, health & aging,* n. 11.2, p. 99, 2007.

[137] L. Broadhurst, «Silicon's elemental benefits,» [Online]. Available: http://www. prolithic. com/hpages/ref_docs/orthosil. html. [Consultato il giorno 19 Sept 2018].

[138] L. A. e. a. Ba, «Tellurium: an element with great biological potency and potential,» *Organic & biomolecular chemistry,* n. 8.19 , pp. 4203-4216, 2010.

[139] F. e. a. Yang, «Purification and in vitro antioxidant activities of tellurium-containing phycobiliproteins from tellurium-enriched Spirulina platensis,» *Drug design, development and therapy,* n. 8, p. 1789, 2014.

[140] A. J. Bradley, «The crystal structures of the rhombohedral forms of selenium and tellurium,» *The London, Edinburgh, and Dublin Philosophical Magazine and Journal of Science,* n. 48.285 , pp. 477-496, 1924.

[141] B. M. N. a. A.-R. S. Zare, «Tracing tellurium and its nanostructures in biology,» *Biological trace element research ,* n. 180.2, pp. 171-181, 2017.

[142] V. e. a. Ignatiev, «Intergranular tellurium cracking of nickel-based alloys in molten Li, Be, Th, U/F salt mixture,» *Journal of Nuclear Materials,* n. 440.1-3, pp. 243-249, 2013.

[143] K. Zweibel, «The impact of tellurium supply on cadmium telluride photovoltaics,» *Science,* n. 328, pp. 699-701, 2010.

[144] X. e. a. Lu, «Selenium-and tellurium-based antioxidants for modulating inflammation and effects on osteoblastic activity,» *Antioxidants,* n. 6, p. 13, 2017.

[145] R. e. a. Yalew, «Antibacterial effects of the tellurium compound OTD on E. coli isolates,» *Archives of microbiology,* n. 196, pp. 51-61, 2014.

[146] I. L. e. a. Calderón, «Tellurite-mediated disabling of [4Fe–4S] clusters of Escherichia coli dehydratases,» *Microbiology,* n. 155, pp. 1840-1846, 2009.

[147] G. H. D. a. H. K. El-Damrawi, «Characterization of new categories of bioactive based tellurite and silicate glasses.,» *Silicon,* n. 9, pp. 503-509, 2017.

[148] M.-G. e. a. Ma, «Synthesis and characterization of the tellurium/calcium silicate nanocomposite,» *Materials letters ,* n. 65, pp. 424-426, 2011.

[149] M. e. a. Shakibaie, «Antimicrobial and Antioxidant Activity of the Biologically Synthesized Tellurium Nanorods; A Preliminary In vitro Study,» *Iranian journal of biotechnology,* n. 15, p. 268, 2017.

[150] J. I. e. a. Goldstein, Scanning electron microscopy and X-ray microanalysis, Springer, 2017.

[151] H. Seiler, «Secondary electron emission in the scanning electron microscope,» *Journal of Applied Physics,* n. 54, pp. 1-18, 1983.

[152] S. K. e. a. Sharma, Handbook of Materials Characterization, Springer, 2018.

[153] A. Nanakoudis, «ThermoFisher Scientific,» 7 Jun 2018. [Online]. Available: http://blog.phenom-world.com/what-is-sem. [Consultato il giorno 14 Dec 2018].

[154] «Core Laboratories,» [Online]. Available: https://www.corelab.com/ps/scanning-electron-microscopy. [Consultato il giorno 12 Gen 2019].

[155] M. e. a. Scimeca, «Energy Dispersive X-ray (EDX) microanalysis: A powerful tool in biomedical research and diagnosis,» *European journal of histochemistry: EJH ,* n. 62, 2018.

[156] T. a. H. T. Kokubo, «How useful is SBF in predicting in vivo bone bioactivity?,» *Biomaterials ,* n. 27, pp. 2907-2915, 2006.

[157] J. R. Dean, Practical skills in chemistry, Pearson Education, 2002.

[158] P. J. Haines, Thermal methods of analysis: principles, applications and problems, Springer Science & Business Media, 2012.

[159] R. a. S. K. D. Sah, «Kinetic studies of iron ore–coal composite pellet reduction by TG–DTA,» *Transactions of the Indian Institute of Metals,* n. 64, pp. 583-591, 2011.

[160] L. Fröberg, «Thermal Analysis TGA/DTA,» [Online]. Available: http://web.abo.fi/instut/biofuelsGS-2/kursen/%C5A/lectures/Lectrure_Thermal%20Analysis.pdf.

[161] A. A. B. a. F. B. Marotta, «Nucleation in glass and differential thermal analysis,» *Journal of materials science,* n. 16, pp. 341-344, 1981.

[162] S. A. a. A. H. W. Mikhail, «Thermal Analysis in Metallurgy,» in *Handbook of Thermal Analysis and Calorimetry*, vol. 2, Elsevier Science, 2003, pp. 657-775.

[163] «Hitachi High-Technologies,» [Online]. Available: https://www.hitachi-hightech.com/global/products/science/tech/ana/thermal/descriptions/dta.html.

[164] R. C. a. P. F. S. R. Mackenzie, «Peak areas and heats of transition of DTA temperature standards,» in *Advances in Instrumentation*, Basel, Birkhäuser, 1972, pp. 441-452.

[165] B. E. Warren, X-ray Diffraction, Courier Corporation, 1990.

[166] D. M. a. R. C. R. Moore, X-ray Diffraction and the Identification and Analysis of Clay Minerals, Oxford: Oxford university press, 1989.

[167] Furiouslettuce, «Wikipedia,» 10 April 2009. [Online]. Available: http://en.wikipedia.org/wiki/File:DiffractionPlanes.png. [Consultato il giorno 24 Jan 2019].

[168] B. B. He, Two-dimensional X-ray diffraction, John Wiley & Sons, 2018.

[169] [Online]. Available: https://nptel.ac.in/courses/103103026/module2/lec12/2.html. [Consultato il giorno 01 Feb 2019].

[170] A. Le Bail, Powder diffraction: theory and practice, Royal Society of Chemistry, 2008.

[171] O. Faix, «Fourier transform infrared spectroscopy,» in *Methods in lignin chemistry*, Berlin, Springer, 1992, pp. 83-109.

[172] John, «Instrumentation Forum,» 18 Jun 2018. [Online]. Available: https://instrumentationforum.com/t/fourier-transform-infrared-spectroscopy-ftir-principle/4980. [Consultato il giorno 07 Jan 2019].

[173] J. J. a. M. D. Ojeda, «Fourier transform infrared spectroscopy for molecular analysis of microbial cells,» *Microbial Systems Biology,* pp. 187-211, 2012.

[174] B. Stuart, «Infrared spectroscopy,» *Kirk-Othmer Encyclopedia of Chemical Technology,* pp. 1-18, 2000.

[175] P. R. a. J. A. D. H. Griffiths, Fourier transform infrared spectrometry, John Wiley & Sons, 2007.

[176] R. A. Gilstrap Jr, *A colloidal nanoparticle form of indium tin oxide: System development and characterization,* Georgia, 2009.

[177] X. a. B. T. J. Hou, «Inductively coupled plasma/optical emission spectrometry,» in *Encyclopedia of analytical chemistry*, Chichester, John Wiley & Sons Ltd, 2000, p. 9468–9485.

[178] V. a. V. A. Cavrini, Principi di analisi farmaceutica, Bologna: Società Editrice Esculapio, 2018.

[179] C. B. a. K. J. F. Boss, Concepts, instrumentation and techniques in inductively coupled plasma optical emission spectrometry, 1999.

[180] A. a. S. Z. Mitra, Basics of marine and estuarine ecology, Springer, 2006.

[181] J. W. Olesik, «Elemental analysis using ICP-OES and ICP/MS,» *Analytical Chemistry,* n. 63, pp. 12-21, 1991.

[182] D. D. Bhanot, «Lab-Training.com,» 26 June 2015. [Online]. Available: Available: http://lab-training.com/2015/06/26/what-are-the-differences-between-raman-and-ir-spectroscopy/. [Consultato il giorno 28 Oct 2018].

[183] D. A. Long, Raman spectroscopy, New York, 1977.

[184] P. Larkin, Infrared and Raman spectroscopy: principles and spectral interpretation, Elsevier, 2017.

[185] G. S. a. R. M. S. Bumbrah, «Raman spectroscopy–Basic principle, instrumentation and selected applications for the characterization of drugs of abuse,» *Egyptian Journal of Forensic Sciences,* n. 6, pp. 209-215, 2016.

[186] U. F. L. a. A. S. Boonyang, «Hierarchical structures and shaped particles of bioactive glass and its in vitro bioactivity,» *Journal of Nanomaterials ,* n. 2013, p. 8, 2013.

[187] H. e. a. Aguiar, «Structural study of sol–gel silicate glasses by IR and Raman spectroscopies,» *Journal of Non-Crystalline Solids,* n. 355, pp. 475-480, 2009.

[188] M. e. a. Mačković, «Bioactive glass (type 45S5) nanoparticles: in vitro reactivity on nanoscale and biocompatibility,» *Journal of Nanoparticle Research ,* n. 14, p. 966, 2012.

[189] M. D. e. a. O'Donnell, «The effect of phosphate content on the bioactivity of soda-lime-phosphosilicate glasses,» *Journal of Materials Science: Materials in Medicine,* n. 20, pp. 1611-1618, 2009.

[190] G. H. D. a. H. K. El-Damrawi, «Characterization of new categories of bioactive based tellurite and silicate glasses,» *Silicon,* n. 9, pp. 503-509, 2017.

[191] F. e. a. Bonino, «In situ Raman study to monitor bioactive glasses reactivity,» *Journal of Raman Spectroscopy: An International Journal for Original Work in all Aspects of Raman Spectroscopy, Including Higher Order Processes, and also Brillouin and Rayleigh Scattering ,* n. 39, pp. 260-264, 2008.

[192] D. e. a. Bellucci, «In situ Raman spectroscopy investigation of bioactive glass reactivity: Simulated body fluid solution vs TRIS-buffered solution,» *Materials characterization,* n. 62, pp. 1021-1080, 2011.

[193] A. K. a. P. S. Yadav, «A review of the structures of oxide glasses by Raman spectroscopy,» *Rsc Advances,* n. 5, pp. 67583-67609, 2015.

[194] M. e. a. Dziadek, «Structural variations of bioactive glasses obtained by different synthesis routes,» *Ceramics International,* n. 42, pp. 14700-14709, 2016.

[195] R. Mazze, «Growth of Hydroxyapatite crystals from solutions with pH controlled by novel vapor diffusion techniques. Effects of temperature and of the acidic phosphoprotein osteopontin on crystals growth,» *Periodico Di Mineralogia,* n. 78, pp. 19-43, 2009).

[196] T. e. a. De Caluwé, «Bioactivity and biocompatibility of two fluoride containing bioactive glasses for dental applications,» *Dental Materials,* n. 32, pp. 1414-1428, 2016.

[197] A. e. a. Chagraoui, «Glasses formation, characterization, and crystal-structure determination in the Bi 2 O 3–Sb 2 O 3–TeO 2 system prepared in an air,» *Journal of materials science ,* n. 46, pp. 5439-5446, 2011.

[198] R. A. e. a. Martin, «Characterizing the hierarchical structures of bioactive sol–gel silicate glass and hybrid scaffolds for bone regeneration,» *Philosophical Transactions of the Royal Society A: Mathematical, Physical and Engineering Sciences,* n. 370, pp. 1422-1443, 2012.

[199] G. I. A. A. a. J. T. G. Xu, «Continuous crystalline carbonate apatite thin films. A biomimetic approach,» *Journal of the American Chemical Society ,* n. 123, pp. 2196-2203, 2001.

[200] Nanophoton, «Nanophoton,» 2016. [Online]. Available: https://www.nanophoton.net/raman/raman-spectroscopy.html. [Consultato il giorno 26 Feb 2019].

[201] R. L. I. E. G. a. L. J. Cunha, «A glimpse on biological activities of tellurium compounds,» *Anais da Academia Brasileira de Ciências,* n. 81, pp. 393-407, 2009.

[202] D. E. Taylor, «Bacterial tellurite resistance,» *Trends in microbiology,* n. 7, pp. 111-115, 1999.

[203] R. H. V. N. U. a. E. A. P. Kretsinger, Encyclopedia of Metalloproteins, Springer, 2013.

[204] B. e. a. Sarecka-Hujar, «Scanning electron microscopy and X-ray energy dispersive spectroscopy–useful tools in the analysis of pharmaceutical products,» *Journal of Physics: Conference Series,* vol. 931, n. 1, 2017.

Acknowledgements

While i was writing this speech, i agonized for days over who to thank first. The successful and final outcome of this work required lots of guidance and assistance from many people and i am extremely fortunate to have completed my assignment work. I would like to show my gratitude Ms. Vernè Enrica, associate professor and chair in the Department of Applied Science and Technology, Politecnico di Torino and Ms. Miola Marta, university researcher and chair in the Department of Applied Science and Technology, Politecnico di Torino for giving me a good guideline for assignment throughout numerous consultations and valuable comment suggestions to improve my assignment. Thank you for all your tireless work even in the face of overwhelimg odds, your sensible advice and your willingness to listen when i needed it the most. You helped me turn on so many lightbulbs in my head, and i'm eternally grateful for all of your help and encouragement. In addition, a thank you to Mr. Massera Jonathan, Academy Research FellowMember of Research Group, Tampere University of Technology, who provided insight and expertise that greatly assisted the research and giving me exposure to the realities of academic life and a working environment in which i most probably have been able to overcome challenges more independently. I also thank the Politecnico di torino who gave me a scholarship, materials and ran my program and University of Tampere for giving me the opportunity to work on this project abroad.

Actually, i have no doubt my familiy has made a lot for me. Whatever i have done is only due to such guidance and assistance and i should not forget to thank them. This assignment could not be completed without the help of my parents. You were there for me in my happiest and saddest moments. In fact they played a part in the preparation of this work since they helped me focus on my goal and my attitude at every opportunity. Thank you for always pushing me in the right direction and supporting me every step of the way. I can never repay you for the support you have provided. If not for your efforts, I wouldn't be where I am today. I would have been here years ago. Thanks for teaching me that absolutely nothing can stand in the way of my success.

I might even thank all my friends and my girlfriend since they made my student life bearable and helped me through the long, arduous process that is getting a master’s degree. Moreover, a special mention is reserved for my cousin who helped me so much to review my thesis.

Thank you to those who helped me along the way